Investigation of system performance of two cascaded organic Rankine cycles using low global warming potential working fluids

zur Erlangung des akademischen Grades

DOKTOR DER INGENIEURWISSENSCHAFTEN (Dr.-Ing.)

der Fakultät für Maschinenbau

der Universität Paderborn

genehmigte

DISSERTATION

von

Wameedh Abbas, M.Sc

aus Salahuddin / Irak

Tag des Kolloquiums: 10.07.2023

Betreuer der Dissertation: Prof. Dr.-Ing. habil. Jadran Vrabec

Koreferent: Prof. Dr. rer. nat. Burak Atakan

"Knowledge is better than wealth. Knowledge guards you while you guard wealth; when knowledge is distributed, it increases, and when wealth is distributed, it decreases.
The collectors of wealth die, while the scholars exist forever. Their bodies have disappeared, but their teachings and wisdom are ingrained in the hearts."

Ali ibn Abi Talib (600-661)

Acknowledgments

First and foremost, I am highly grateful to my supervisor, Prof. Dr. Jadran Vrabec, for his invaluable advice, continuous support and patience during my PhD study. His immense knowledge and great experience have encouraged me throughout my academic research and daily life. He is my mentor and an excellent advisor for my doctorate study.

I would like to thank Dr. Gerhard Herres for his great help when I was writing my publications and for answering all questions during my PhD studies. My gratitude extends to Elmar Baumhögger for his technical support in the laboratory. I also appreciate the experimentally professional work of Rüdiger Pflock, Dennis Themm and Norbert Temborius.

I would like to extend my sincere thanks to Dr. Frithjof Dubberke and Dr. Matthias Linnemann for their great support which was influential in shaping my experimental methods and for critiquing my results. Additionally, I would like to express my gratitude to my former colleagues Jutta Jäger, Andreas Paul, Michael Reineke, Andreas Elsner, Prof. Dr. Dieter Gorenflo, Marco Grefe, Dr. Tatjana Janzen, Dr. René Spencer Chatwell, Matthias Heinen, Dr. Andreas Köster, Dr. Gabor Rutkai, Dr. Gerrit Sonnenrein, Stefan Eckelsbach, Dr. Yonny Mauricio Muñoz Muñoz and Dr. Robin Fingerhut for the cherished time spent together at the University of Paderborn.

I am deeply grateful to the Deutscher Akademischer Austauschdienst (DAAD) for the financial and administrative support during the scholarship.

I am also grateful to my parents, brothers, sister, friends and acquaintances who remembered me in their prayers for the ultimate success. Without their tremendous understanding and encouragement in the past years, it would have been impossible for me to complete my study.

Finally, my great appreciation goes to my wife Asmaa and my daughter Maria who stood by me and supported me with all their strength to achieve my objective without any obstacles on the way.

Leonberg, 01.04.2023

Wameedh Abbas

Zusammenfassung / Abstract

Diese Dissertation bietet eine experimentelle und simulationsbasierte Bewertung der CORC-Systemleistung durch die Nutzung verschiedener Arbeitsfluide aus verschiedenen physio-chemischen Gruppen. Die Arbeit basiert auf einem 158 kW CORC-System, das aus drei Hauptkreisläufen besteht: Wärmequellenkreislauf, Hochtemperatur-ORC und Niedertemperatur-ORC. In dieser Arbeit wird die Systemleistung anhand des thermischen Wirkungsgrads und des exergetischen Wirkungsgrads gemessen, da sie die abgegebene Leistung im Verhältnis zum zugeführten Wärmestrom wiedergeben. Zusätzlich wird die Leistungsfähigkeit der Hauptkomponenten bewertet, indem der Turbinenwirkungsgrad, die Wärmeübertragung zwischen den kaskadierten ORC-Kreisläufen sowie der Exergieverlust in ihren vier Hauptkomponenten gemessen wird. Darüber hinaus konzentriert sich diese Arbeit auf die Untersuchung der Beziehung zwischen der Systemleistung und den thermophysikalischen Eigenschaften der Arbeitsfluide, wie z.B. der kritischen Temperatur, dem kritischen Druck, der Molasse und der Molekülstruktur. Diese Parameter werden über einen weiten Bereich von Betriebsbedingungen berücksichtigt, einschließlich Wärmequellentemperatur, Turbineneinlassdruck, Massenstrom des Arbeitsfluide, Überhitzungsgrad und Druckverhältnis.

This thesis provides experimental and simulation-based evaluations of CORC system performance by adopting various working fluids from different physico-chemical groups. The work is based on a 158 kW CORC system, consisting of three main cycles: heat source cycle, high-temperature ORC and low-temperature ORC. System performance is measured based on thermal efficiency and exergy efficiency, as they view power output in relation to the heat flow input. In addition, the performance of the main components is evaluated by measuring the turbine efficiency, the heat transfer between the two cascaded ORC as well as the exergy loss in their four main components. Moreover, it is focused on the relationship between system performance and the thermophysical properties of the working fluids, such as critical temperature, critical pressure, molar mass and molecular structure. These parameters are considered over a wide range of operating conditions, including heat source temperature, turbine inlet pressure, mass flow rate of working fluid, superheating degree and pressure ratio.

List of publications

Dubberke F, Linnemann M, Abbas WK, Baumhögger E, Priebe KP, Roedder M, Neef M, Vrabec J. Experimental setup of a cascaded two-stage organic Rankine cycle. Applied Thermal Engineering 2018;131:958–964. DOI: 10.1016/j.applthermaleng.2017.11.137.

Abbas WKA, Linnemann M, Baumhögger E, Vrabec J. Experimental study of two cascaded organic Rankine cycles with varying working fluids. Energy Conversion and Management 2021;230:113818. DOI: 10.1016/j.enconman.2020.113818.

Abbas WKA, Vrabec J. Cascaded dual-loop organic Rankine cycle with alkanes and low global warming potential refrigerants as working fluids. Energy Conversion and Management 2021;249:114843. DOI: 10.1016/J.ENCONMAN.2021.114843.

Abbas WKA, Baumhögger E, Vrabec J. Experimental investigation of organic Rankine cycle performance using alkanes or hexamethyldisiloxane as a working fluid. Energy Conversion and Management: X 2022;15;100244. DOI: 10.1016/J.ECMX.2022.100244.

Contents

Aknowledgments **i**

Zusammenfassung / Abstract **ii**

List of publications **iii**

1 Introduction **1**

1.1 Background 1

1.2 Objective and aims 4

1.3 Thesis outline 5

2 ORC system **7**

2.1 ORC history 8

2.2 Thermodynamics of the ORC 10

2.3 Comparison of ORC and SRC 11

2.4 ORC market 13

3 Working fluid **15**

3.1 Working fluid categories 15

3.2 Working fluid selection criteria 16

3.3 Working fluids considered in this work 19

4 CORC system **24**

4.1 CORC test rig 26

5 Publications **31**

5.1 Experimental setup of a cascaded two-stage organic Rankine cycle 31

5.2 Experimental study of two cascaded organic Rankine cycle with varying working fluids 32

5.3 Cascaded dual-loop organic Rankine cycle with alkanes and low global potential refrigerants as working fluid 46

5.1 Experimental investigation of organic Rankine cycle performance using alkanes or hexamethyldisiloxane 61

5 Summary and conclusions **75**

Bibliography **77**

Appendix **84**

1. Introduction

1.1. Background

During the past two decades, global energy demand has increased dramatically due to population increase that was paralleled with technological, industrial and urban development. Demand for the consumption of energy will further increase over the next two decades, with an expected world population rise to about nine billion. Figure 1 presents the increase of global energy consumption for the period from 2000 to 2022, indicating an expected rise to about 620 Exajoules in 2022 [1].

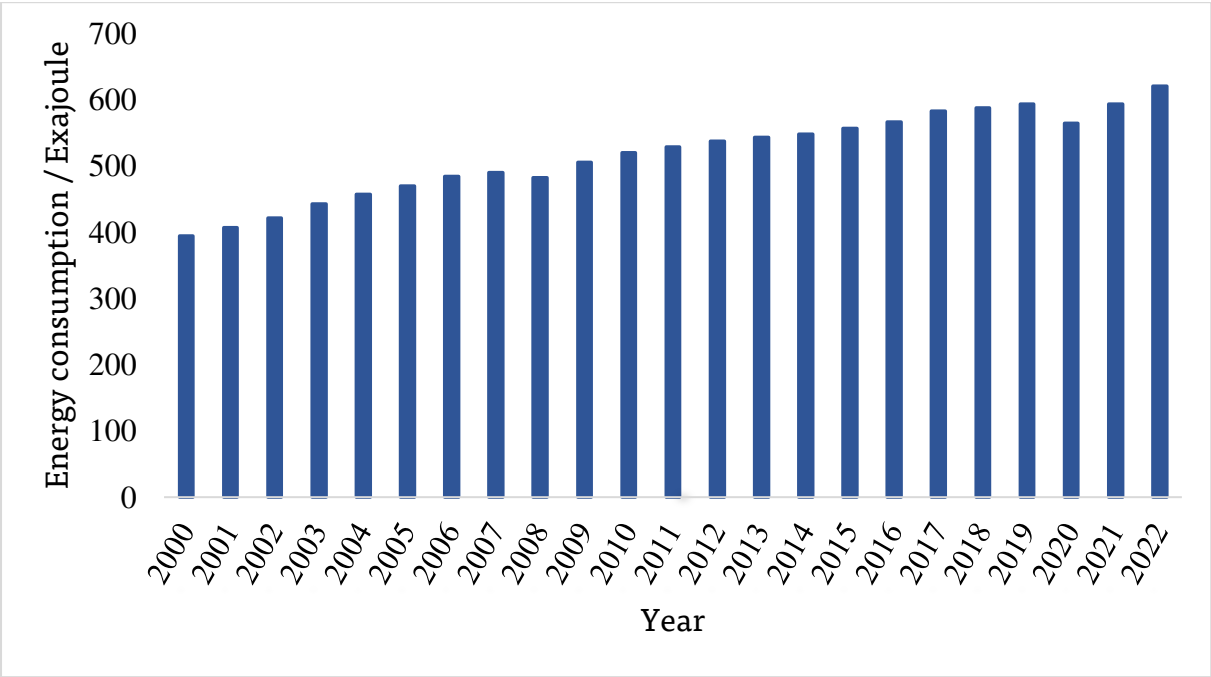

Fig. 1. Global energy consumption since the year 2000 [1].

The latest report issued by British Petroleum (BP) showed that the energy demand recorded a historical rise during the last 50 years. According to the statistical review published by BP, current global energy consumption has recorded an increase of 5.5% in 2021, representing the fastest growth since the beginning of the 1970s. This report also reflects the quickest growth in energy consumption since 1970, showing a strong global demand spike after the decline in 2020 due to the COVID-19 pandemic [2].

By reviewing the sources of global energy consumption, it is clear that fossil fuels dominate with about 80%, while the percentage from renewable and clean sources is only in the range of 16%. Nevertheless, crude oil still covers nearly a third of the world's energy consumption, as shown in Fig. 2. In 2021, the world used 94.1 million barrels of oil per day, an increase of 6%

over 2020, which is still 3.7% less than the consumption in 2019 [1,3]. Moreover, the impact of the Corona pandemic still dominated the statistics of energy use and consumption, as energy consumption and production decreased significantly in 2020, but since then the demand has rebounded again [3].

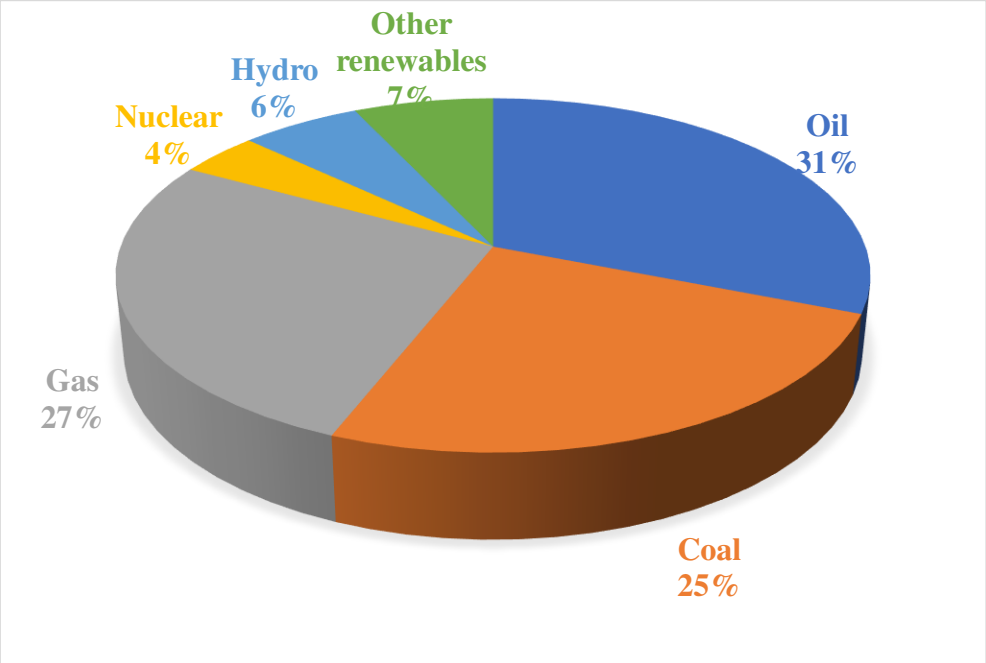

Fig. 2. Comparison of global use of fossil fuels and renewable energy [3,4].

The choice of fossil crude oil-based fuels as the primary energy source worldwide did not come about randomly. It was driven by availability and ease of use, transportation and storage, as crude oil can be refined, and other types of fuel can be extracted from it. The use of fossil fuels leads to many pollutants, including CO_x, SO_x, NO_x, volatile organic compounds, particulate and greenhouse gases, such as N_2O, CO_2 and CH_4, directly or indirectly related to combustion of fossil fuels to produce electricity or drive transport. In this context, global CO_2 emissions have recovered from 2020 levels, growing by 5.9% in 2021. However, this is still about 1% below the record levels set in 2018 and 2019 [5,6]. In parallel, the Intergovernmental Panel Climate Change (IPCC) reported in August 2021 that global warming will reach or exceed 1.5 °C in the next two decades. Key challenges are reducing the pollutants that affect climate change and using much more renewable energy. Many agreements and treaties have been made during the past two decades to reduce pollution and global warming, including the Paris Agreement, which aims to keep the mean global temperature rise below 2 °C and preferably limit the increase to 1.5 °C. However, emissions must be reduced by approximately 50% until 2030 to keep global warming below 1.5°C, with less reliance on fossil fuels and an increase of clean energy use by 20% [7].

To avoid the worst consequences of climate change, pollutant emissions must be halved by 2030 and brought to zero in 2050. This goal can be achieved by reducing the dependence on fossil fuels and investing more in alternative clean energy sources for power supply. In addition, a balance must be struck between the large demand for energy and the preservation of the environment by finding effective alternatives, increasing their efficiency, and preserving the environment.

To achieve this purpose, international communities have started to generate power from alternative and clean sources, including solar, wind, biomass, hydro and waste heat from industrial process. The past decade has seen a steady increase in alternative energy exploitation, with the proportion of alternative energy increasing from 3% to about 16% of the total global energy consumption [4].

One of the techniques to generate clean power is exploiting heat sources with low or medium temperature that are naturally available or emerge as waste heat during industrial processes. The organic Rankine cycle (ORC) is one of the best technologies to generate electric power from different heat sources at low and medium heat source temperature. In ORC systems, an organic working fluid with a low boiling point is used instead of water, which makes it practical to exploit heat from low and medium temperature sources. This feature has made ORC units available in the market with a capacity ranging from several kilowatts to several megawatts that are adopted in many applications. The ORC can exploit several heat sources, including solar, biomass and industrial waste heat. The widespread use of the ORC for power generation worldwide is due to several technical reasons, including simple structure, ease of maintenance and operation, preferred temperature and pressure conditions, safety and flexibility. In addition, small ORC units were established in the range of one to ten kilowatts, which are efficient in generating electricity in rural areas, small commercial buildings or remote areas [8,9]. Since the adoption of the ORC, many improvements, designs and new architectures have been introduced to increase the system's thermal efficiency, leading to a better utilization of the heat source. Different architectures aim to implement various technologies to improve the performance of ORC systems and to handle many other conditions that are not well accessible with regular ORC. In the last 20 years, different ORC architectures have been studied, e.g. single-stage regenerative ORC, dual-stage regenerative ORC, reheat ORC, ORC with recuperator, dual-loop ORC, cascaded two-ORC or cascaded dual-loop ORC (CORC) [10].

One of the architectures investigated over the past years is the CORC system, which contains two power generation cycles, instead of one, to maximize thermal energy utilization.

This system consists of two cycles, a high-temperature cycle (HT-ORC) and a low-temperature cycle (LT-ORC), containing two working fluids with different critical temperatures. The HT-ORC exploits the main heat source, while the LT-ORC utilizes the residual heat from the HT-ORC or uses a secondary heat source. Usually, the working fluid in the LT-ORC has a critical temperature lower than that of the HT-ORC to exploit the waste heat from the HT-ORC [11].

This thesis presents an experimental and simulation study of the CORC system under different conditions considering various working fluids from various physico-chemical groups to explore system performance. Consequently, the relationship between the thermodynamic properties of working fluids, such as critical temperature, pressure and system efficiency was studied. The criteria adopted to qualify system performance are thermal and exergy efficiencies, since they asses the generated net power output with respect to the heat flow input.

The present work presents the development and investigation of the CORC system to utilize heat sources at different temperature levels. This type of ORC architecture allows using several heat sources and various working fluids with their respective properties in both the HT-ORC and LT-ORC. The heat source of the employed test rig was given by four electrical heaters with an adjustable temperature. Electrical heaters allow for simple control and regulation and are little demanding concerning safety and hazard requirements. Furthermore, they can operate over a wide temperature range. The performance of the CORC system was assessed by adopting different groups of working fluids, covering a wide range of critical temperature and critical pressure. The investigated working fluids belong to three groups, namely alkanes, refrigerants and siloxanes.

Despite the considerable quantity of research published on the ORC, there is a massive lack of work that practically tests CORC system performance. Therefore, this work is based on introducing and studying a CORC with a flexible design that can concurrently use heat sources with different temperature levels. In addition, the main components can be used under many conditions and with varying working fluids.

1.2. Objective and aims

A lot of research has dealt with and explained ORC technology together with its use in various fields driven by different heat sources. However, only a few covered the CORC extensively, while testing and comparing the system's efficiency in practice with various working fluids is almost completely missing. The main goal of this work was to investigate the performance of the CORC as a technique for exploiting low and medium temperature heat sources and

providing clean power by increasing thermal efficiency. The work is based on a CORC unit with an external power of 158 kW, designed and practically set up at the University of Paderborn.

The objectives of this PhD thesis were:

- A literature review of the published works on the ORC, especially the CORC, a study of its characteristics, working fluids and an assessment of its performance.
- Practical investigation using different working fluids, including alkanes, refrigerants, siloxanes, and evaluation the CORC system performance by comparing the results.
- A practical study of system components, such as the heat exchangers, turbine and condenser, by testing the heat transfer between the HT-ORC and LT-ORC, as well as the turbine efficiency and connecting it with system performance.
- Simulation of the CORC system to study its performance by adopting thermal and exergy efficiencies as indicators, as well as employing many working fluids with a low global warming potential (GWP) and zero ozone depletion potential (ODP).
- Test how system performance relates to the thermodynamic properties of working fluids, such as critical temperature and critical pressure.
- Comparison of thermal efficiency between a conventional ORC and a CORC system at different heat source temperatures.
- Parametric analysis of the CORC system under different operational conditions.

1.3. Thesis outline

This work is comprised two essential parts: the first part is an overview, and the second one includes four papers that were published in peer-reviewed scientific journals.

The first chapter presents the background of global energy consumption during the last 20 years. In addition, the increase of fossil fuel consumption and its negative impact on the environment is addressed. It highlights the utilization of clean energy consumption from different sources and its percentage of global clean energy consumption.

The second chapter explains the importance of the ORC as a technology for power generation from low and medium temperature heat sources. Therefore, it was essential to address the history of the ORC and its development over the past two centuries by looking at the ORC market of and the number of currently installed units. This chapter contains an explanation of the ORC system in terms of thermodynamics. A comparison between it and the Clausius-Rankine steam cycle from thermodynamic and economic aspects is presented.

Chapter 3 deals with working fluids, their types and how to select a suitable working fluid for ORC systems. It discusses the criteria used to select appropriate working fluids and the importance of each criterion. The focus of this work was laid on three groups of working fluids: alkanes, refrigerants and siloxanes. In addition, it contains a literature review and a statement on the importance of each working fluid group.

Chapter 4 is a presentation of the CORC system with a detailed explanation. It highlights its importance by presenting the main aspects of this technique. A literature review was made of the works that tested CORC units and the most important findings are outlined. Some publications dealt with the differences between the regular and CORC systems. This work is based on the experimental and simulative investigation of a CORC test rig. This test rig is explained, highlighting its essential components, operational conditions and basic cycles. Further, the reasons behind such designs and applications are discussed.

Chapter 5 contains four papers published in peer-reviewed journals. The first paper deals with designing, installing and setting up the CORC test rig with the system's main components and operational conditions. Two publications deal with an experimental investigation of system performance using alkanes and siloxanes as working fluids. The fourth paper deals with the simulation of the CORC test rig using low-GWP alkanes and refrigerants as working fluids. The research highlights the system's thermal and exergy efficiencies and their relationship with several other parameters, including heat source temperature and internal pressure. In addition, the efficiency of the components was studied by looking at turbine efficiency, heat transfer and pinch point temperature difference (PPTD). The relationship between system efficiency and thermophysical properties of working fluids was also studied.

2. ORC system

Steam turbines, which use water vapor as the working fluid, are often used as heat engines, especially in large power plants. However, the thermodynamic properties of water vapor make it unsuitable as a working fluid, if heat sources with a relatively low temperature are utilized, like heat from geothermal sources. In such cases, the principle of ORC is used as an alternative to the Clausius-Rankine cycle (CRC) that contains conventional steam turbines. The word "organic" means that some organic matter (in the sense of chemistry) is used as a working fluid. Working fluids of ORC systems have a lower boiling temperature so that waste heat flows with temperatures below 350 °C can also be used to generate power. The working fluid can be silicone oils, hydrocarbons, like butane, or refrigerants, like fluorinated hydrocarbons. This feature means that the process can work at lower temperatures and pressures than the conventional water cycle so that it can be used in the large-scale conversion of industrial waste heat into power. ORC working fluids have in common that they have relatively low boiling points compared to water, which allows them to be operated at low temperatures. In contrast to the steam Rankine cycle (SRC), the ORC operates at relatively low temperatures so that excess heat in factories can be utilized. It can also generate power from renewable sources, such as solar or geothermal [12].

The term "ORC" only describes the basic physical principle, but not a specific technical implementation. It does not even state whether a turbine is used to expand the steam or a reciprocating engine. The tendency is to use a turbine for higher output, while reciprocating engines can be cheaper for lower output power.

The system must be optimized for the respective conditions in terms of heat source and heat sink temperatures, performance and the working fluid to achieve an optimal efficiency. Therefore, providing a standard steam turbine with a different working fluid is impossible. However, the basic processes are the same as in conventional steam turbines. For example, evaporators and superheaters are often used to obtain a dry vapor with higher enthalpy. The turbine or engine drives a generator that yields electrical power. The efficiencies achieved in practice are usually well below the Carnot efficiency, which describes the theoretical potential [13].

The rising interest in alternative energy sources has increased attention to ORC technology. ORC consist mainly of the four components of SRC: a pump, an evaporator, a turbine and a condenser.

The ORC is a smaller-sized power source ranging from several kilowatts to several megawatts that can use a heat source temperature ranging from 80 °C to 350 °C. Therefore, ORC can utilize many heat sources from nature, industries or engines, including solar, biomass, geothermal and waste heat. In addition, the ORC is used for heating processes in various applications [12].

2.1. ORC history

ORC history dates to the beginning of the 19th century, when it began as a marginal technique and became widely applied in the 21st century. The history of the ORC started about a hundred years after the invention of the steam engine. In his work published in 1824, S. Carnot proposed the use of an alternative working fluid instead of water in heat engines. T. Howard, in 1826, used ether as a working fluid in an engine [14].

In 1829, A. Ainger proposed a CORC system design, where each cycle uses a different working fluid. In this design, the evaporator acts as a condenser for the next cycle. The residual heat from the HT-ORC is used to drive the LT-ORC. This design was considered the first proposal to define the CORC system and use two working fluids in one system [15]. In 1853, the French engineer V. Du Tremblay introduced a binary heat engine, where water was used as a working fluid in the HT-cycle, while ether was used in the LT-cycle. In this unit, the generated water vapor was used to evaporate the ether to generate power [16]. At the end of the 19th century, F.W. Ofeldt developed engines based on the ORC principles using naphtha as a working fluid. Ofeldt's invention has been adopted in hundreds of engines built in the United States [17].

The beginning of the 20th century saw the suggestion of using different working fluids, such as ether, chloroform, ammonia, carbon disulfide and sulfurdioxide. Already then, solar energy was adopted as a heat source in many units, where a 20 kW ORC unit was built in Missouri in 1904. F. Shumann built in 1907 a small-scale ORC, where the output power was about 2.6 kW by utilizing ether as a working fluid [18].

T. Romagnoli in Italy developed ORC systems in 1923. In these units, water vapor was used to heat ethyl chloride and the output power generated by motors was about 1.5 kW [19].

L. D' Amelio established the first modern application of the ORC principles in 1935. This system was driven by solar energy and adopted ethyl chloride as a working fluid. The evaporation and condensation temperatures were 55 °C and 23 °C, respectively, where the thermal efficiency was low and estimated at 3.6%. Nevertheless, D' Amelio's technology has

been adopted in many small units with a capacity of 2.6 kW to generate power from geothermal heat sources [18].

The technology of the ORC has witnessed many developments, as the first commercial units that depended on geothermal heat sources were adopted in Congo, where refrigerants were utilized as working fluids in the middle of the 20th century. These units were used to generate power for small villages and mining companies, where they depended on heat source temperatures ranging from 85 °C to 90 °C, and the produced power output was between 200 kW and 670 kW [16,20].

In the mid-1960s, ORC units with capacities of up to 10 kW were invented by Tabor and Bronicki using monochlorobenzene as a working fluid. These units depended on solar heat sources and had little need for maintenance and a high efficiency characterized these units at the time. The same researchers conducted a study and established criteria for selecting a working fluid based on molecular mass and boiling point. In 1967, A 500 kW ORC was built in Kamchatka, Soviet Union using a geothermal heat source and R12 as a working fluid. In the sixties and seventies of the last century, many ORC units were designed by the Ormat (1964) and Turboden (1970) companies, which are still active in the design and production of ORC systems around the world. In the 1970s, the evolution of ORC technology continued and saw the construction of units with greater power and new working fluids, such as R133 and perchloroethylene [18].

In 1979, a ORC unit was established, exploiting the waste heat from iron and steel industry in Kawasaki, Japan, with a capacity of 2.9 MW, using R11 as a working fluid. In the same year, a CORC unit was established with a capacity of 12.5 MW, where isopentane and butane were used as working fluids in the HT-ORC and LT-ORC, respectively [21].

Later, ORC technology witnessed many developments and additional components, and new architectures were introduced to enhance the efficiency of these units. A CORC power plant appeared in 1979 in California. It utilized isobutane in the HT-cycle, while propane was used in the LT-cycle. It was driven by geothermal heat and produced an output power of 12.5 MW [20].

By 1981, the number of installed ORC units increased significantly, and the number of working fluids used reached about 16 in commercial units. Moreover, more than 20 companies were established that manufactured the components of ORC [18].

The past two decades witnessed a significant and remarkable development of ORC technology through increased research and dozens of commercially installed units. In parallel, the number of experimental test rigs expanded, and tens of working fluids were tested. The evolution of ORC technology has experienced growth, as many new working fluids have been introduced and different heat sources have been adopted. Today, there are about 2,000 ORC units worldwide, with a total installed capacity of around 5 GW [22].

2.2. Thermodynamics of the ORC

The ORC has four main components: pump, evaporator, turbine and condenser as shown in Fig. 3. First, the working fluid in its liquid state is pumped from low to high pressure (process 1 to 2). Next, the high-pressure working fluid in the liquid state enters the evaporator, which is heated by an external heat source and turns into vapor or superheated gas state when required (process 2 to 3). The working fluid steam expands through the turbine, generating mechanical power, usually converted into electricity by the generator. During expansion, the temperature and pressure of the working fluid decrease (process 3 to 4). The expanded working fluid enters the condenser, where the phase change process occurs at almost constant pressure, and the vapor turns into a liquid (processes 4 to 1). Finally, the working fluid is returned to the pump and pressurized to repeat the process, of Fig. 3.

The thermodynamic efficiency of the ORC is a function of the evaporation and condensation temperatures, component efficiency and working fluid properties. The most important criteria for evaluating ORC system performance are thermal efficiency and exergy efficiency, where both represent the ratio of the turbine power output in relation to the heat input to the system. Exergy efficiency is defined as the maximum amount of power which can be produced from a flow of matter, if it would come to equilibrium with a reference environment. Both refer to the amount of net power generated by the system and its relationship to the input heat [8,9].

The thermal efficiency of the ORC is given by the ratio of net power to heat flow input

$$\eta_{th} = \frac{\dot{W}_{net}}{\dot{Q}_{in}} \tag{1}$$

where $\dot{W}_{net}$ is the signed sum of turbine output power and pump power.

The exergy efficiency of the ORC is given by the ratio of net power to exergy flow input $\dot{E}_{in}$

$$\eta_{ex} = \frac{\dot{W}_{net}}{\dot{E}_{in}} \tag{2}$$

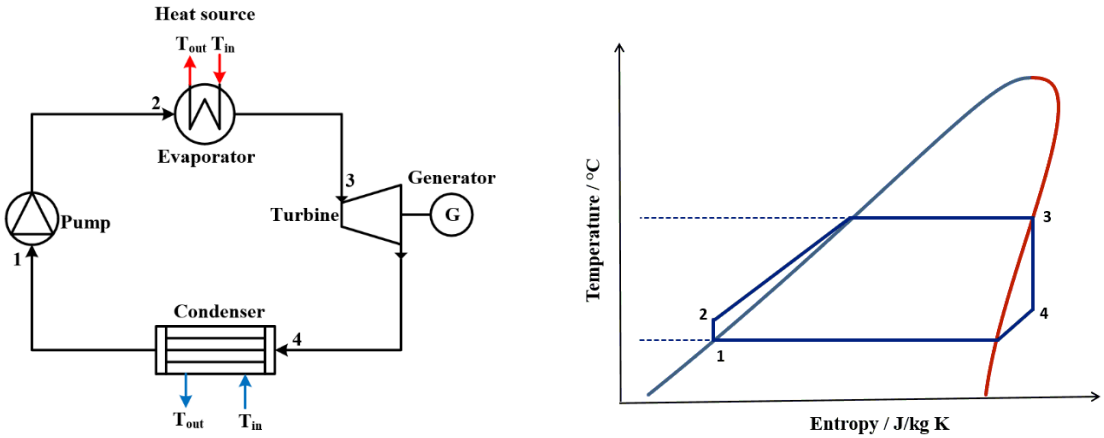

Fig. 3. Layout (left) and temperature-entropy diagram (right) of the basic ORC system.

The net power output should be as large as possible for a given heat flow input to increase thermal efficiency. This can be achieved by reaching the system's highest possible evaporation temperature and the lowest possible condensation temperature. In addition to the temperature levels of the heat source and heat sink, the evaporation temperature is related to the vapor pressure, which is supplied by the pump, while the condensation temperature is related to the condensation pressure. Therefore, the significant difference between the evaporation and condensation pressure leads to greater net power output and, thus, to an increase of thermal efficiency. Moreover, the efficiency of essential equipment, such as turbine, pump, evaporator and condenser, plays a crucial role in increasing system performance. In parallel, the working fluid itself significantly influences system performance [23,25]. The selection of the working fluid is subject to several criteria, including thermodynamic properties, environmental friendliness, availability in the market, cost and other qualities that are discussed below in detail.

2.3. Comparison between ORC and SRC

In this section, a comparison is made between the ORC and the SRC concerning working fluids, operating conditions, components, system complexity, cost, performance and the impact on the environment. The most important feature of the ORC is its ability to exploit low and medium temperature heat sources so that it is a superior technology to take advantage of solar, biomass, geothermal and industrial waste heat. These properties make the ORC suitable for generating power without adverse environmental effects due to the combustion of fossil fuel. Although SRC and ORC utilize the same thermodynamic principles, they have many differences with respect to the heat source, operating temperature and system construction. The advantages of the ORC can be explained by utilizing working fluids with a critical temperature lower than

that of water (373.95 °C), which makes them suitable to employ low or medium temperature heat sources and waste heat recovery [12]. Astolfi et al. [24] reported that ORC systems allow for a better match between the working fluid temperature and the heat source temperature, which reduces the exergy loss and increases the evaporator's exergy efficiency during heat transfer. In addition, ORC systems can work at lower evaporation temperature/pressure and a reasonable mass flow rate when utilizing low or medium temperature heat sources. These advantages allow for the design of ORC systems with less construction effort and less component layout complexity than SRC systems. Therefore, ORC systems are suitable for waste heat recovery from different industrial processes, like cement production, ceramic and steel industry. Moreover, ORC technology also allows for the implementation of small-scale systems with an output of around 2 kW and more compact sizes, which means that they are usable in the transport sector for waste heat recovery from internal combustion engines. Further benefits of the ORC system consist of favorable operating conditions, little maintenance and autonomous operation [25,26].

Economically, ORC systems are less expensive than SRC systems, available in capacities ranging from several kilowatts to several megawatts. Temperature and pressure in ORC are lower than those in SRC so that the total cost, safety and maintenance requirements are lower. ORC systems can exploit dry working fluids that do not require superheating before entering the expander, unlike water in SRC systems. The condenser pressure in ORC is often higher than the atmospheric pressure due to the low critical temperature of the working fluid. In contrast, in the SRC, the condensing pressure is lower than the atmospheric pressure, which may increase the possibility of leakage that affects system performance. The pressure rate in ORC is low. Therefore, the enthalpy difference across the turbine is comparably small, which makes it convenient to use a single turbine. In SRC, due to the high pressure rate, the use of a turbine with several stages is common. In addition, the small enthalpy difference across the turbine of ORC leads to the direct use of the generator without needing a core box. Most of the working fluids in the ORC are used directly without primary treatment, while typical SRC need primary water treatment. In summary, the ORC is characterized by its effectiveness, ease of installation, excellence in generating electricity with small units in remote areas, ease of maintenance and reasonable cost. In contrast, the SRC is characterized by a higher thermal efficiency, which is often above 30%, while the ORC maximum thermal efficiency is about 25%. Compared to the working fluids of the ORC, the benefits of water are availability, low cost and low viscosity, entailing a minimal pressure drop in heat exchangers and piping. The differences between the

ORC and SRC can be summarized in that the ORC is preferred when the heat source temperature is low or medium [25,27,28].

2.4. ORC market

Since the emergence of the ORC as a clean technology for generating power from varying heat sources, interest in it has increased and its market has developed significantly. Currently, there are about 2,700 ORC projects around the world, with a total capacity of about 5 GW. The capacity of individual units varies from several kilowatts to several megawatts. Since 2016, the ORC market has witnessed a tremendous development, with increases of 40% in the terms of capacity (about 1.2 GW) and 46% in terms of installed units (about 900). The significant increase of the total installed ORC unit capacity during the past four years is because most units use geothermal sources, which have a typical capacity of 10 MW, while the capacity of units that depend on biomass and waste heat recovery does not exceed one or two megawatts. By reviewing the currently installed ORC units, it can be found that geothermal heat is the dominant heat source for ORC units with 77.4%, while the percentage of waste heat recovery and biomass are 11.6% and 10.1%, respectively [22,29,30].

Furthermore, by reviewing the geographical distribution of ORC technology, it can be seen that most units are spread in the Middle East and North America, and use geothermal heat sources, as in the USA and Turkey. On the other hand, most units in Europe use biomass and waste heat recovery as heat sources, as in Germany and Italy. Many companies manufacture and install ORC units, but the market is dominated by three companies, which share about 78% of the market, namely Ormat, Turboden and Exergy. ORC markets were affected by the COVID-19 pandemic, as component manufacturing and installation operations were slowed, but they recovered after restrictions were lifted in most countries and industrial activity rebounded. Technical and economic studies anticipate a further development of the ORC market, especially in Asia and Europe, which play a major role in manufacturing components of ORC. According to a report issued by Grandview research, the global ORC market size was 415.1 million US$ in 2021 and is expect expand by an annual rate of about 3.3% in the next ten years. Some suppliers of ORC technology expect an increase of more than 3.3% due to the increasing trend to use renewable energy. Moreover, the longer life cycle and relatively low cost of operation and maintenance of ORC are some of the significant drivers globally. On the other hand, ORC technology faces stiff competition from the availability of classic fossil fuel technology such as SRC. This increase is the result of the interest of many countries in finding clean energy sources

and exploiting waste heat in major industrialized countries, such as USA, China, Germany and Canada [31].

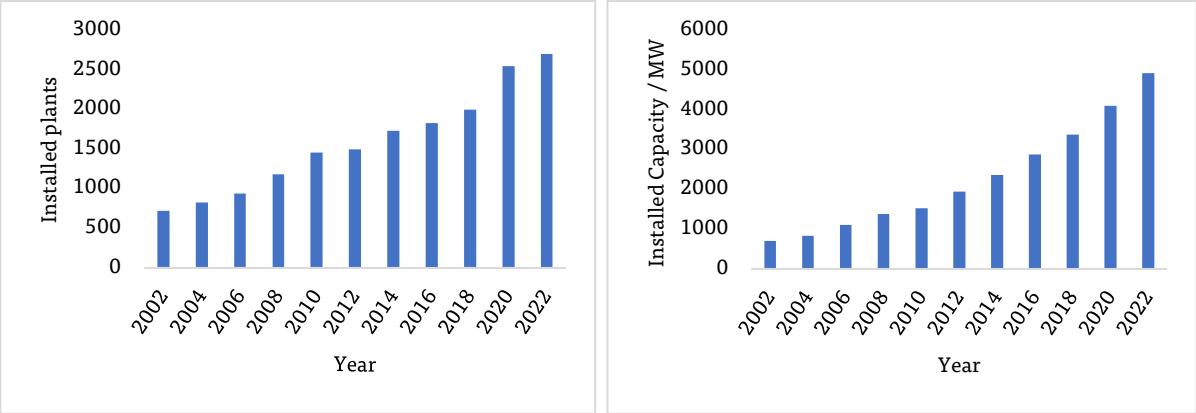

Fig. 4. Historical trend of the installed plants (left) and installed capacity (right) [29-31].

3. Working fluid

ORC mainly exploit low and medium temperature heat sources, so water is not a suitable working fluid for this technology. For this reason, working fluids with a low or medium boiling point are adopted. The selection of the working fluid depends on the type of ORC system, heat source, system components, expansion device, safety and environmental considerations. The thermodynamic properties influence the system's thermal efficiency, since the working fluid's critical temperature is strongly related to the heat source temperature. During the development of ORC technology, many working fluids belonging to different physico-chemical groups were used, both in test rigs and units used worldwide for power generation. Generally, the working fluids used in ORC belong to different groups, such as alcohols, ethers, inorganic fluids, hydrocarbons, refrigerants, chlorofluorocarbons, mixtures and other [32,33].

3.1. Working fluid categories

Working fluids can be divided into three categories according to the saturated vapor line in the temperature-entropy diagram. A negative slope ($ds/dT < 0$) refers to wet working fluids, which means that entropy increases with falling saturation temperature. A positive slope ($ds/dT > 0$) refers to dry working fluids, which means that entropy decreases with falling saturation temperature. The third category are isentropic fluids, where the slope almost vertical ($ds/dT = 0$), which means constant entropy. The terms wet, dry and isentropic also refer to the vapor quality after the expansion. The vapor quality is an essential factor in selecting the expander device. The disadvantage of wet liquids is that they need to be superheated. Moreover, using wet fluids may reduce the turbine efficiency and require a heat exchanger with a larger heat exchange area to provide the required superheating degree. Dry and isentropic working fluids are preferred in ORC as they do not require superheating and thus better protect the turbine from corrosion and increase its efficiency [34,35].

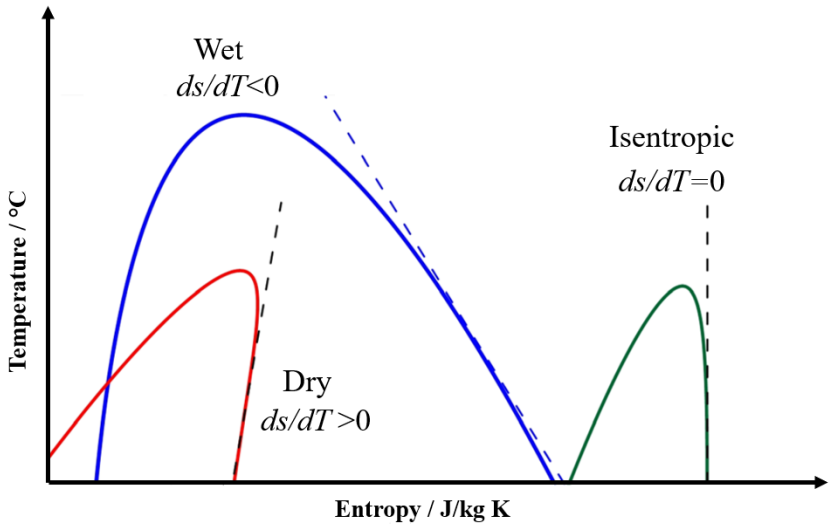

Fig. 5. Types of working fluid [34,35].

3.2. Working fluid selection criteria

Water is an ideal working fluid in classic high-temperature SRC units. However, this feature cannot be applied to units with low and medium heat source temperatures due to the thermodynamic properties of water. This renders water most suitable, if the heat source temperature is between 700 K and 800 K. Therefore, if the heat source temperature is lower than that, a substance other than water should be used. The temperature of natural heat sources, such as solar and geothermal, is classified within the low and medium temperature range that needs working fluids other than water. The selection of the working fluid is one of the crucial factors for the design of ORC systems. Working fluids affect not only the efficiency of the system, but also the temperature and pressure levels inside the system, which directly affect the selection of the remaining components. Other factors that influence the selection of the working fluid include expander type, size of the heat exchangers, condensation and evaporation pressure as well as availability in the market. In addition to the above, the selection of the working fluid is subject to the following criteria:

- Thermodynamic and physical properties

The critical properties of the working fluid must be compatible with the operating conditions, including the maximum temperature and pressure, where the working fluid should have a critical temperature above the heat source temperature. The critical temperature is very important for selecting the working fluid, as it plays a vital role for the system's thermal efficiency. It is also essential for the design of the components for heat transfer, such as the evaporator and condenser. In addition, the selected working fluid must have an appropriate

boiling point to create vapor at the applied temperature. Another critical factor is the freezing point of the working fluid, which must be below the lowest temperature during system operation [9,36].

- Density, enthalpy of evaporation

Density is one of the crucial characteristics that must be considered when choosing a working fluid. A high density is preferable to provide a large mass flow rate during operation, which is positively reflected in the increase turbine power output. When the other parameters are defined during the operation, the working fluid should have a large enthalpy of evaporation, which will reflect positively on increasing the system performance by rising the turbine power output. This enthalpy difference plays a vital role in reducing moisture during the expansion process, affecting the turbine's working life and reducing maintenance. Moreover, a large enthalpy difference may increase recovery efficiency and improve thermal efficiency. In brief, the working fluid with a high density and large enthalpy difference may increase system performance [37,38,42].

- Molecular weight

High molecular weight fluids are preferred because they result in a greater mass flow rate and increase turbine efficiency with lower rotational speeds and reduced number of expansion stages [39].

- Thermal conductivity and viscosity

The thermal conductivity of the working fluid should be high to obtain a large heat transfer coefficient during the heat exchange processes in the evaporator and condenser, which increases thermal and exergy efficiencies. The viscosity of the working fluid should be low to reduce drag and thus dissipation, which directly affects the turbine power output and thermal efficiency [40,41].

- Chemical stability and compatibility

It is imperative that the working fluid is suitable for the components of the system and does not interact chemically with them, as it is economically reflected in reducing maintenance costs and increasing the performance of the devices that constitute the system. In addition, the working fluid should be chemically stable to avoid decomposition at high temperature and pressure, which may result in ignition, explosion or corrosion of materials [42,43].

- Environmental aspects

Environmental considerations have become one of the essential factors for selecting the working fluid, especially after the emergence of environmental problems due to some refrigerants. The ORC is one of the technologies used to produce clean power, so a working fluid with a low GWP and ODP must be selected. Because refrigerants have effectively entered as a working fluid in ORC systems, environmental aspects must be considered when selecting refrigerants, since some of them have to be excluded due to their adverse effects on ozone layer depletion [9,42].

- Safety and toxicity

The working fluid should be non-toxic and non-flammable due to safety considerations. The use of flammable working fluids requires the consideration of more safety factors, which rises the operational cost of the ORC system, since they may be dangerous for workers, especially at high temperature and pressure [9,42].

- Availability and cost

Working fluids must be reasonably priced in the market to reduce the ORC units' operating costs [9].

In order to achieve a high thermal efficiency and a better use of the heat source, the working fluid must be selected carefully. Several studies concluded that there is no optimal working fluid for all operating conditions and all ORC types. This is due to the presence of differences related to heat source temperature, different types of ORC architecture, operating conditions and the presence of several criteria for evaluating system performance [10].

Matching of the working fluid's critical properties with the heat source is essential for several reasons, such as adequate heat transfer between the heat source and the working fluid, optimal use of the heat source and reduced irreversibility. A large temperature difference between the heat source and the turbine inlet temperature leads to an increase in the exergy loss and a decrease of the system's thermal efficiency [44].

A growing body of literature deals with the relationship between system performance and the thermophysical properties of working fluids, including Jacob number [45], boiling point [46], critical temperature [47] and molar mass [48].

Aljundi [49] as well as Mann and Barse [50] reported an important relationship between the critical temperature of the working fluid and system performance. Song et al. [51] also pointed out that a high critical temperature of the working fluid might enhance the system's thermal efficiency.

Some studies linked the selection of the working fluid and the difference between the heat source temperature and the critical temperature of the working fluid. For example, Zhai et al. [52] found that ORC systems achieved a better thermal efficiency when the difference between the heat source temperature and the critical temperature of the working fluid is between 35 °C and 50 °C, while Vivian et al. [53] reported that the suitable temperature difference is 35 °C. Braimakis et al. [11] also showed that a small difference between the critical temperature of the working fluid and the heat source temperature is favorable.

Chen et al. [54] studied 35 working fluids and confirmed that dry and isentropic working fluids are more suitable for ORC systems than wet working fluids. Their study was based on several factors, including thermophysical properties, thermal stability, safety, availability in the market and environmental aspects.

Branchini et al. [55] emphasized that selecting the optimal working fluid for the ORC must be based on several considerations, including thermal efficiency, expansion ratio, mass flow rate, recovery efficiency and heat transfer area.

3.3. Working fluids considered in this work

3.3.1 Alkanes

In organic chemistry, alkanes (formerly often addressed as paraffins) are a group of simple, saturated hydrocarbons without multiple bonds between the atoms. Like all hydrocarbons, they consist of the two elements carbon (C) and hydrogen (H) only and belong to the saturated compounds. The basic structure of the alkanes can consist of unbranched and branched chains or rings. The first two types, n-alkanes and iso- or neo-alkanes, form a homologous series with the general molecular formula C_nH_{2n+2}. The ring-shaped molecules are called cycloalkanes and differ from the chain-like alkanes in terms of their thermo-physical and chemical properties [56-58].

Alkanes represent a remarkably uniform group of substances that build the framework for many other groups of organic substances. Due to the different molecular topologies, however, cycloalkanes have properties that sometimes differ significantly from those of linear alkanes.

Alkanes, both linear and cyclic types, comprise a wide range of working fluids with different thermodynamic properties that suit different types of ORC systems. In general, alkanes have an appropriate critical temperature and critical pressure, good thermal stability, material compatibility, low toxicity and are environmentally friendly (low GWP and zero ODP). Moreover, it was shown that alkanes exhibit properties that are desired for the ORC, i.e. good performance in the components and high efficiency [59].

Many studies have focused on the effectiveness of alkanes as working fluids in ORC systems. For example, Zhai et al. [60] presented that the thermal efficiency is affected by the molecular structure of the working fluid. They found that working fluids with a cyclic structure and double bonds achieved higher efficiencies than linear alkanes.

Siddiqi et al. [61] and Lai et al. [62] reported that alkane-based working fluids are suitable for high-temperature ORC to achieve a good system performance. Quoilin et al. [63] studied a small-scale ORC system using refrigerants and alkanes as working fluids. They concluded that working fluid selection must be based on thermodynamics and economics, which reflects on the selection of system components.

Shu et al. [64] investigated different alkane-based working fluids for exhaust heat recovery in diesel engines. The authors reported that cyclic alkanes show a good performance in terms of net power output, thermal efficiency and exergy loss. They indicated that alkane-based ORC systems might be more practical than regular steam cycles for waste gas heat recovery. Li et al. [65] showed that cyclic alkanes are suitable working fluids for high-temperature ORC due to their ability to achieve a high turbine inlet temperature before the expansion process.

Braimakis et al. [11] evaluated the exergetic efficiency of CORC systems by adopting four alkanes and refrigerants as working fluids. The authors found that alkanes are promising for HT-ORC and LT-ORC for a heat source temperature between 100 °C and 300 °C.

3.3.2. Siloxanes

Siloxanes are organic compounds with the general formula $R_3Si{-}[O{-}SiR_2]_n{-}O{-}SiR_3$, where R can be hydrogen or alkyl. There are no Si−Si bonds in this group of substances; the silicon atoms are linked to their neighbouring silicon atom by one intermediary oxygen atom. Siloxanes are widely applied in electrical and textile industries and in household detergents manufacture. Global production of siloxanes reaches several million tons per year. The word siloxane is derived from silicon, oxygen and alkane. In some cases, siloxanes are composed of different types of groups; they are labelled according to the number of Si-O bonds. M-units:

$(CH_3)_3SiO_{0.5}$, D-units: $(CH_3)_2SiO$, T-units: $(CH_3)SiO_{1.5}$. Generally, siloxanes are divided into linear and cyclic molecules according to their Si-O bonds. Linear siloxanes consist of two M-units such as hexamethyldisiloxane (MM), octamethyltrisiloxane (MDM), decamethyltetrasiloxane (MD_2M) and dodecamethylpentasiloxane (MD_3M). Cyclic siloxanes consist only of D-units, such as hexamethylcyclotrisiloxane (D_4), decamethylcyclopentasiloxane (D_5) and dodecamethylcyclohexasiloxane (D_6). The critical temperature of siloxanes rises with the number of units per molecule, starting with D_2 for cyclic siloxanes and MM for linear siloxanes. Siloxanes are characterized by good thermodynamic properties, limited flammability, low/non-toxicity, good thermal stability, suitable lubricating properties, low GWP and zero ODP [56,66-69].

Many studies indicated that siloxanes, such as MM and MDM, are desirable working fluids for high-temperature ORC due to their high critical temperature, low flammability, thermal stability, reasonable cost and environmental friendliness. Fernandez et al. [69] studied several linear and cyclic siloxanes as working fluids of ORC systems under different conditions, including saturated, superheated, subcritical and supercritical. They found that MM and D_4 are the best option for supercritical cycles. On the other hand, MDM yielded a high thermal efficiency for a heat source temperature above 200 °C.

In their experimental work, Dai et al. [70] reported that MM is a suitable working fluid for ORC systems due to its thermal stability. Loni et al. [71] reviewed ORC systems driven by solar thermal energy as a heat source. They reported that MM is the best option for high-temperature ORC, while butane is suitable for low-temperature ORC. Sorgulu et al. [72] reported favorable energy and exergy analyses of an ORC system that was integrated with drying and combustion subsystems using MM as a working fluid.

3.3.3. Refrigerants

Since their invention and initial use, the task of refrigerants has been to transfer heat due to their distinct properties. The use of refrigerants dates back to the 19th century, when the refrigerant ethyl ether was used, followed by many uses of natural refrigerants, such as ammonia, carbon dioxide or hydrocarbons. However, a remarkable transformation in the world of refrigerants took place after the invention of dichlorodifluoromethane (R12) in 1928 by T. Midgley, which led to a significant development in the field of refrigerants [73,74].

The use of refrigerants as working fluids in ORC units began early in many experimental and commercial units. The use of refrigerants as working fluids spread in the 1960s, such as in the

one in 1967 in Kamchatka, Soviet Union, where R12 was used. That ORC system was operating with a heat source temperature of 80 °C, adopting geothermal heat as a source, where the power output was about 680 kW. The distinctive properties of refrigerants, including their low critical temperature, make them suitable for heat recovery from low-temperature sources such as geothermal and industrial waste heat [18].

Refrigerants have been used as working fluids in different ORC systems due to their thermodynamic characteristics, safety and chemical stability. However, the diversity of refrigerants and the expansion of their use as working fluids in many applications showed that some of them cause environmental problems, including ozone layer depletion and global warming [75]. As a result, many conventions and treaties have been established to address the environmental problems resulting from the use of refrigerants, including the Montreal Protocol (1987) [76], the Copenhagen amendment (1992) [77], the Kyoto Protocol (1997) [78] and the EU F-gas regulation [79]. These agreements aimed to phase out and limit refrigerants that cause ozone layer depletion.

In general, refrigerants can be classified according to their chemical composition:

- Chlorofluorocarbons (CFC)

These refrigerants contain chlorine, fluorine and carbon atoms, such as R11, R12, R13, R113 and R114. They are considered to be among the safest refrigerants and they are odourless, non-toxic and chemically stable. There were widely used until the 1990s in various applications due to their distinct properties. However, according to the Montreal Protocol, CFC refrigerants were phased out due to their very high GWP and ODP [80].

- Hydrochlorofluorocarbons (HCFC)

These second-generation refrigerants and were offered as an alternative because they are more environmentally friendly than CFC refrigerants, having a lower GWP and ODP. They are composed of hydrogen, carbon, chlorine and fluorine atoms, such as R123 and R22. However, according to the Montreal Protocol, the production of HCFC refrigerants has been limited, and their production will be stopped by 2030 [81].

- Hydrofluorocarbons (HFC)

This third generation of refrigerants is characterized by having less impact on the environment than CFC and HCFC refrigerants so that they are considered as an excellent alternative to them, as they are chlorine-free. These refrigerants are composed of hydrogen, carbon and fluorine

atoms, such as R32, R152a, R134a and R227ea. In addition, they are characterized by their specific thermophysical properties that make them suitable for many applications [9,82].

- Hydrofluoroolefins (HFO)

These refrigerants are composed of hydrogen, carbon and fluorine atoms, such as R1234yf, R1336mzz(Z) and R1233zd. They are environmentally friendly, characterized by a low GWP and zero ODP, while they are an excellent alternative to CFC, HCFC and HFC refrigerants. HFO refrigerants have boiling and freezing points that are suitable for many applications and are considered as non-toxic and inert, i.e. chemically stable [9,83].

- Hydrocarbons (HC)

Hydrocarbon refrigerants contain carbon and hydrogen atoms only, such as propane, butane and isobutane. Because they have a negligible GWP and zero ODP, they are considered as an alternative for the excluded refrigerants, but their flammability has made them less desirable in some applications. Nevertheless, they have thermodynamic properties that are appropriate for many refrigeration applications and as working fluids in ORC systems [9,84].

- Mixtures

Mixture refrigerants are produced by mixing two or more pure compounds to obtain refrigerants with distinctive properties that reduce undesirable characteristics. Refrigerant mixtures can be categorized into:

Azeotropic mixtures, such as R433A, R436A and R444A. These mixtures have the advantage of behaving like a pure compound, evaporating and condensing at a constant temperature and pressure.

Zeotropic mixtures, such as R510 and R511. These mixtures are composed of different compounds with different boiling points. At constant pressure, evaporation and condensation are associated with a temperature variation, i.e. the phase change occurs with a temperature glide [9,85,86].

4. CORC system

The ORC is accepted as a useful technology for converting the heat flow from sources at different temperature levels into power. In addition, it is designed for simple operation with less maintenance as a source of clean power. Due to these properties that are in very high demand today, the number of ORC plants worldwide is increasing to utilize heat from various sources. As a result, regular ORCs are being introduced in the industry in many fields. The next logical step was to develop new ORC architectures for an optimized utilization of heat sources to increase system performance and lifting the potential of new working fluids. The past decades have witnessed great interest in developing the ORC systems in various respects, but the focus on testing new architectures needs to be sharpened. However, new architectures typically contain more components and more complex than regular ORC systems. In addition, few practical data are available on tests of new architectures under different conditions [87].

One of the architectures that researchers have focused on is the multi-loop or multi-cycle ORC system. Many studies showed theoretically that multi-loop ORC may achieve a better system performance in terms of net power output and thermal efficiency than conventional ORC systems. Moreover, they can concurrently recover heat from different sources. Multi-cycle or loop ORC consist of several ORC cycles, where each one operates under different conditions (temperature, pressure and mass flow rate). Generally, cascaded two-ORC consist of a high-temperature ORC (HT-ORC) and a low-temperature ORC (LT-ORC). The HT-ORC (topping ORC) utilizes the primary heat source, while the LT-ORC (bottoming ORC) utilizes residual heat from the HT-ORC or is driven by a secondary heat source. Each cycle consists of the main components, i.e. turbine, condenser, evaporator and pump. The two-ORC system may improve thermal efficiency due to a better temperature match between the heat source and the working fluid of the HT-ORC. The disadvantage of multi-cycle systems is their larger complexity in terms of devices, sensors and operational parameters that must be coordinated. Such systems are also characterized by higher cost because they consist of more components than regular ORC [11].

CORC systems can maximize heat source exploitation mainly when one heat source is used, where the residual heat from the HT-ORC is used to drive the LT-ORC, leading to a higher thermal efficiency. Several studies have investigated the advantages of CORC systems to enhance system performance. As a result, it was shown that multi-loop ORC could theoretically reach a better thermal efficiency and more turbine power than regular ORC. Therefore, several

researchers have published reports highlighting the importance and advantages of CORC systems by comparing their system performance with regular ORC systems [9].

One of the early studies of the CORC system was conducted by Bryszewska-Mazurek, whose system consisted of several heat exchangers and expansion stages. The results proved that the highest efficiency was obtained using the multi-ORC system, outmatching regular ORC [88].

Yun et al. [89] compared regular ORC and CORC systems for waste heat recovery of exhaust gas discharged from marine engines. They presented that a two-ORC system achieved a higher net power output and better thermal efficiency than regular ORC. The authors reported that a two-ORC system is a suitable technology to recover waste heat from marine engines, where about 115% more net power output can be obtained than with regular ORC.

Ayachi et al. [90] investigated the performance of regular ORC and two-ORC systems for waste heat recovery, adopting refrigerants as working fluids at a heat source temperature of 150 °C and 165 °C. They found that the inclusion of an additional cycle (LT-ORC) into the system to use the residual heat from the HT-ORC led to an increase of the exergy efficiency by about 33% compared to regular ORC.

Chen et al. [91] proposed that the CORC system can generate about 8% more net power output than regular two-ORC systems. In addition, the authors presented that the heat exchanger volume of the CORC system was 18% smaller than for conventional ORC.

Rashwan et al. [92] conducted a parametric comparative study between the CORC system and conventional ORC. Their results showed that the thermal and exergy efficiencies were enhanced by 8% and 21%, respectively. In addition, they found that the exergy loss was reduced by 27%. Therefore, the authors suggested utilizing CORC systems for heat source temperatures above 200 °C.

White et al. [93] compared regular ORC and CORC systems for waste heat recovery applied at 200-300 °C. Their results indicated that CORC system could produce 10.5% more output power than regular ORC. In previous publications [94,95], the same authors found that the CORC system could produce about 4-6% more power output than the regular ORC at temperatures above 250°C. In addition, the authors presented that the CORC also allows for the expansion process to be divided into two parts due to the two constituting cycles, which means that the total volume expansion ratio was reduced. This feature increases turbine efficiency, reduces exergy loss and entails lower maintenance costs because the turbine does not have to operate at its maximum capacity, as in the case of regular ORC.

Kane et al. [96] considered a mini-scale CORC system using R123 and R134a as working fluids in the HT-ORC and LT-ORC, respectively. They reported a good stability of the CORC system over a wide range of the operational conditions.

The advantage of CORC systems in terms of exergy efficiency was studied by Braimaiks et al. [11]. The authors used low GWP refrigerants and hydrocarbons as working fluids for waste heat recovery. Their study included performance comparisons between CORC systems and regular ORC by utilizing a heat source temperature between 100 °C and 300 °C. They found that the exergy efficiency of the CORC system is about 25% greater when compared to conventional ORC. They noted that a CORC system is preferred when the difference between the heat source temperature and the critical temperature of the working fluid is small.

The literature review above emphasizes the importance and advantages of CORC systems in increasing system performance regarding turbine power, thermal and exergy efficiencies. The advantages offered by CORC systems make them more suitable for the exploitation of heat from different sources and from several sources at the same time. In addition, they can operate with different working fluids having different thermodynamic properties. One of the advantages of the CORC is that it can exploit high-temperature heat sources.

4.1. CORC test rig

The schematic diagram of the CORC test rig that was employed in this work is shown in Fig. 6. The HT-ORC utilizes the heat flow from the heating cycle (HC), while the LT-ORC exploits the residual heat flow from the HT-ORC. The heating cycle and the HT-ORC have a shared heat exchanger (HE1) to evaporate the working fluid, while the HT-ORC and the LT-ORC also have a shared heat exchanger (HE2). The HE2 represents the condenser of the HT-ORC and the evaporator of the LT-ORC. This combined heat exchanger reduces the heat dissipated to the environment and reuses it again in the LT-ORC, which leads to an increase of the thermal efficiency by a more optimal utilization of the heat source. The CORC unit design and its features allow for a use of heat from two different sources, where the primary heat source is used by the HT-ORC, while the secondary heat source is used by the LT-ORC.

The scope of this work was to optimize the system performance of the CORC system in terms of thermal and exergy efficiencies by studying different parameters. Due to the structure of the test rig, no recuperator was required. The CORC system set-up was designed to cope with different working fluids and a wide range of heat source temperatures. The test rig comprised heating, cooling and power generation cycles, consisting of the HT-ORC and LT-ORC.

The system had fast-acting valves and controllers. Safety considerations to avoid reaching critical situations were embedded technically and protected users and system components from damage.

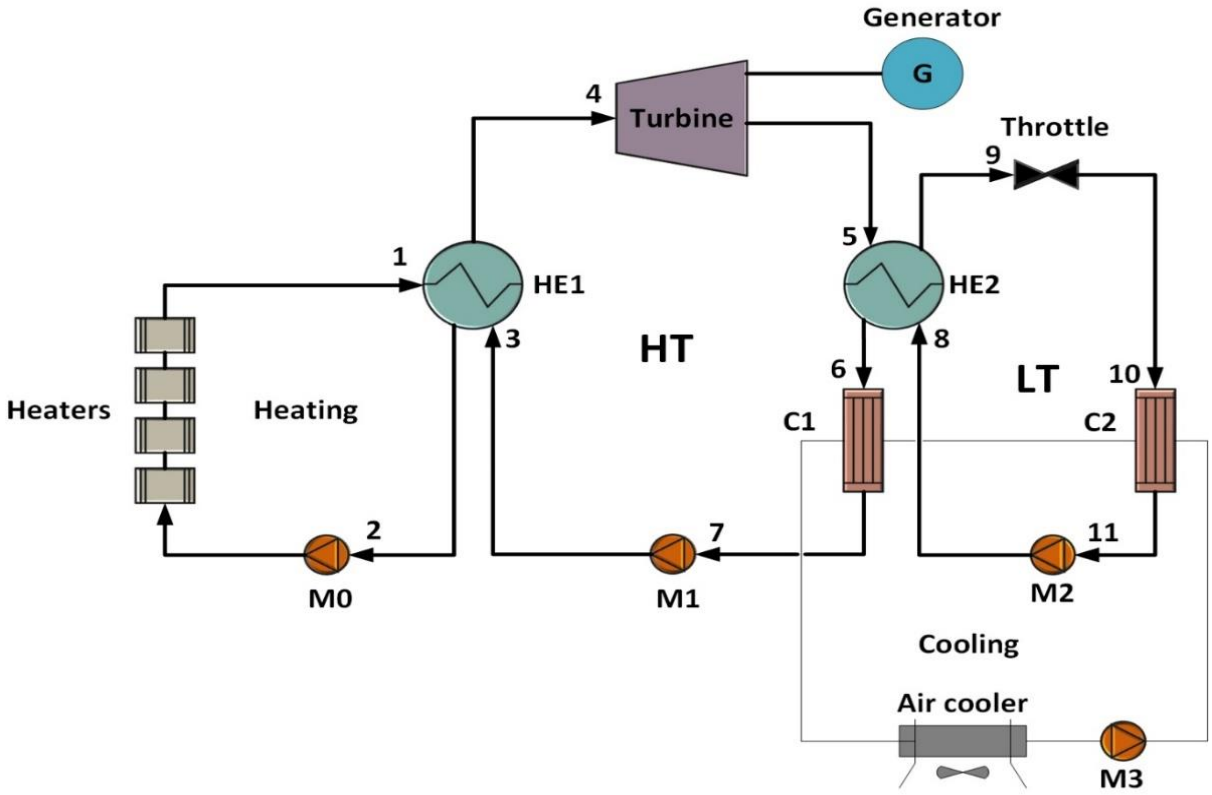

Fig. 6 Layout of the present CORC test rig.

Moreover, the CORC system was designed such that a wide range of operating conditions in terms of mass flow rate, working fluid, heat source temperature and pressure became accessible. In addition, temperature and pressure sensors were placed at the inlet and outlet of each component connected to software for control, giving effectively access the results. Improving CORC system performance is not straightforward, and different parameters should be optimized in concert to enhance system performance. These parameters include PPTD, condensation temperature and pressure, evaporation temperature and pressure as well as the temperature difference between the heat source and turbine inlet.

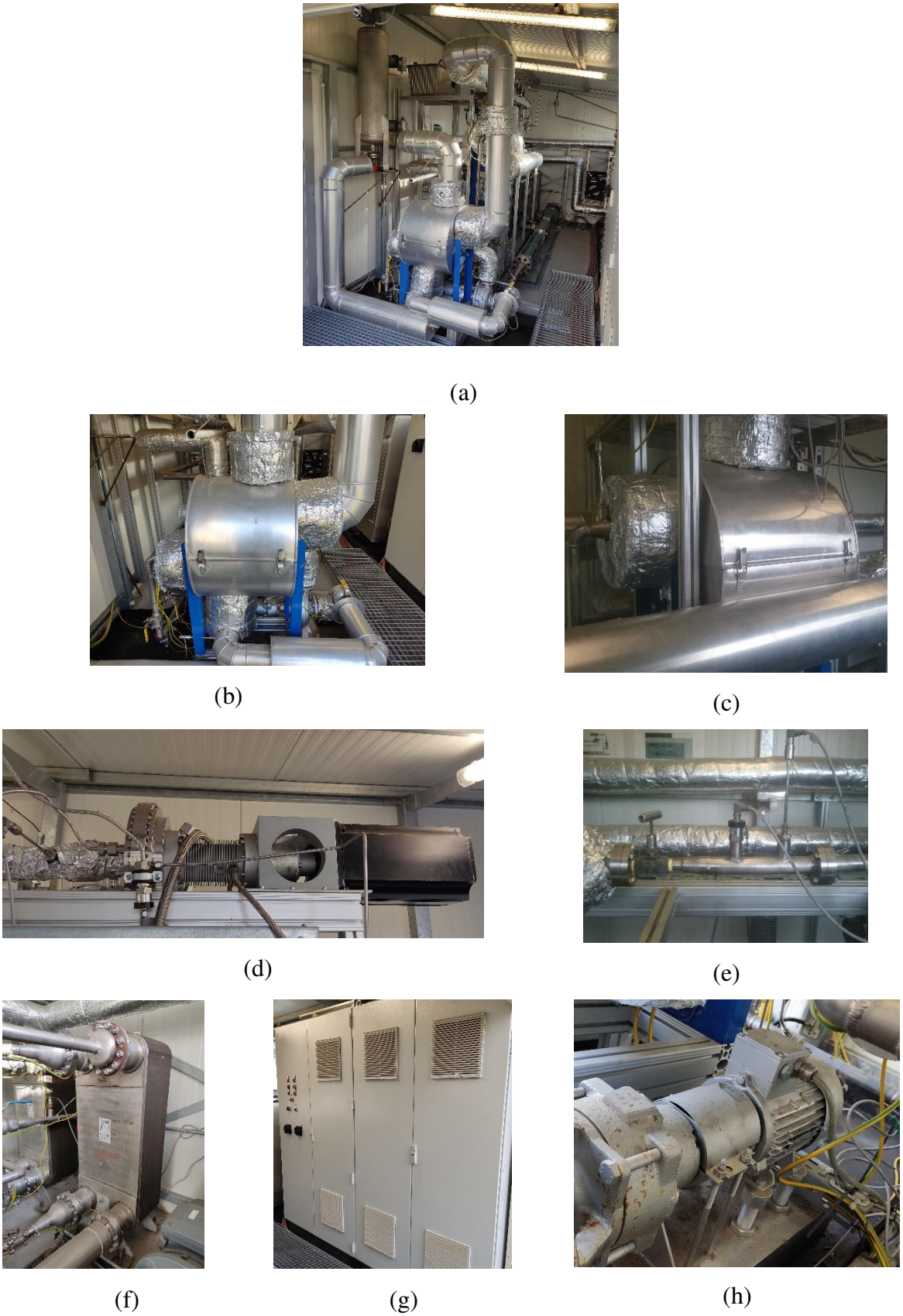

Fig. 7. (a) The cascaded two-ORC test rig, (b) HT cycle heat exchanger, (c) LT cycle heat exchanger, (d) HT cycle turbine and generator, (e) LT cycle throttle, (f) HT and LT heat condensers, (g) power and control cabinet, (h) M0 pump.

The optimization of the HT-ORC is the most critical factor that directly affects the overall system performance, since the HT-ORC is the primary cycle and represents the heat source of the LT-ORC. Selecting parameters only to increase the turbine power output may harm the overall thermal and exergy efficiencies. This is because increasing the turbine power output may require absorbing more heat from the source, leading to a decrease of net power output and thus reducing the thermal and exergy efficiencies [11]. Fig. 7 shows the layout of the CORC test rig. The main components of the CORC test rig and their operating range are listed in Table 1.

4.1.1. Heating cycle

Heat was generated by four electric heaters with a maximum power of 158 kW. Each electric heater consisted of three standard rods controlled by thyristors to set the heat source temperature. The electric heaters are simple to control and can be easily set up, allowing the system to be tested over a wide heat source temperature range. Moreover, electric heaters provide high temperatures with low operating risk and reduce the uncertainty of heat flow input. In the heating cycle, a heat transfer fluid (Therminol 66) was employed to transfer the heat to the working fluid in the HT-ORC via HE1. Employing Therminol 66 and electrical heaters allowed for a good modulation of the thermal power, reducing the uncertainty in the heating cycle during the experiments. Furthermore, Therminol 66 allows for a high heat source temperature (up to 300 °C) at atmospheric pressure. Moreover, it avoids corrosion and freezing, reducing maintenance cost. Therminol 66 is characterized by low toxicity, good heat transfer properties, suitable price and is usable in a wide temperature range. Therminol 66 was heated by electric heaters and pumped by the pump (M0) to the heat exchanger (HE1) to transfer heat to the working fluid in the HT-ORC.

4.1.2. Cooling cycle

The role of the cooling cycle was to dissipate the residual heat of the working fluid after the expansion process in the turbine. The cooling cycle in the CORC test rig was located outside the laboratory and consisted of an air cooler connected to a plate heat exchanger. The working fluid in the cooling cycle was a mixture of ethylene-glycol/water, circulated by the pump (M3). After the expansion process, the residual heat in the working fluid was absorbed by the ethylene-glycol/water mixture and released to the ambient by the air cooler. The design of the cooling cycle allowed to operate the CORC system as a dual cycle or only the HT-ORC as a single cycle.

4.1.3. Power generation cycles

The power generation cycles consisted of the HT-ORC and the LT-ORC, which were connected as a cascade that shared a heat exchanger HE1 so that the HT-ORC can be driven by the residual heat of the HT-ORC. Each cycle contained the four essential components of the ORC system, i.e. pump, evaporator, turbine and condenser. However, the LT-ORC contained an expansion valve instead of a turbine for the present investigation purposes. The working fluid was compressed to a higher pressure through pump M1 (process 7-3), then entered the evaporator (process 3-4), where it was preheated, evaporated and superheated before it entered the turbine (4-5), where it expanded to generate the power output. After the expansion, the working fluid was still at a high temperature, where its residual heat was used in the LT-ORC. After that, it entered the condenser to reject the remaining heat, and the same process was repeated. In the LT-ORC, the working fluid absorbed residual heat from the HT-ORC fluid via the second heat exchanger (HE2) (process 8-9). The working fluid was thereby converted into steam and entered the expansion valve (process 9-10). After the expansion process, the working fluid rejected its residual heat via the condenser C2 (process 10-11), and then entered the pump to be pressurized to a higher pressure before entering the evaporator (process 11-8), as shown in Fig. 6.

Table 1: Basic components of the CORC test rig.

Component	Type	Range
Flow heaters	GC heat D01-00508	0 – 158 kW
M0	Allweiler NTWH 25 200	max. 0.3 kW
M1	Progressive cavity-NETZSCH	-20 – 200 °C
M2	Progressive cavity-NETZSCH	-20 – 200 °C
HE1	Plate & Shell, VAHTERUS	-20 – 280 °C, -1 – 60 bar
HE2	Plate & Shell, VAHTERUS	-20 – 250 °C, -1 – 100 bar
C1	Heat exchanger, WP 10 L-100	max. 25 bar, -195 – 195 °C
C2	Heat exchanger, WP 10 L-100	max. 25 bar, -195 – 195 °C
Turbine	Radial flow	max. 325 °C
Generator	Six pole synchronous servomotor	max. 12 kW

5. Publications

In this section, four publications were presented, where three publications are first author contributions, and one publication is a second author contribution. The main objective of the publications was to test CORC system performance for a wide range of operating conditions. The publications included experiments and simulations of overall system and component performance. In these papers, the working fluids were selected according to environmental considerations, thermodynamic properties and availability in the market.

5.1. Experimental setup of a cascaded two-stage organic Rankine cycle

Dubberke F, Linnemann M, Abbas WK, Baumhögger E, Priebe KP, Roedder M, Neef M, Vrabec J. Experimental setup of a cascaded two-stage organic Rankine cycle. Applied Thermal Engineering 2018;131:958–964. DOI: 10.1016/j.applthermaleng.2017.11.137.

With permission of Elsevier reprinted from the journal Applied Thermal Engineering (Copyright 2018).

This paper involved testing and installing a CORC system using cyclopentane and propane in the HT-ORC and LT-ORC, respectively. One of the primary purposes of the work was to review system components, specifications and operating conditions. The work included the measurement of turbine power output, thermal efficiency, in addition to the heat transfer between HT-ORC and LT-ORC and PPD evaluation. The results showed that system performance should be tested over a wide range of heat source temperature using different working fluids. The calculations in this work depended on a fixed heat source temperature of 220 °C and turbine input pressure of 16.32 bar.

Design and layout of the system was done by Frithjof H. Dubberke and Klaus-Peter Priebe. Elmar Baumhögger and Rüdiger Pflock supported the construction and set up process. The measurement and data evaluation were performed by the author of this thesis and Mathiaas Linnemann. Jadran Vrabec revised the manuscript.

5.2. Experimental study of two cascaded organic Rankine cycles with varying working fluids

Abbas WKA, Linnemann M, Baumhögger E, Vrabec J. Experimental study of two cascaded organic Rankine cycles with varying working fluids. Energy Conversion and Management 2021;230:113818. DOI: 10.1016/j.enconman.2020.113818.

With permission of Elsevier reprinted from the journal Energy Conversion and Management (Copyright 2021).

System performance was experimentally tested in terms of thermal efficiency, exergy efficiency and turbine power output. Cyclopentane, pentane, butane and propane were selected as working fluids. The system performance was measured over a wide range of heat source temperature and turbine inlet pressure. Moreover, the component performance was discussed by evaluating turbine efficiency and enthalpy difference across the turbine. In addition, the heat transfer between HT-ORC and LT-ORC and PPTD was studied. It was shown that the CORC system can be considered suitable for exploiting different levels of heat source temperature.

The author of this thesis determined the operating conditions, selected working fluids and conducted experiments. The experiments were supported by Elmar Baumhögger and Mathiaas Linnemann. The paper was written by the author of this thesis and was revised by Jadran Vrabec.

Energy Conversion and Management 230 (2021) 113818

Contents lists available at ScienceDirect

Energy Conversion and Management

journal homepage: www.elsevier.com/locate/enconman

Experimental study of two cascaded organic Rankine cycles with varying working fluids

Wameedh Khider Abbas Abbas [a], Matthias Linnemann [b], Elmar Baumhögger [a], Jadran Vrabec [b,*]

[a] Thermoynamics and Energy Technology, University of Paderborn, Warburger Straße 100, 33098 Paderborn, Germany
[b] Thermodynamics and Process Engineering, Technical University of Berlin, Ernst-Reuter-Platz 1, 10587 Berlin, Germany

ARTICLE INFO

Keywords:
Organic Rankine cycle
Two-ORC system
Heat source temperature
Working fluids
Pinch point temperature difference

ABSTRACT

Organic Rankine cycles convert low-temperature heat from different sources, like solar, geothermal or biomass, into electricity and may thus help to meet the energy demand in an environmentally friendly way. While single ORC systems have been studied extensively, there are only very few experimental works on systems consisting of two cascaded organic Rankine cycles (two-ORC). In this work, an experimental study is carried out on the performance of a two-ORC system that consists of a high temperature (HT) cycle and a low temperature (LT) cycle. Each cycle is composed of the four significant components, i.e. expander, evaporator, condenser and pump, while the LT cycle is equipped with a throttle as expansion device. The HT cycle utilized heat from electrical heaters, while the LT cycle was driven by the waste heat from the HT cycle. The test rig utilizes Therminol 66 as a source that is heated up by electrical heaters with a power of 158 kW. Propane, butane, pentane and cyclopentane are chosen as working fluids for the present experiments. Parameter variations are carried out to study the thermodynamic characteristics of each cycle. The aim is to investigate the HT cycle performance considering turbine power output, thermal efficiency and exergy efficiency. The effect of the HT cycle on the LT cycle is examined by studying the heat transfer rate between the two cycles, characteristics of heat exchangers and pinch point temperature difference. A further goal is to explore the system performance under different conditions to maximize the exergetic utilization of the heat source. The results confirm that turbine power output and thermal efficiency increase with heat source temperature and turbine inlet pressure in the HT cycle. The maximum achieved thermal and exergy efficiencies are 5.5% and 20.2%, respectively, while the maximum turbine power output is 4.92 kW. Heat transfer measurements show that the maximum transferred heat flow from the HT cycle to the LT cycle is 23 kW when pentane is used as a working fluid. Temperature profiles and the pinch point temperature difference in the heat exchangers of both cycles are assessed under conditions where the highest turbine power is obtained. The experimental tests are promising and show that the two-ORC system is suitable to utilize heat sources in various temperature ranges.

1. Introduction

Global warming and its impact on climate change has received much attention in recent years. Consequently, many alternative technologies and solutions have been introduced to reduce the dependence on fossil fuels. The organic Rankine cycle (ORC) is a suitable technology for power generation because it can be driven by heat from different sources. ORC may generate power from low-temperature and waste heat that might otherwise be emitted into the environment [1,2]. The heat source has an essential role in the design process of such plants. Therefore, ORC systems have been devised for various low- and medium-temperature sources [3]. The ORC has the same operating scheme as the Rankine cycle, but utilizes organic fluids instead of water. The working fluid selection is a key step for the design and optimization of ORC under given heat source characteristics. A large number of studies highlighted the importance of selecting appropriate working fluids [4].

Saleh et al. [5] tested 31 working fluids for different ORC layouts in the context of geothermal plants with temperatures varying from 30 °C to 100 °C. The authors demonstrated that supercritical fluids recovered the largest amount of heat, while the situation was reversed for high-boiling subcritical fluids. Bao et al. [6] reviewed different working fluids and turbines for ORC plants. Their analysis included a study of thermo-physical properties of working fluids and their influence on ORC

* Corresponding author.
E-mail address: vrabec@tu-berlin.de (J. Vrabec).

https://doi.org/10.1016/j.enconman.2020.113818
Received 22 September 2020; Received in revised form 22 September 2020; Accepted 28 December 2020
Available online 9 January 2021
0196-8904/© 2020 Elsevier Ltd. All rights reserved.

Nomenclature

C	Condenser [–]
HT	High temeprature cycle [–]
LT	Low temperature cycle [–]
LNG	Liquefied natural gas [–]
M0	Heat cycle pump [–]
M1	High temperature cycle pump [–]
M2	Low temperature cycle pump [–]
M3	Cooling cycle pump [–]
PPTD	Pinch point temperature difference [K]
TIP	Turbine inlet pressure [MPa]
c_p	Isobaric heat capacity [kJ/(kg K)]
$\dot{E}_{in}$	Exergy flow input [kW]
$\dot{m}_{HC}$	Mass flow rate in heating cycle [kg/s]
$\dot{m}_{HT}$	Mass flow rate in high temperature cycle [kg/s]
$\dot{m}_{LT}$	Mass flow rate in low temperature cycle [kg/s]
p_c	Critical pressure [MPa]
M	Molar mass [g/mol]
$\dot{Q}$	Heat flow [kW]
T_b	Boiling point temperature [K]
T_c	Critical temperature [K]

performance, along with a comparison of working fluids that are pure components or mixtures. It was pointed out that mixtures with an appropriate composition may improve overall system efficiency. Ma et al. [7] published a study on system performance of medium- and low-temperature ORC systems. Their study included a systematic screening of 70 working fluids with different thermo-physical properties and reported a major dependence of specific turbine volume and thermal efficiency on their critical point temperature.

Many researchers focused on the selection of suitable heat sources for different ORC systems to modify the objective functions, like output power, thermal efficiency, exergy efficiency or heat transfer. The selection included solar energy [12], geothermal energy [13], biomass [14] or liquefied natural gas (LNG) [15].

A considerable number of investigations focused on developing different ORC architectures. In this context, ORC systems with multi-cycle layouts have received attention in recent years [9]. One of these architectures is the two-ORC system, where each cycle has a different working fluid, different temperature and pressure levels as well as different mass flow rates. Generally, a two-ORC system consists of a HT cycle (topping ORC) and a LT cycle (bottoming ORC). The HT cycle is driven by the main heat source, while the LT cycle utilizes the residual heat from HT cycle or a secondary heat source [10]. Several theoretical investigations have been presented to identify the advantages of multi-ORC systems. Wang et al. [8] studied a two-ORC system driven by waste heat of a diesel engine using R245fa and R134a as working fluids. The authors assessed the influence of turbine efficiency, evaporation pressure of the HT cycle and condensation temperature of the LT cycle on the system performance. They reported that the use of a two-ORC system can improve the net power by up to 22%. Braimakis et al. [10] considered seven working fluids to explore the exergetic optimization of a two-ORC system, where the heat source temperature ranged from 100 °C to 300 °C. The authors developed a routine to calculate the optimal evaporation pressure as well as the pinch point temperature difference during evaporation and condensation to increase power output. Thereby, the exergetic efficiency increased up to 25% by employing cyclopentane and butane for the HT and the LT cycle, respectively. They found that the two-ORC layout is suitable when the critical temperature difference between the working fluids in the HT and LT cycles is low. Sung and Kim [16] analyzed a two-ORC system to recover waste heat from engine exhaust. They revealed that the proposed two-ORC system may enhance the performance of the engines such that the net power output may be 5% higher than that of regular ORC systems. The authors reported that pentane and R125 are the best option for the HT cycle and the LT cycle, respectively. Mehrpooya et al. [17] optimized a two-ORC layout by studying the influence of 11 thermodynamic parameters on the system performance. The authors also reported a relation between the improvement of the exergy efficiency and the investment cost of the ORC layout. Yang et al. [18] proposed a two-ORC layout for heat recovery from a compressed natural gas engine. The authors investigated the effect of evaporation pressure and condensation temperature of the HT cycle on the system performance, while the same parameters were kept constant in the LT cycle. Their results indicated that the maximum power output and the thermal efficiency are 23.62 kW and 10.19%, respectively. Kosmadakis et al. [19] studied 33 refrigerants to select the optimal working fluid for the use in the HT cycle of a two-ORC layout. They discussed the environmental effects and performance of working fluids under high-temperature conditions. They found that R245fa has the best properties among the selected working fluids according to its high turbine power, good thermal efficiency and low impact on the environment. The thermodynamic analysis of a two-ORC system was discussed in the work of Xue et al. [20]. The authors presented numerical thermodynamic models to investigate the effect of different parameters on the system performance. They showed that the maximum achieved net power output was 1.78 MW, with maximum thermal and exergy efficiency of 25.64% and 31.02%, respectively. Preissinger et al. [21] made an exergy analysis of a biomass-fired two-ORC system, investigating 35 different working fluids. The study concluded that the achieved thermal and exergy efficiencies were 36% and 60%, respectively. The authors showed that the exergy efficiency is affected by the LT cycle working fluid more than by the HT cycle working fluid. Ayachi et al. [22] assessed the exergy efficiency of regular and two-ORC systems, reporting that the two-ORC system may provide an exergy efficiency of about 42%, which is higher than that of regular ORC systems. Their study also points out a strong relation between critical temperature of the working fluid and exergy efficiency. In addition, the highest efficiencies may be achieved by subcritical cycles. Yun et al. [23] proposed a parallel two-ORC system for marine applications, comparing it with regular ORC systems for waste heat recovery. They studied the advantages of two-ORC layouts and considered four models based on actual sailing data of a container ship. They demonstrated that the two-ORC system may generate more power output than regular ORC. Their paper reported that the proposed two-ORC system can be considered for different marine applications due to its ability to recover waste heat under different operational conditions. Choi et al. [24] studied multi-ORC (two- and three-ORC) systems for LNG cold energy recovery for power production. The authors presented that cycle efficiency, thermal efficiency and turbine power output increase with the number of system cycles. The highest turbine power output was gained with a three-ORC system by using propane as a working fluid. Li et al. [25] proposed a cascaded two-ORC power generation plant using LNG and solar energy as heat source and they also investigated the influence of working fluids on system performance. The authors discussed the design of turbines for ORC and found that the volume ratio of their expanders is much smaller than that of regular ORC. Shu et al. [26] analyzed a two-ORC layout with respect to system performance to recover waste heat from high-temperature exhaust and engine coolant. They utilized water and six refrigerants for the HT cycle and the LT cycle, respectively. Their results revealed that the maximum achieved power output and exergy efficiency are 36.77 kW and 55%, respectively. The selection of the working fluids for the two-ORC system was discussed in the paper of Emadi et al. [14]. They studied the applicability of two-ORC technology for waste heat recovery from a solid-oxide fuel cell system integrated with a gas turbine. The authors investigated 20 combinations of working fluids and proposed the combination of pentane and ethane for the HT and the LT cycle, respectively. According to their study, the two-ORC system produced electrical power of 1040 kW with an exergetic efficiency of 51%.

This literature review of theoretical studies indicates that articles dealing with two-ORC systems are devoted to the effectiveness of this architecture and may contribute to the environmentally friendly power supply [28]. Despite many publications on two-ORC technology, there is still a lack of experimental studies and practice in turning theoretical research into tangible results.

Experimentally, Linnemann et al. [27] assessed a cascaded two-ORC system. Their study presented a thermodynamic analysis of different parameters by utilizing waste heat from a biogas combined heat and power plant. They found that the maximum achievable thermal efficiency of the HT cycle was 15.20% by using toluene as working fluid, while it was 8.90% for the LT cycle by using SES36 as a working fluid. Ntavou et al. [42] practically tested and compared the system performance for both regular and two-ORC systems over a wide range of heat flow input. Their results showed a thermal efficiency of 7% and turbine power of 6.30 kW for a regular ORC, while the values of the two-ORC improved to 9.9% and 7.7 kW, respectively. Yu et al. [11] investigated a cascaded steam-ORC experimentally, which consisted of a HT cycle and a LT cycle to recover waste heat from a diesel engine. They pointed out that the maximum power output was 12.7 kW.

The rather large literature review of the present work indicates that the two-ORC system may be highly promising and effective for waste heat recovery applications, as elaborated in numerous theoretical studies. However, the very few experimental studies found that two-ORC systems are considered to be immature and there is a significant increase of complexity with respect to the operating conditions of two-ORC systems. To improve this technology, further practical investigations are thus necessary, which was the aim of this work. It was attempted to fill some of the gaps with experimental investigations for two-ORC system technology by applying a wide range of operating conditions and parameters.

This paper presents an experimental investigation of a cascaded two-ORC system by considering four hydrocarbon working fluids. The first goal is to investigate HT cycle performance concerning turbine power output, thermal efficiency and exergy efficiency under different heat source temperatures and turbine inlet pressures. The second goal is to measure the heat transfer rate from the HT cycle to the LT cycle under different heat source temperatures and heat exchanger inlet pressures. The pinch point temperature difference (PPTD) was studied for various conditions to explore the temperature profiles and heat exchanger characteristics. These investigations provide sufficient knowledge for the optimization of future system operation with various combinations of working fluids.

2. System description

The investigated cascaded two-ORC test rig was designed and set up in practice at the University of Paderborn [29]. A schematic of this system is displayed in Fig. 1 and its basic components are listed in Table 1. The test rig contained two essential cycles, the HT cycle and the LT cycle. Heat was supplied by four electrical heaters with an adjustable temperature. Electrical heaters allow for simple control and regulation and are benign with respect to safety and hazard requirements. Furthermore, electrical heaters can be sources over a wide range of temperature [47]. In addition to the two working cycles, the test rig had four supporting cycles. The heating cycle (HC) contained a heat transfer fluid (Therminol 66) which was thermostated by electrical heaters to supply heat to the HT cycle. The mass flow rate of Therminol 66 in the HC was controlled via the rotational frequency of the radial pump M0. The temperature of the HC was controlled via a fully adjustable

Table 1
Basic components of the cascaded two-ORC test rig.

Component	Type	Range
M0	Allweiler NTWH 25 200	Max.: 0.3 kW, 0.7 kg/s, 0.8 MPa, 350 °C
Flow heaters	GC heat D01-00508	0–158 kW
M1	Progressive cavity-NETZSCH	−20 to 200 °C,
M2	Progressive cavity-NETZSCH	−20 to 200 °C,
HE1	Plate & Shell, VAHTERUS	−20 to 350 °C, −1 to 6 MPa
HE2	Plate & Shell, VAHTERUS	−20 to 250 °C, −1 to 10 MPa
C1	Heat exchanger, WP 10 L-100	Max. 2.5 MPa, −195 to 195 °C
C2	Heat exchanger, WP 10 L-100	Max. 2.5 MPa, −195 to 195 °C
Turbine	Radial flow	Max. 325 °C
Generator	Six pole synchronous servomotor	Max. 14 kW

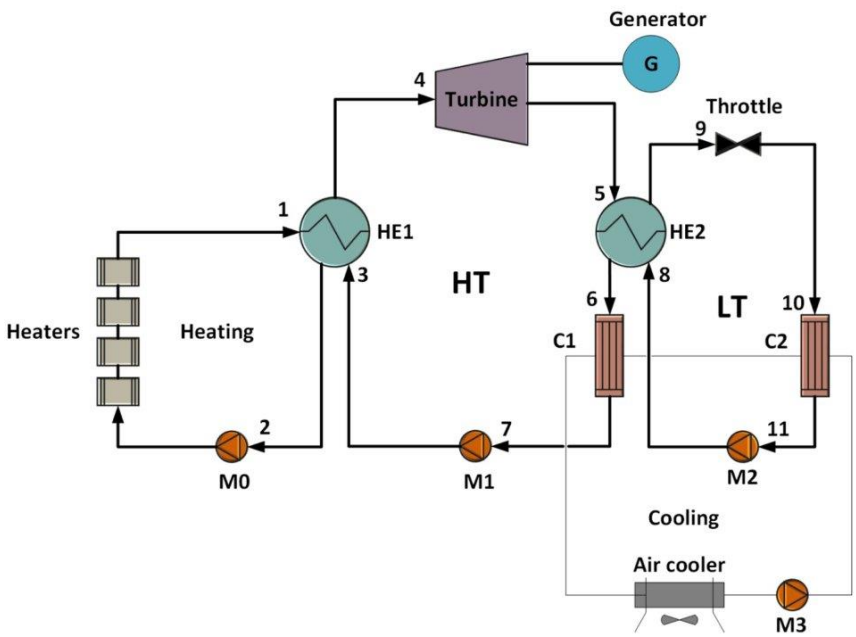

Fig. 1. Layout of the cascaded two-ORC system investigated experimentally in the present work.

thyristor-controlled heater (TCH), while three power contactor heaters (PCH) were in use as well. The temperature of Therminol 66 was raised by the flow heaters up to a maximum temperature of 623 K to avoid its thermal decomposition. Cyclopentane was employed as a working fluid in the HT cycle, while the working fluid in the LT cycle was varied, i.e. propane, butane and pentane. The HT cycle consisted of the essential components of the Rankine cycle, i.e. centrifugal radial turbine coupled to a generator, condenser, plate and shell heat exchanger (as an evaporator) as well as a progressive cavity pump. The LT cycle consisted of the same elements, but the turbine was substituted by a manually adjustable throttle. Fig. 2 shows the cascaded two-ORC system and the basic components of the HC, HT and LT cycles.

In the HT cycle, cyclopentane was compressed by the progressive cavity pump M1, was then heated up and evaporated in the first heat exchanger (HE1), followed by the expansion in the turbine. Because cyclopentane was subsequently still at a high temperature, its residual heat was employed to drive the LT cycle. In the LT cycle, the working fluid was heated up in the second heat exchanger (HE2) and expanded through the throttle. Its residual heat was not used further because the according temperature was low. Therefore, the working fluid was condensed via heat discharge to the environment to reach its initial state.

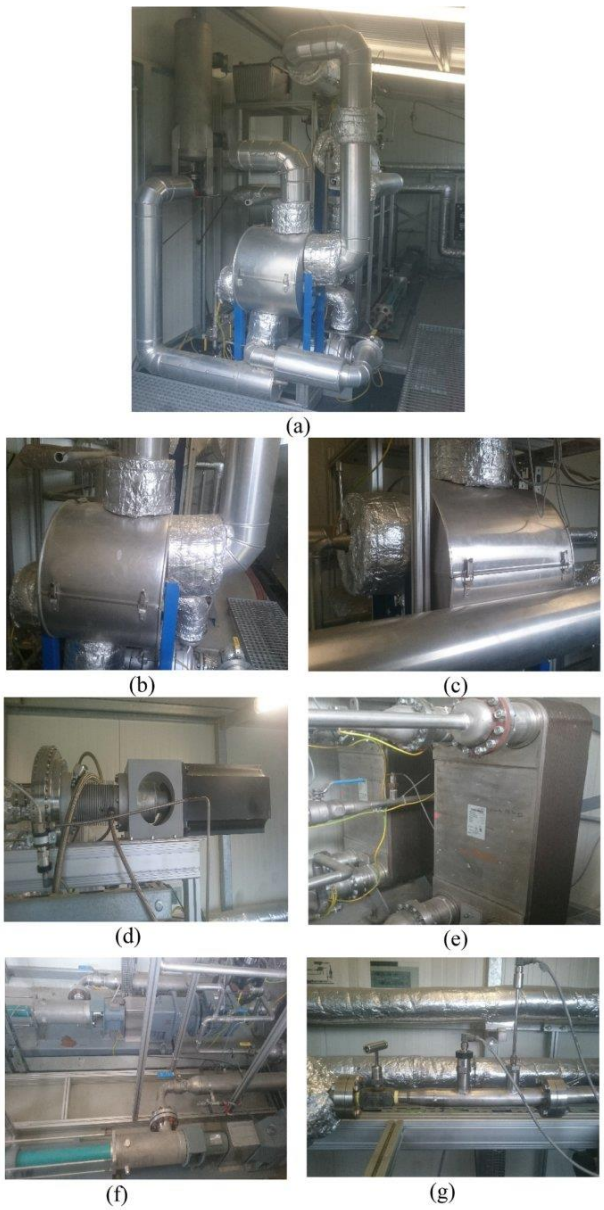

Fig. 2. (a) The cascaded two-ORC test rig was in a container due to safety considerations, (b) HT cycle heat exchanger, (c) LT cycle heat exchanger, (d) HT cycle turbine and generator, (e) condensers of HT and LT cycles, (f) pumps of HT and LT cycles, (g) LT cycle throttle.

The HE2 is the connection and the main component for the heat transfer between the HT cycle and the LT cycle. Therefore, it was important to explore the performance of the HE2 under different process conditions. The system performance concerning turbine power output, thermal efficiency, exergy efficiency and the heat transfer between the two cycles was investigated under different operational conditions. The long-term target of the experimental investigations is to achieve a maximum exergetic utilization of the heat source and the system optimization for future operation. The heat source temperature, turbine inlet pressure (TIP) and the mass flow rate were varied to investigate the HT cycle's system performance. In contrast, the LT cycle was examined by varying the HE2 inlet pressure for a wide range of heat source temperature.

Temperature, pressure and mass flow rate sensors were located at the inlet and outlet of the components to measure the thermodynamic states and process parameters of the cascaded two-ORC system. Parameter selection to improve only the turbine power output of the HT cycle may have a negative effect on the performance of the LT cycle and the overall system. Optimization of HT cycle parameters has a significant influence on the LT cycle's inlet parameters, which are equal to the outlet conditions of the HT cycle. Thermal and exergy efficiency are suitable criteria for rating the system performance. Thermal efficiency gives the percentage of the heat input being converted into turbine power output. In contrast, the exergy efficiency is an indicator for efficient utilization of the given heat source. Moreover, higher exergy efficiency refers to higher energy quality utilized in the system [29,48].

The heat source temperature and TIP were selected as independent variables to investigate turbine power output, thermal efficiency and exergy efficiency as dependent variables of the HT cycle. The turbine power output is notably dependent on the mass flow rate and the enthalpy difference across the turbine. Thermal and exergy efficiencies may not depend directly on the heat source temperature and TIP, but these two parameters directly affect the net power and input heat flow amount. The thermal efficiency depends on the net power and input heat flow, while thermal exergy depends on two parameters, i.e. net power and exergy flow input. In the LT cycle, heat source temperature and the HE2 inlet pressure were selected as independent variables to investigate the heat transfer rate between the HT cycle and the LT cycle.

All measurements represent average values of temperature and pressure at each state point. The basic sensors of the cascaded two-ORC system are listed in Table 2.

Table 2
Measuring devices of the cascaded two-ORC test rig.

Variable	Sensor type	Range	Uncertainty
p (HC)	Jumo	0 to 0.6 MPa	±0.5%
T_1, T_2 (HC)	Pt 1000	−40 to 380 °C	±0.1%
$\dot{m}_{HC}$ (HC)	Pressure difference	0 to 2.5 MPa	±0.1%
T_3, T_4, T_5, T_6, T_7 (HT)	Pt 1000	−40 to 380 °C	±0.1%
p_3, p_4 (HT)	APT	0 to6 MPa	±0.5%
p_5, p_6, p_7 (HT)	APT	0 to 1.6 MPa	±0.5%
$\dot{m}_{HT}$(HT)	SITRANS P DS III	0 to 10 MPa	≤0.065%
T_8, T_9 (LT)	Pt 1000	−40 to 380 °C	±0.1%
T_{10}, T_{11} (LT)	Pt 1000	−40 to 380 °C	±0.1%
p_8, p_9 (LT)	APT	0 to 6 MPa	±0.5%
p_{10}, p_{11} (LT)	APT	0 to 1.6 MPa	±0.5%
$\dot{m}_{LT}$ (LT)	SITRANS P DS III	0 to 10 MPa	≤0.065%

3. Thermodynamic analysis

The expressions and equations employed to define the performance of different operation modes of the cascaded two-ORC system are discussed in the following. In this thermodynamic analysis, the equations were built on the assumptions that there is no significant pressure drop in heat exchangers, condensers or tubes and that the turbine does not exchange heat with the environment. These assumptions are standard practice in the literature. They have also been validated in preceding work of our group and with experimental investigations [43–46].

In the HC, the flow heaters supply Therminol 66 with the heat flow

$$\dot{Q}_{HC} = \dot{m}_{HC} \cdot c_p \cdot (T_2 - T_1) \tag{1}$$

where T_1 and T_2 are temperatures of Therminol 66 at the inlet and outlet of HE1, respectively.

The heat flow $\dot{Q}_{HC}$ into the heating cycle is equal to the heat flow driving the HT cycle

$$\dot{Q}_{HC} = \dot{Q}_{HE,1} = \dot{m}_{HT} . (h_4 - h_3) \tag{2}$$

where $\dot{m}_{HT}$is the mass flow rate of cyclopentane in the HT cycle, h_3 and h_4 are cyclopentane enthalpies at the inlet and outlet of the heat exchanger HE1, respectively.

The turbine power output is

$$\dot{W}_{HT}^{T} = \dot{m}_{HT} . (h_4 - h_5) \tag{3}$$

where h_4 and h_5 are cyclopentane enthalpies at the inlet and outlet of the turbine, respectively.

After the expansion, cyclopentane was cooled before entering the pump. The heat transferred via the condenser is given by

$$\dot{Q}_{C1} = \dot{m}_{HT} . (h_6 - h_7) \tag{4}$$

where h_6 and h_7 are cyclopentane enthalpies at the inlet and outlet of the condenser C1, respectively.

The work of the pump was calculated by

$$\dot{W}_{HT}^{P} = \dot{m}_{HT} . (h_3 - h_7) \tag{5}$$

where h_7 and h_3 are cyclopentane enthalpies at the inlet and outlet of the pump M1, respectively.

The thermal efficiency of the HT cycle was calculated as the ratio of net power to heat flow input

$$\eta_{th,HT} = \frac{\dot{W}_{net}}{\dot{Q}_{HC}} \tag{6}$$

$$\dot{W}_{net} = \dot{W}_{HT}^{T} - \dot{W}_{HT}^{P}$$

The exergy efficiency of the HT cycle was calculated as the ratio of net power to exergy flow input

$$\eta_{ex,HT} = \frac{\dot{W}_{net}}{\dot{E}_{in}} \tag{7}$$

Therein, $\dot{E}_{in}$ is the exergy flow from the heat source, which was calculated by

$$\dot{E}_{in} = \dot{m}_{HT}[(h_4 - h_3) - T_0(s_4 - s_3)]$$

whereT_0 is the ambient temperature, h_3 and h_4 are cyclopentane enthalpies at the inlet and outlet of HE1, respectively, while s_3 and s_4 are the corresponding entropies.

The turbine efficiency of the HT cycle can be calculated by

$$\eta_T = \frac{h_4 - h_5}{h_4 - h_{5s}} \tag{8}$$

where h_{5s} is the enthalpy of cyclopentane at the outlet of a hypothetic isentropic turbine.

The heat flow through the heat exchanger HE2 was calculated by

$$\dot{Q}_{HE,2} = \dot{m}_{LT} . (h_9 - h_8) \tag{9}$$

where $\dot{m}_{LT}$ is the mass flow rate of the working fluid in the LT cycle, while h_8 and h_9 are its enthalpies at the inlet and outlet.

The energy balance of condenser C2 is

$$\dot{Q}_{C2} = \dot{m}_{LT} . (h_{10} - h_{11}) \tag{10}$$

where h_{10} and h_{11} are the working fluid enthalpies at the inlet and outlet of the condenser C2, respectively.

The work of the pump was calculated by

$$\dot{W}_{LT}^{P} = \dot{m}_{LT} . (h_8 - h_{11}) \tag{11}$$

where h_{11} and h_8 are the working fluid enthalpies at the inlet and outlet of the pump M2, respectively.

4. Selection of working fluids

The selection of working fluids is the most significant key to the performance of ORC cycles. There are many categories of working fluids for ORC systems, which differ considerably from each other in terms of their thermo-physical properties.

Generally, working fluids are divided according to the slope of their saturated vapor line in the temperature-entropy diagram: A positive slope refers to dry fluids, a negative slope refers to wet fluids, while a nearly vertical slope refers to isentropic fluids. Isentropic and dry working fluids are favored in ORC systems because they cannot condense in the turbine [30].

In this work, three dry fluids (butane, pentane and cyclopentane) and one wet fluid (propane) were investigated. The advantages of these hydrocarbons are their low price, environmental friendliness (low GWP and ODP) and thermodynamic attractiveness. The disadvantages are mainly safety related because all of these fluids are very combustible.

The selection of the working fluids was based on their thermodynamic properties, which were calculated with REFPORP 9.0 [31]. The selection was also based on the experimental and simulation results of references [10,17,18,32–38]. Table 3 presents the basic properties of these working fluids. Cyclopentane, that has the highest critical temperature, was selected for the HT cycle, while propane, butane or pentane were alternatively selected for the LT cycle. 40 kg of cyclopentane was used in the HT cycle, while about 20 kg of working fluid was used in the LT cycle.

5. Operational conditions of the experiments

Different parameters were investigated to assess the system performance. The HT cycle performance considering turbine power output, exergy efficiency, thermal efficiency, enthalpy difference and turbine efficiency was investigated under different conditions. Under condition 1, the HT cycle performance was studied for a heat source temperature from 453 K to 533 K at 10 K intervals. The maximum heat source temperature was limited to the critical temperature of cyclopentane due to safety considerations. Under condition 2, the heat source temperature was kept constant at 533 K (the maximum temperature under condition 1), while the TIP was varied from 2.0 MPa to 3.0 MPa.

The LT cycle was driven by the residual heat flow from the HT cycle so that its output represents the input of the LT cycle and the overall performance depends on the amount of heat flow transferred between the cycles. The influence of the HT cycle on the LT cycle was investigated by looking at the heat transfer between the two cycles. For that purpose, two additional conditions were investigated. Under condition 3, the heat source temperature was varied from 453 K to 533 K. Under condition 4,

Table 3
Properties of the selected working fluids.

Substance	M [g/mol]	T_b [K]	T_c [K]	p_c [MPa]	Type	GWP	ODP	Ref.
Propane	44.096	231.036	369.89	4.25	Wet	3	0	[39]
Butane	58.122	272.66	425.13	3.79	Dry	4	0	[40]
Pentane	72.149	309.21	469.70	3.37	Dry	4	0	[35]
Cyclopentane	70.133	322.375	511.72	4.57	Dry	<1	0	[41]

the heat source temperature was kept constant at 503 K and 533 K, while the heat transfer was measured for different HE2 inlet pressures. Moreover, the PPTD, which is one of the most important factors affecting the heat transfer, was investigated for different conditions in HE1 and HE2. Under conditions 1 and 2, the PPTD was investigated at points where the maximum turbine power output was achieved. Under conditions 3 and 4, the PPTD was investigated where the largest amount of heat was transferred from the HT cycle to the LT cycle for each working fluid. The HE2 is the device for the heat transfer between the HT cycle and the LT cycle. Therefore, it was important to explore its performance under different process conditions. Basic parameters and operational conditions of the present two-ORC system are listed in Table 4. The selected operational conditions and different parameters are related to the thermo-physical properties of working fluids and the design aspects of various components of the cascaded two-ORC system.

6. Results and discussion

The heat source consisted of four electrical flow heaters in the HC cycle with a maximum power of 158 kW in total. These heaters allowed for adjusting the heat source temperature, both manually and with automatic controllers. The heat flow amount during the experiments was varied by means of the temperature and mass flow rate of Therminol 66 in the HC cycle. The cascaded two-ORC system was studied for heat source temperatures in the range between 453 K and 533 K and the TIP was varied between 2.0 MPa and 3.0 MPa. The impact of these important parameters is discussed for each cycle.

Table 4
Basic parameters and operational conditions of the present experiments with the cascaded two-ORC test rig.

Parameter	Range
Condition 1	
Temperature of heat source	453–533 K
Mass flow rate (HC)	0.48–0.55 kg s^{-1}
Ambient temperature	278.15–288.15 K
Ambient pressure	0.1013 MPa
Mass flow rate (HT)	0.08–0.12 kg s^{-1}
Condition 2	
Temperature of heat source	533 K
Turbine inlet pressure	2.0–3.0 MPa
Mass flow rate (HC)	0.48–0.55 kg s^{-1}
Mass flow rate (HT)	0.12–0.15 kg s^{-1}
Condition 3	
Temperature of heat source	453–533 K
Mass flow rate (HC)	0.48–0.55 kg s^{-1}
Mass flow rate (HT)	0.12 kg s^{-1}
Mass flow rate (LT)	0.030–0.035 kg s^{-1}
Condition 4	
Temperature of heat source	533 K
HE2 inlet pressure	1.2–3.6 MPa
Mass flow rate (HC)	0.48–0.55 kg s^{-1}
Mass flow rate (HT)	0.12 kg s^{-1}
Mass flow rate (LT)	0.035–0.048 kg s^{-1}

6.1. Effects of heat source temperature on the HT cycle performance (condition 1)

The first step was to study the impact of the heat source temperature on the cascaded two-ORC system performance. Thermal efficiency, turbine power output and exergy efficiency were investigated for different heat source temperatures. The mass flow rate of cyclopentane was thereby also varied from 0.08 kg/s to 0.12 kg/s. The maximum heat source temperature was selected to keep the turbine inlet temperature below the critical temperature of cyclopentane to avoid supercritical states.

For the variation between 453 K and 533 K, the impact of heat source temperature on the turbine power output can be seen in Fig. 3 (a). As the heat source temperature increases, the turbine power output rises. A comparison between the three configurations shows that the maximum turbine power output was 4.64 kW at a heat source temperature of 533 K and a mass flow rate of 0.12 kg/s. Furthermore, the turbine power output varied from 0.65 kW to 2.86 kW at a mass flow rate of 0.08 kg/s, while it varied between 1.09 kW and 3.64 kW at a mass flow rate of 0.10 kg/s. The observed increase of turbine power output can be explained by the fact that with the rise of the heat source temperature, the ratio between inlet and outlet pressure of the turbine increases. This means that the increasing heat source temperature increased both inlet and outlet pressure of the turbine. Nevertheless, the increasing rate of the inlet pressure outweighs the increasing rate of the outlet pressure. This leads to a larger enthalpy difference across the turbine, as shown in Fig. 4 (a), so that its power output increases. The enthalpy difference across the turbine increases for all three working fluid mass flow rates with rising heat source temperature. The results indicate that the impact of enthalpy drop across the turbine on the turbine power output is more significant than that of mass flow rate.

The thermal efficiency as a function of the heat source temperature is depicted in Fig. 3 (b). When the heat source temperature rises from 453 K to 533 K for a cyclopentane mass flow rate of 0.08 kg/s, the thermal efficiency increases from 1.84% to 4.80%. At a mass flow rate of 0.10 kg/s, the thermal efficiency rises from 2% to 5.3%. The maximum thermal efficiency in this experiment was 5.50% at a temperature of 533 K, where the mass flow rate was 0.12 kg/s. The increase of thermal efficiency with heat source temperature indicates that the increasing net power rate is higher than that of the heat flow input to the HT cycle so that the thermal efficiency increases gradually.

The variation of the exergy efficiency as a function of heat source temperature for different mass flow rates of cyclopentane is shown in Fig. 3 (c). As expected, the three investigated cases ($\dot{m}$=0.08, 0.10 and 0.12 kg/s) show an increasing trend. The maximum exergy efficiency of 20.2% was obtained for a mass flow rate of 0.12 kg/s and a heat source temperature of 533 K. It was throughout observed that the exergy efficiency rises with the heat source temperature. The main reason is that the net power increases with heat source temperature and the increasing rate is higher than that of exergy flow input.

The variation of the turbine efficiency with heat source temperature is shown in Fig. 4 (b). The results demonstrate that the turbine efficiency rises with heat source temperature, which can be related to the increase of enthalpy difference across the turbine. As seen in Fig. 4 (a), the enthalpy difference increased with the heat source temperature leading to a higher turbine efficiency. The maximum measured turbine efficiency was 39.12% at a heat source temperature of 533 K.

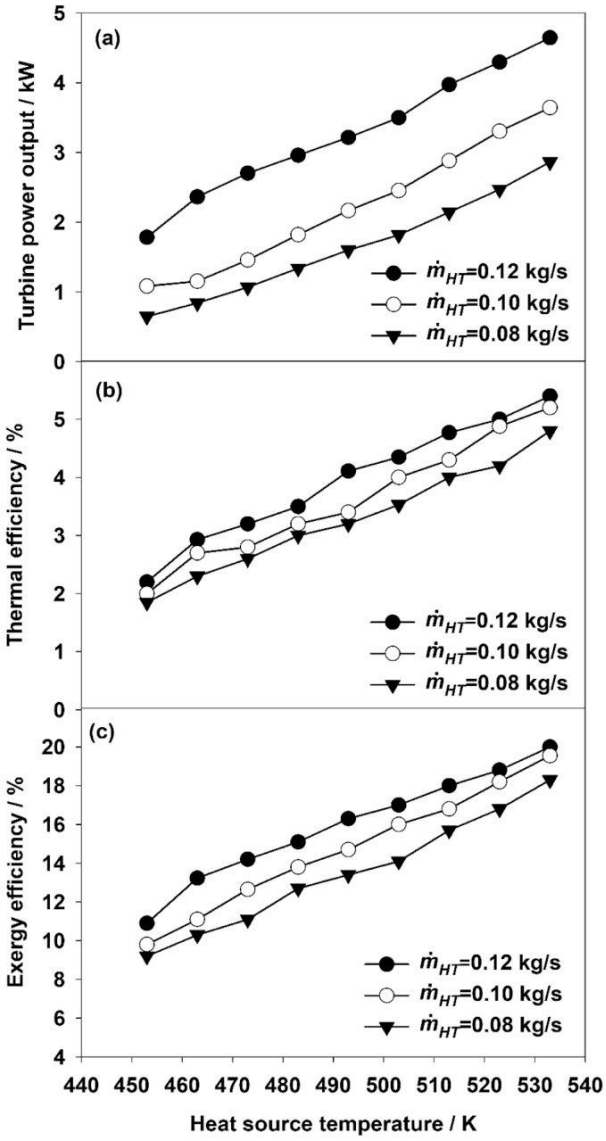

Fig. 3. Variation of (a) turbine power output, (b) thermal efficiency and (c) exergy efficiency of the HT cycle as a function of heat source temperature for a varying cyclopentane mass flow rate.

6.2. Effects of TIP on the HT cycle performance (condition 2)

In this section, the impact of the TIP on the cascaded two-ORC system performance was studied. The heat source temperature was kept constant at 533 K, where the highest HT cycle performance was achieved under condition 1. The mass flow rate of cyclopentane was varied from 0.12 kg/s to 0.15 kg/s by adjusting the rotational frequency of the pump M1. The inlet pressure was again kept throughout below the critical pressure of cyclopentane to avoid supercritical states.

Fig. 5 shows the impact of the TIP on the turbine output power, thermal and exergy efficiencies and demonstrates the variation of turbine power output with TIP. When the TIP rises from 2.0 MPa to 3.0 MPa, the turbine power output increases slightly from 3.18 kW to 4.92 kW for a mass flow rate between 0.12 kg/s and 0.15 kg/s. However, the turbine power output is related to turbine inlet and outlet pressure and both were increased during this experiment. The higher pressure ratio in this test entails a larger enthalpy drop across the turbine and more

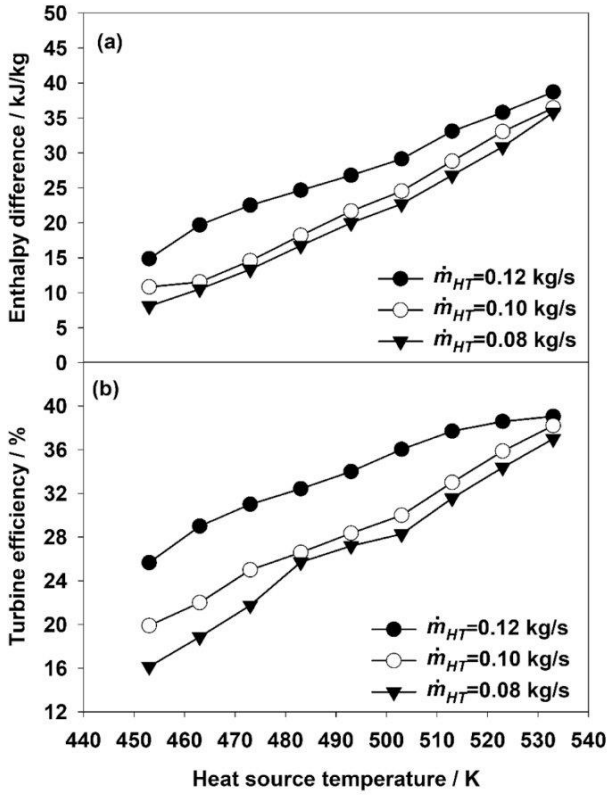

Fig. 4. Variation of (a) enthalpy difference across the turbine and (b) turbine efficiency as a function of heat source temperature for a varying cyclopentane mass flow rate.

power output was generated as depicted in Fig. 6. When the TIP increases, the enthalpy difference across the turbine rises as well and causes an increase of the turbine power output.

The variation of the thermal efficiency versus TIP is also shown in Fig. 5. It can be concluded that the thermal efficiency increased slightly from 4.17% to 4.60% as the TIP increased from 2.0 MPa to 3.0 MPa. The rise of the TIP led to a larger heat flow transferred from the HC cycle to the HT cycle, while pump work increased as well. However, the increasing rate of net power slightly outweighs that of the increasing rate of the heat flow input $\dot{Q}_{HC}$, which led to a slight increase in thermal efficiency according to Eq. (6).

The influence of the TIP on exergy efficiency is also shown in Fig. 5. It can be noted that the exergy efficiency increases with TIP. When the TIP increases from 2.0 MPa to 3.0 MPa, the exergy efficiency rises from 16.30% to 17.11%. This increasing trend is expected, as the TIP increases, the enthalpy difference across the turbine increases, which results in a higher turbine power output and a better exergy efficiency. In other words, the ratio of net power to exergy flow input $\dot{E}_{in}$ increases with increasing TIP.

Fig. 6 displays the turbine efficiency and the enthalpy difference across the turbine upon variation of the TIP. As the TIP increased, the enthalpy difference rises from 26.87 kJ/kg to 32.82 kJ/kg, while the turbine efficiency increased from 29.1% to 31.6%. Generally, by comparing condition 1 with condition 2, the highest turbine power output was gained under condition 2 at a heat source temperature of 533 K and a TIP of 3.0 MPa, which is due to the positive impact of the higher TIP. The thermal and exergy efficiencies under condition 2 were lower than under condition 1. This can be explained as follows: Increasing the TIP required more pump work during the experiment. Moreover, the HT cycle absorbed more heat from the HC cycle under

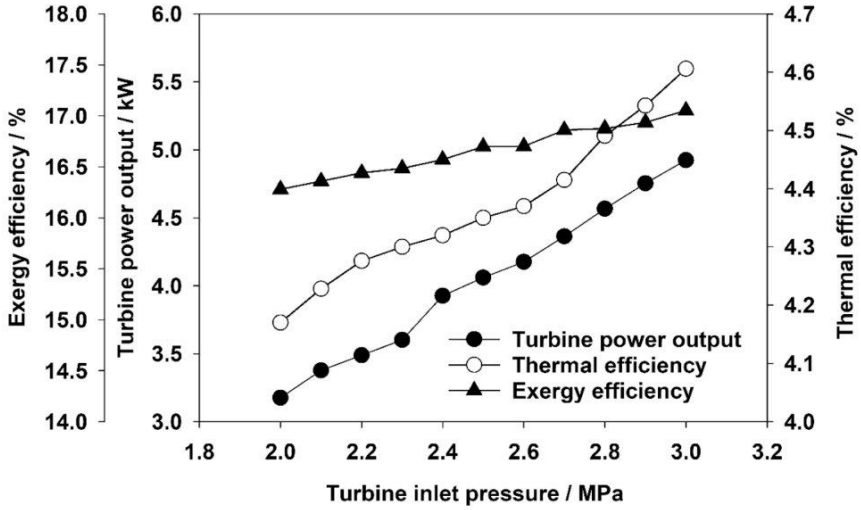

Fig. 5. Variation of turbine power output, thermal efficiency and exergy efficiency as a function of turbine inlet pressure.

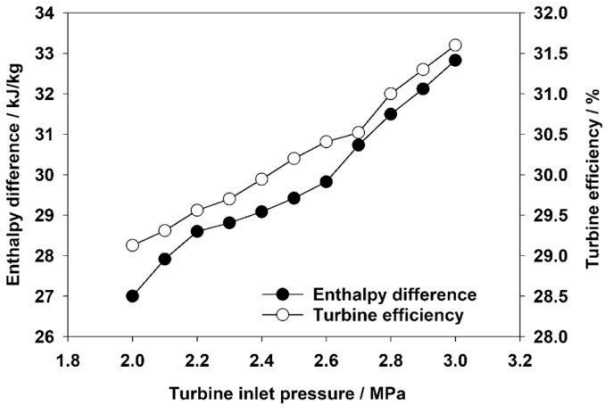

Fig. 6. Variation of enthalpy difference and turbine efficiency as a function of turbine inlet pressure.

condition 2. This results in a lower thermal efficiency, which is related to turbine power output, pump work and heat flow input. Increasing the pump work reduced the increasing rate of the net power which directly affected the exergy efficiency. The system achieved the maximum thermal and exergy efficiencies under condition 1, where the heat source temperature was 533 K and the mass flow rate 0.12 kg/s. In contrast, the maximum turbine power output was obtained under condition 2, where the heat source was 533 K, TIP 3.0 MPa and the mass flow rate 0.15 kg/s. Solely turbine power output does not reflect system performance improvement because focusing on selected parameters may have a negative impact on the overall system performance. In the case of a two-ORC system, it is better to adopt thermal and exergy efficiencies as criteria for the system performance [10].

Fig. 7 depicts the heat transfer and temperature profiles in HE1 under conditions 1 and 2 at operating parameters where the maximum turbine power output was achieved. State points 1 and 2 refer to the inlet and outlet of Therminol 66 in the HC cycle, respectively. Moreover, HE1 was divided for both conditions into three sections: preheating (3-3a), evaporation (3a-3b) and superheating (3b-4). Fig. 7 also shows PPTD under conditions 1 and 2, which is the minimum temperature difference between Therminol 66 and cyclopentane in HE1. The PPTD was calculated by the following equations according to Figs. 2 and 7.

Under condition 1:

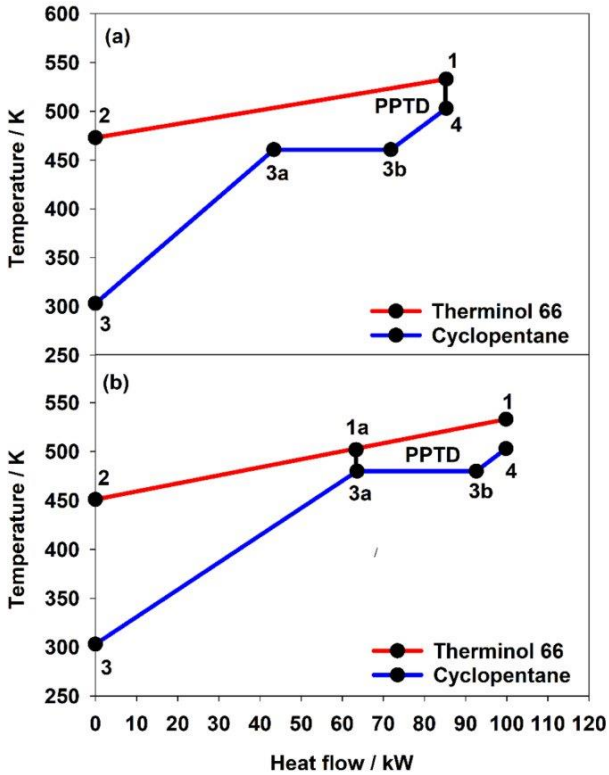

Fig. 7. Comparison of heat transfer, temperature profiles and PPDT in the heat exchanger HE1 under (a) condition 1 and (b) condition 2.

$$\mathrm{PPDT} = T_1 - T_4 \tag{12}$$

Under condition 2:

$$\dot{Q}_{3-3a} = -\dot{Q}_{2-1a} \tag{13}$$

$$\dot{Q}_{3-3a} = \dot{m}_{HT} \cdot (h_{3a} - h_3) \tag{14}$$

$$\dot{Q}_{2-1a} = \dot{m}_{HC} \cdot c_p \cdot (T_2 - T_{1a}) \tag{15}$$

$$T_{1a} = \frac{\dot{Q}_{2-1a}}{\dot{m}_{HC} \cdot c_p} + T_2 \quad (16)$$

$$\text{PPDT} = T_{1a} - T_{3a} \quad (17)$$

The heat flow-temperature diagram gives a clearer picture of the heat exchanger's performance and the matching between Therminol 66 and the cyclopentane during evaporation for optimal exergy utilization of the heat source temperature. Furthermore, an optimal PPTD during the heat transfer from the heat source to the HC cycle and to the HT cycle may reduce exergy losses.

Fig. 7 (a) represents the operation parameters where the maximum turbine power output of 4.6 kW was gained under condition 1. At a heat source temperature of 533 K, a heat flow of 83 kW was transferred from the HC cycle to the HT cycle. The transferred heat flow was utilized for preheating, evaporating and superheating a mass flow rate of 0.12 kg/s of cyclopentane from state point 3 to state point 4. The PPTD under condition 1 was 30 K and was located at the HE1 outlet.

Fig. 7 (b) depicts the operation parameters where the maximum turbine power output of 4.9 kW was yielded under condition 2. At a heat source temperature of 533 K, the HC cycle transferred a heat flow of 99.82 kW to the LT cycle. The heat flow was employed for preheating, evaporating and superheating 0.15 kg/s of cyclopentane from state point 3 to state point 4. The PPTD was 23 K and was located at the beginning of the evaporation section (3a-3b). However, the location of the PPTD depends on the temperature profiles in HE1, the amount of the heat flow from the HC cycle and system performance. The PPTD is a significant factor affecting the heat flow from the HC cycle to the HT cycle. Moreover, the PPTD is related to the heat exchange surface area and the performance of the heat source fluid. Optimal PPTD lead to small exergy losses between the two streams in the HE1, but require a large heat exchange surface area to transfer the heat flow from Therminol 66 to cyclopentane in the HT cycle. The variation in the PPTD values in Fig. 7 (a) and (b) is due to several factors, which are the difference in mass flow, the amount of transferred heat flow and the inlet and outlet temperature of HE1 in both cases. At the highest heat source temperature of 533 K, the heat flow under condition 2 was higher than that under condition 1, but the thermal and exergy efficiencies were lower. That means the amount of transferred heat flow that was converted into useful work and the utilization of source heat temperature under condition 2 was lower than that under condition 1.

6.3. Effects of heat source temperature on the LT cycle performance (condition 3)

During the present experiments, three working fluids, i.e. propane, butane and pentane, were used to investigate the heat transfer from the HT cycle to the LT cycle. The throttle in the LT cycle was manually adjusted to provide an appropriate expansion process according to the properties of the working fluids and the operational conditions of the system.

Since the present test rig was designed as a cascaded two-ORC system, the second heat exchanger HE2 was a crucial component in this experiment for the heat transfer between the HT cycle and the LT cycle. It was important to investigate the different parameters and operational conditions related to HE2 characteristics, such as inlet temperature, mass flow rates and HE2 inlet pressure.

Fig. 8 shows a comparison of the heat transfer rate form the HT cycle to the LT cycle for the three organic fluids. The mass flow rate of the working fluids in the LT cycle was varied from 0.030 kg/s to 0.035 kg/s. The heat source temperature in the HC cycle for pentane and butane ranged from 453 K to 533 K in increments of 10 K, while the heat source temperature for propane was in a smaller range from 453 K to 503 K because of its low critical temperature (369.89 K). A comparison between the three configurations shows that among the three working fluids, pentane is the one with the highest transferred heat flow rates.

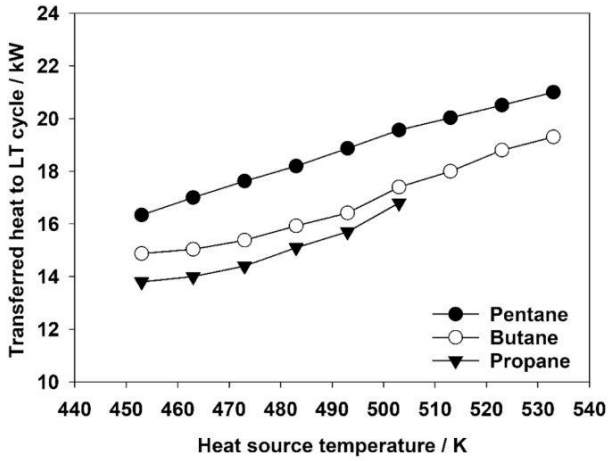

Fig. 8. Variation of heat flow from the HT cycle to the LT cycle as a function of heat source temperature for three different LT cycle working fluids.

The maximum transferred heat flow to the LT cycle was 21 kW, obtained at a mass flow rate of 0.035 kg/s and a heat source temperature of 533 K. Because the heat source temperature was not fixed, the heat absorbed by the LT cycle varied and rose with an increase of the heat source temperature. As the heat source temperature was raised from 453 K to 503 K, the transferred heat flow grew from 13.80 kW to 16.82 kW in case of propane and from 14.90 kW to 19.30 kW for butane, while the according numbers were 16.35 kW to 21.00 kW for pentane. Generally, the amount of transferred heat flow depends on the thermo-physical properties of the working fluids and the process parameters of the LT cycle, such as temperature and the mass flow rate. As the amount of transferred heat flow increased with the rising heat source temperature, it was primarily expected that the maximum transferred heat flow in the case of propane is lower. This is primarily because the maximum heat source temperature was lower than that of pentane and butane.

6.4. Effects of HE2 inlet pressure on the LT cycle performance (condition 4)

This test was carried out at a heat source temperature of 533 K, where the highest amount of heat flow was transferred from the HT cycle to the LT cycle under condition 3 by using pentane and butane as working fluids. The heat source temperature for propane was 503 K because of its low critical temperature. The mass flow rate of the working fluids was varied in the range from 0.035 kg/s to 0.048 kg/s. The variation of HE2 inlet pressure and the heat transfer to the LT cycle can be seen in Fig. 9. For all working fluids, an increase of the HE2 inlet pressure led to a gradual increase of the heat transfer from the HT cycle to the LT cycle. The transferred heat flow for propane increased from 14.88 kW to 19.30 kW at a heat source temperature of 503 K, as the HE2 inlet pressure rises in the limited range from 3.2 MPa to 3.6 MPa to avoid critical conditions. Moreover, when using butane as a working fluid, the HE2 inlet pressure varied from 2.2 MPa to 2.7 MPa, while the transferred heat flow increased from 16.21 kW to 21.00 kW. The maximum achievable heat transfer during these experiments was 23 kW by employing pentane as working fluid, when the HE2 inlet pressure was raised from 1.2 MPa to 1.7 MPa. As mentioned earlier, it was expected that the amount of transferred heat flow in the case of propane is lower since the maximum heat source temperature is less than that in the case of pentane or butane.

The heat transfer rate values under condition 4 are higher than under condition 3 for all working fluids. The main reason is that the variation of the mass flow rate of working fluids under condition 1 was larger than that under condition 3. For all working fluids under condition 4, the

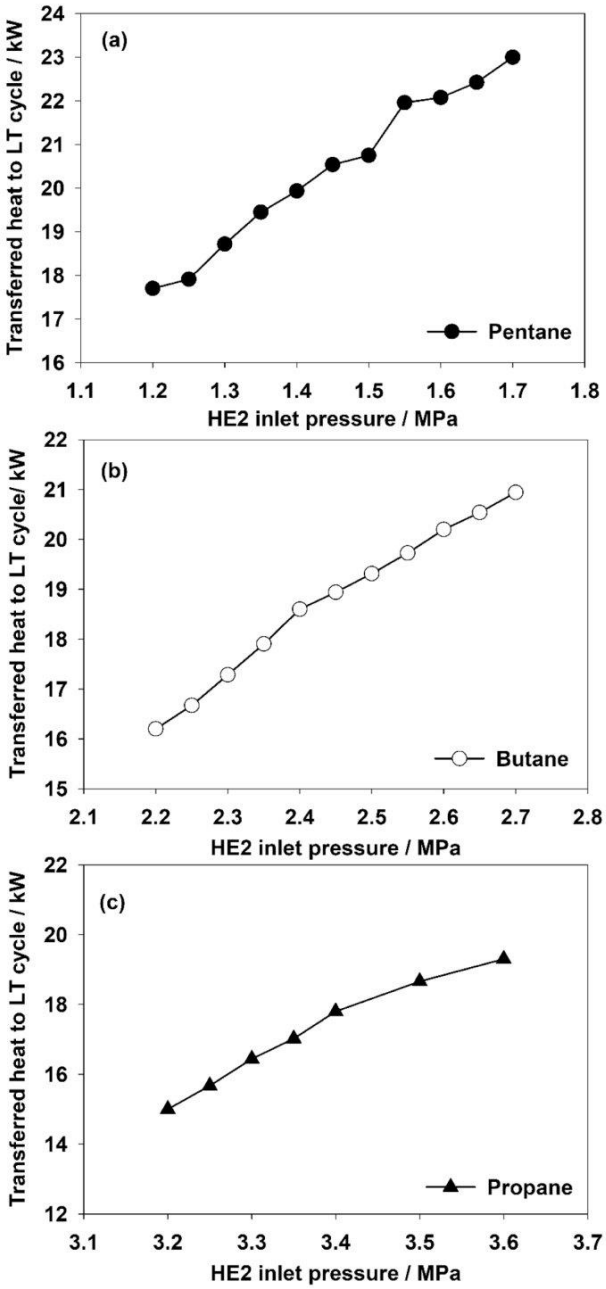

Fig. 9. Variation of heat transfer from the HT cycle to the LT cycle as a function of inlet pressure of heat exchanger HE2, by using (a) pentane, (b) butane and (c) propane as a working fluid in the LT cycle.

mass flow rate varied from 0.035 kg/s to 0.048 kg/s and led to an increase of the HE2 inlet pressure and an increase of the absorbed heat flow rate from the HT cycle. Furthermore, the HE2 inlet pressure had a more significant effect on the heat transfer rate values than the heat source temperature variation. Since the LT cycle employed a throttle as an expansion device, it was important to explore the heat transfer between the two cycles and the PPTD to examine the performance of HE2, which is helpful for designing the LT cycle's turbine.

Fig. 10 shows the temperature profile, heat flow and PPTD at the operating condition where the maximum amount a heat flow was transferred from the HT cycle to the LT cycle under condition 3 in the

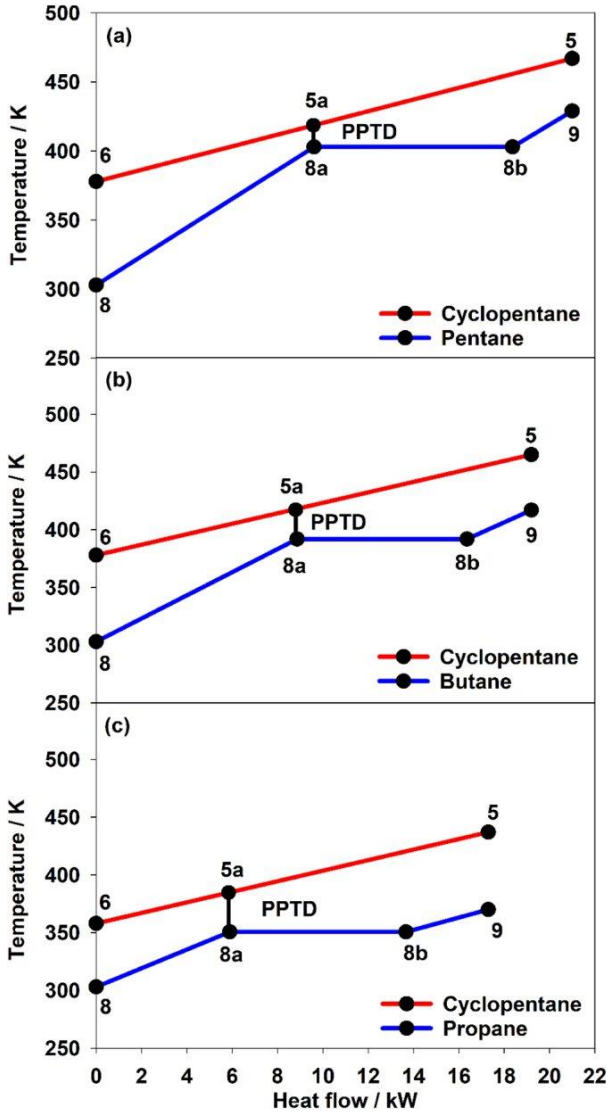

Fig. 10. Comparison of heat transfer, temperature profiles and PPTD in heat exchanger HE2 under condition 3, by using (a) pentane, (b) butane and (c) propane as a working fluid in the LT cycle.

HE2. The PPTD under these conditions was calculated by

$$\dot{Q}_{9-8a} = -\dot{Q}_{5-5a} \tag{18}$$

$$\dot{Q}_{9-8a} = \dot{m}_{LT}\cdot(h_9 - h_{8a}) \tag{19}$$

$$\dot{Q}_{5-5a} = \dot{m}_{HT}\cdot c_p\cdot(T_5 - T_{5a}) \tag{20}$$

$$T_{5a} = \frac{\dot{Q}_{5-5a}}{\dot{m}_{HT}\cdot c_p} + T_5 \tag{21}$$

$$\mathrm{PPDT} = T_{5a} - T_{8a} \tag{22}$$

Fig. 10 (a) shows operating parameters where the maximum heat flow was transferred under condition 3 in the HE2 by using pentane as a working fluid. At a heat source temperature of 533 K and a mass flow rate of 0.12 kg/s, cyclopentane from the HT cycle supplied the LT cycle a heat flow of 21 kW. The absorbed heat was utilized for preheating, evaporating and superheating a mass flow rate of 0.035 kg/s of pentane

from state point 8 to state point 9. The PPTD was 19 K and was located at the beginning of the evaporation section (8a-8b).

Fig. 10 (b) shows the temperature profile, heat flow and PPTD where the maximum heat flow absorbed by butane under condition 3 in the HE2. A heat flow of 19.30 kW was transferred from the HT cycle to the LT cycle. The absorbed heat was used for preheating, evaporating and superheating 0.035 kg/s of butane from the state point 8 to state point 9. The PPTD was 25 K and located at the beginning of evaporation section (8a-8b).

Fig. 10 (c) shows the same properties when propane was employed as a working fluid. The mass flow rate of cyclopentane was raised to 0.12 kg/s at a heat source temperature of 503 K. A heat flow of 16.82 kW was transferred from the HT cycle to the LT cycle for preheating, evaporating and superheating 0.04 kg/s of propane. The PPTD was 33 K and was located at the beginning of the evaporation section (8a-8b).

Fig. 11 shows the heat transfer, temperature profiles and the PPTD in HE2 at operating parameters where the maximum heat flow was transferred from the HT cycle to the LT cycle under condition 4. In the HT cycle, the mass flow rate of cyclopentane was raised up to 0.12 kg/s at a heat source temperature of 533 K. A heat flow of 23.00 kW was transferred to the LT cycle from the HT cycle. The heat flow was utilized for preheating, evaporating and superheating 0.04 kg/s of pentane at a pressure of 1.7 MPa from state point 8 to state point 9 as shown in Fig. 11 (a). The PPTD was 13 K and was located at the beginning of the evaporation section (8a-8b).

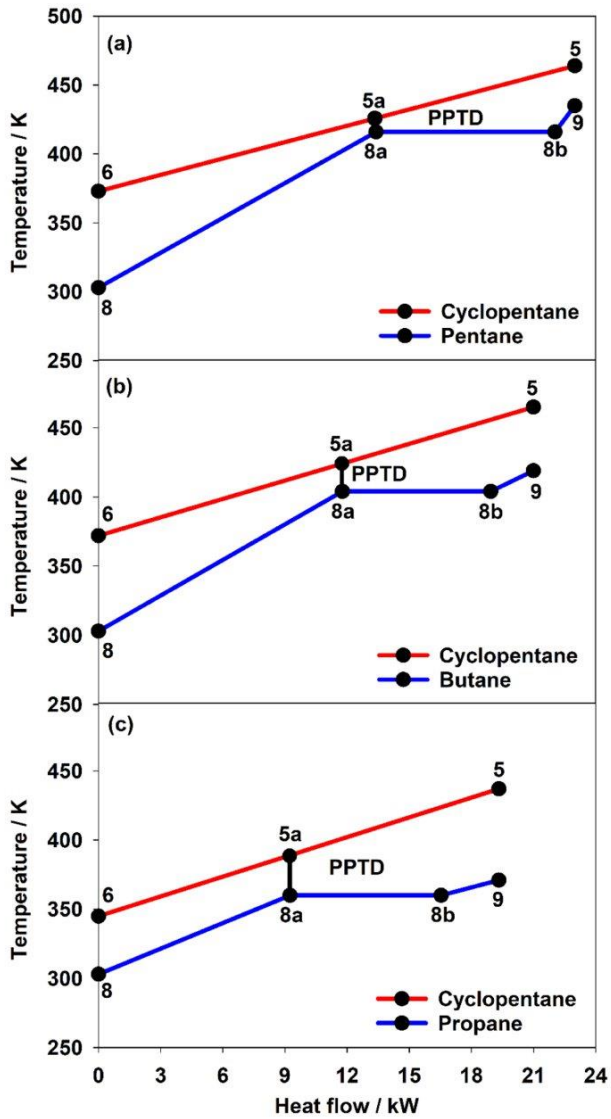

Fig. 11. Comparison of heat transfer, temperature profiles and PPTD in heat exchanger HE2 under condition 4, by using (a) pentane, (b) butane and (c) propane as a working fluid in the LT cycle.

Fig. 11 (b) shows the same properties in HE2 under condition 4 by using butane as a working fluid. A heat flow of 21.00 kW was transferred to the LT cycle for preheating, evaporating and superheating 0.04 kg/s of butane at a heat source temperature of 533 K and a pressure of 2.7 MPa. The PPTD was 21 K and located at the beginning of the evaporation section (8a-8b).

Fig. 11 (c) is analogous for propane as a working fluid. At a heat source temperature of 503 K, propane was pressurized to 3.6 MPa. A heat flow of 19.30 kW was transferred to the LT cycle for preheating, evaporating and superheating a mass flow rate of 0.048 kg/s of propane from state point 8 to state point 9. The PPTD was 30 K and located at the beginning of the evaporation section (8a-8b).

The PPTD is an important factor for the heat exchanger effectiveness and is related to the overall system performance. The lower PPTD led to an increase of the absorbed heat flow from the HT cycle. Moreover, the amount of transferred heat flow to the LT cycle and the PPTD location depend on the HT cycle performance, the temperature profile of the HE2, thermo-physical properties of the working fluid and process parameters of the LT cycle. By comparing Figs. 10 and 11, the PPTD values under condition 4 are lower than under condition 3 for all working fluids and the maximum transferred heat flow for all working fluids is higher than that under condition 3. This variation may be explained as follows: Under condition 4, the mass flow rate variation of the working fluids was larger than that under condition 3. This led to an increase in the absorbed heat flow from the HT cycle, which was higher under condition 4. Therefore, under condition 4, the PPTD values were lower than those under condition 3 in the HE2 for the same working fluids.

7. Conclusion

A cascaded two-ORC system was studied experimentally, filling the gap in scientific research with respect to testing the two-ORC system for a wide range of temperatures and pressures. Various parameters were employed to provide practical results that can be used for system improvements and optimization. Cyclopentane was used in the HT cycle, while pentane, butane and propane were alternatively employed as working fluids in the LT cycle. The purpose of this work was to investigate the cascaded two-ORC system performance under different operating parameters. Results were presented for the performance of the HT cycle and the LT cycle for a heat source temperature between 453 K and 533 K as well as different values of the mass flow rate and the turbine inlet pressure. The maximum power output of the HT cycle was 4.92 kW for a heat source temperature of 533 K and working fluid mass flow rate of 0.15 kg/s. The maximum thermal efficiency was 5.5% for a heat source temperature of 533 K and a mass flow rate of 0.12 kg/s, while the maximum exergy efficiency was 20.15% under the same condition. Since the LT cycle employed a throttle as an expansion device, it was important to explore the heat transfer between the two cycles and the PPTD to examine the performance of HE2. The heat transfer rate between the HT cycle and the LT cycle was examined by employing three working fluids. The results illustrate that part of the residual heat from the HT cycle was absorbed by the working fluid in the LT cycle and the remainder was dissipated by the cooling cycle. Heat transfer measurements showed that the best option among the considered fluids was pentane. The maximum heat transferred to the LT cycle and absorbed by pentane was 23 kW. However, the majority of the heat flow from HT cycle was not transferred to the LT cycle. The present experimental results demonstrate that more work is needed to enhance the system performance. The experimental investigations were promising and

showed that the two-ORC system is suitable to utilize heat sources under different operational conditions. The present paper is encouraging further experimental and theoretical examinations for clarifying the advantages of cascaded two-ORC systems.

Furthermore, to present the convenience of cascaded two-ORC systems, a new turbine must be designed and built to study the power output, thermal and exergy efficiency of the LT cycle. In addition, the HT cycle performance should be studied for varying working fluids.

Author contribution

Wameedh Khider Abbas Abbas has written the manuscript, developed the cycle calculation, carried out the field tests and analyzed the results. He conducted the cycle test and selected the working fluids and operational conditions. Matthias Linnemann and Elmar Baumhögger supported the test operation. Jadran Vrabec supported the team over the entire time of this research project and contributed to the manuscript's revision.

Declaration of Competing Interest

The authors declare that they have no known competing financial interests or personal relationships that could have appeared to influence the work reported in this paper.

Acknowledgements

We gratefully acknowledge the German Academic Exchange Service (DAAD) for financial support and the help provided by Dr. Gerhard Herres, University of Paderborn.

References

[1] Tchanche BF, Lambrinos Gr, Frangoudakis A, Papadakis G. Low-grade heat conversion into power using organic Rankine cycles – a review of various applications. Renew Sustain Energy Rev 2011;15(8):3963–79. https://doi.org/10.1016/j.rser.2011.07.024.
[2] Bamorovat Abadi G, Kim KC. Investigation of organic Rankine cycles with zeotropic mixtures as a working fluid: advantages and issues. Renew Sustain Energy Rev 2017;73:1000–13. https://doi.org/10.1016/j.rser.2017.02.020.
[3] Zhai H, An Q, Shi L, Lemort V, Quoilin S. Categorization and analysis of heat sources for organic Rankine cycle systems. Renew Sustain Energy Rev 2016;64:790–805. https://doi.org/10.1016/j.rser.2016.06.076.
[4] Vivian J, Manente G, Lazzaretto A. A general framework to select working fluid and configuration of ORCs for low-to-medium temperature heat sources. Appl Energy 2015;156:727–46. https://doi.org/10.1016/j.apenergy.2015.07.005.
[5] Saleh B, Koglbauer G, Wendland M, Fischer J. Working fluids for low-temperature organic Rankine cycles. Energy 2007;32(7):1210–21. https://doi.org/10.1016/j.energy.2006.07.001.
[6] Bao J, Zhao Li. A review of working fluid and expander selections for organic Rankine cycle. Renew Sustain Energy Rev 2013;24:325–42. https://doi.org/10.1016/j.rser.2013.03.040.
[7] Ma W, Liu T, Min R, Li M. Effects of physical and chemical properties of working fluids on thermodynamic performances of medium-low temperature organic Rankine cycles (ORCs). Energy Convers Manage 2018;171:742–9. https://doi.org/10.1016/j.enconman.2018.06.032.
[8] Wang EH, Zhang HG, Fan BY, Ouyang MG, Yang FY, Yang K, Wang Z, Zhang J, Yang FB. Parametric analysis of a dual-loop ORC system for waste heat recovery of a diesel engine. Appl Therm Eng 2014;67(1-2):168–78. https://doi.org/10.1016/j.applthermaleng.2014.03.023.
[9] Lecompte S, Huisseune H, van den Broek M, Vanslambrouck B, De Paepe M. Review of organic Rankine cycle (ORC) architectures for waste heat recovery. Renew Sustain Energy Rev 2015;47:448–61. https://doi.org/10.1016/j.rser.2015.03.089.
[10] Braimakis K, Karellas S. Exergetic optimization of double stage Organic Rankine Cycle (ORC). Energy 2018;149:296–313. https://doi.org/10.1016/j.energy.2018.02.044.
[11] Yu G, Shu G, Tian H, Huo Y, Zhu W. Experimental investigations on a cascaded steam-/organic-Rankine-cycle (RC/ORC) system for waste heat recovery (WHR) from diesel engine. Energy Convers Manage 2016;129:43–51. https://doi.org/10.1016/j.enconman.2016.10.010.
[12] Gang P, Jing Li, Jie Ji. Design and analysis of a novel low-temperature solar thermal electric system with two-stage collectors and heat storage units. Renewable Energy 2011;36(9):2324–33. https://doi.org/10.1016/j.renene.2011.02.008.
[13] Fu W, Zhu J, Li T, Zhang W, Li J. Comparison of a Kalina cycle based cascade utilization system with an existing organic Rankine cycle based geothermal power system in an oilfield. Appl Therm Eng 2013;58(1-2):224–33. https://doi.org/10.1016/j.applthermaleng.2013.04.012.
[14] Drescher U, Brüggemann D. Fluid selection for the Organic Rankine Cycle (ORC) in biomass power and heat plants. Appl Therm Eng 2007;27(1):223–8. https://doi.org/10.1016/j.applthermaleng.2006.04.024.
[15] Sun H, Zhu H, Liu F, Ding He. Simulation and optimization of a novel Rankine power cycle for recovering cold energy from liquefied natural gas using a mixed working fluid. Energy 2014;70:317–24. https://doi.org/10.1016/j.energy.2014.03.128.
[16] Sung T, Kim KC. Thermodynamic analysis of a novel dual-loop organic Rankine cycle for engine waste heat and LNG cold. Appl Therm Eng 2016;100:1031–41. https://doi.org/10.1016/j.applthermaleng.2016.02.102.
[17] Mehrpooya M, Ashouri M, Mohammadi A. Thermoeconomic analysis and optimization of a regenerative two-stage organic Rankine cycle coupled with liquefied natural gas and solar energy. Energy 2017;126:899–914. https://doi.org/10.1016/j.energy.2017.03.064.
[18] Yang F, Cho H, Zhang H, Zhang J. Thermoeconomic multi-objective optimization of a dual loop organic Rankine cycle (ORC) for CNG engine waste heat recovery. Appl Energy 2017;205:1100–18. https://doi.org/10.1016/j.apenergy.2017.08.127.
[19] Kosmadakis G, Manolakos D, Kyritsis S, Papadakis G. Comparative thermodynamic study of refrigerants to select the best for use in the high-temperature stage of a two-stage organic Rankine cycle for RO desalination. Desalination 2009;243(1-3):74–94. https://doi.org/10.1016/j.desal.2008.04.016.
[20] Xue X, Guo C, Du X, Yang L, Yang Y. Thermodynamic analysis and optimization of a two-stage organic Rankine cycle for liquefied natural gas cryogenic exergy recovery. Energy. 2015;83:778–87. https://doi.org/10.1016/j.energy2015.02.088.
[21] Preißinger M, Heberle F, Brüggemann D. Exergetic analysis of biomass fired double-stage organic rankine cycle (ORC), Proc. 25th Int. Conf. Effic. Cost, Optim. Simul. Energy Convers. Syst. Process. ECOS 2012. 1 (2012) 155–165.
[22] Ayachi F, Boulawz Ksayer E, Zoughaib A, Neveu P. ORC optimization for medium grade heat recovery. Energy 2014;68:47–56. https://doi.org/10.1016/j.energy.2014.01.066.
[23] Yun E, Park H, Yoon SY, Kim KC. Dual parallel organic Rankine cycle (ORC) system for high efficiency waste heat recovery in marine application. J Mech Sci Technol 2015;29(6):2509–15. https://doi.org/10.1007/s12206-015-0548-5.
[24] Choi I-H, Lee S, Seo Y, Chang D. Analysis and optimization of cascade Rankine cycle for liquefied natural gas cold energy recovery. Energy 2013;61:179–95. https://doi.org/10.1016/j.energy.2013.08.047.
[25] Li P, Li J, Pei G, Munir A, Ji J. A cascade organic Rankine cycle power generation system using hybrid solar energy and liquefied natural gas. Sol Energy 2016;127:136–46. https://doi.org/10.1016/j.solener.2016.01.029.
[26] Shu G, Liu L, Tian H, Wei H, Yu G. Parametric and working fluid analysis of a dual-loop organic Rankine cycle (DORC) used in engine waste heat recovery. Appl Energy 2014;113:1188–98. https://doi.org/10.1016/j.apenergy.2013.08.027.
[27] Linnemann M, Priebe K-P, Heim A, Wolff C, Vrabec J. Experimental investigation of a cascaded organic Rankine cycle plant for the utilization of waste heat at high and low temperature levels. Energy Convers Manage 2020;205:112381. https://doi.org/10.1016/j.enconman.2019.112381.
[28] Shu G, Yu G, Tian H, Wei H, Liang X, Huang Z. Multi-approach evaluations of a cascade-Organic Rankine Cycle (C-ORC) system driven by diesel engine waste heat: Part A – thermodynamic evaluations. Energy Convers Manage 2016;108:579–95. https://doi.org/10.1016/j.enconman.2015.10.084.
[29] Dubberke FH, Linnemann M, Abbas WK, Baumhögger E, Priebe K-P, Roedder M, Neef M, Vrabec J. Experimental setup of a cascaded two-stage organic Rankine cycle. Appl Therm Eng 2018;131:958–64. https://doi.org/10.1016/j.applthermaleng.2017.11.137.
[30] Mago PJ, Chamra LM, Srinivasan K, Somayaji C. An examination of regenerative organic Rankine cycles using dry fluids. Appl Therm Eng 2008;28(8-9):998–1007. https://doi.org/10.1016/j.applthermaleng.2007.06.025.
[31] Lemmon EW, Huber ML, McLinden MO. Reference fluid thermodynamic and transport properties (REFPROP), Version 9.0, in NIST Standard Reference Database 23. Gaithersburg, MD: National Institute of Standard and Technology; 2007.
[32] Schilling J, Lampe M, Gross J, Bardow A. 1-stage CoMT-CAMD: an approach for integrated design of ORC process and working fluid using PC-SAFT. Chem Eng Sci 2017;159:217–30. https://doi.org/10.1016/j.ces.2016.04.048.
[33] Rayegan R, Tao YX. A procedure to select working fluids for Solar Organic Rankine Cycles (ORCs). Renew Energy 2011;36(2):659–70. https://doi.org/10.1016/j.renene.2010.07.010.
[34] Siddiqi MA, Atakan B. Alkanes as fluids in Rankine cycles in comparison to water, benzene and toluene. Energy 2012;45(1):256–63. https://doi.org/10.1016/j.energy.2012.06.005.
[35] Invernizzi CM, Iora P, Manzolini G, Lasala S. Thermal stability of n-pentane, cyclopentane and toluene as working fluids in organic Rankine engines. Appl Therm Eng 2017;121:172–9. https://doi.org/10.1016/j.applthermaleng.2017.04.038.
[36] Zhai H, Shi L, An Q. Influence of working fluid properties on system performance and screen evaluation indicators for geothermal ORC (organic Rankine cycle) system. Energy 2014;74:2–11. https://doi.org/10.1016/j.energy.2013.12.030.
[37] Mahmoudi A, Fazli M, Morad MR. A recent review of waste heat recovery by Organic Rankine Cycle. Appl Therm Eng 2018;143:660–75. https://doi.org/10.1016/j.applthermaleng.2018.07.136.
[38] Qiu G. Selection of working fluids for micro-CHP systems with ORC. Renew Energy 2012;48:565–70. https://doi.org/10.1016/j.renene.2012.06.006.

[39] Lemmon EW, McLinden MO, Wagner W. Thermodynamic properties of propane. III. A reference equation of state for temperatures from the melting line to 650 K and pressures up to 1000 MPa. J Chem Eng Data 2009;54(12):3141–80. https://doi.org/10.1021/je900217v.
[40] Bücker D, Wagner W. Reference Equations of State for the Thermodynamic Properties of Fluid Phase n-Butane and Isobutane. J Phys Chem Ref Data 2006;35(2):929–1019. https://doi.org/10.1063/1.1901687.
[41] Gedanitz H, Davila MJ, Lemmon EW. Speed of sound measurements and a fundamental equation of state for cyclopentane. J Chem Eng Data 2015;60(5):1331–7. https://doi.org/10.1021/je5010164.
[42] Ntavou E, Kosmadakis G, Manolakos D, Papadakis G, Papantonis D. Experimental testing of a small-scale two stage Organic Rankine Cycle engine operating at low temperature. Energy 2017;141:869–79. https://doi.org/10.1016/j.energy.2017.09.127.
[43] Galloni E, Fontana G, Staccone S. Design and experimental analysis of a mini ORC (organic Rankine cycle) power plant based on R245fa working fluid. Energy 2015;90:768–75. https://doi.org/10.1016/j.energy.2015.07.104.
[44] Butcher CJ, Reddy BV. Second law analysis of a waste heat recovery based power generation system. Int J Heat Mass Transf 2007;50(11-12):2355–63. https://doi.org/10.1016/j.ijheatmasstransfer.2006.10.047.
[45] Sung T, Yun E, Kim HD, Yoon SY, Choi BS, Kim K, Kim J, Jung YB, Kim KC. Performance characteristics of a 200-kW organic Rankine cycle system in a steel processing plant. Appl Energy 2016;183:623–35. https://doi.org/10.1016/j.apenergy.2016.09.018.
[46] Zhou N, Wang X, Chen Z, Wang Z. Experimental study on Organic Rankine Cycle for waste heat recovery from low-temperature flue gas. Energy 2013;55:216–25. https://doi.org/10.1016/j.energy.2013.03.047.
[47] Wang P, Zhao P, Lai Y, Wang J, Dai Y. Performance comparison of different combined heat and compressed air energy storage systems integrated with organic Rankine cycle. Int J Energy Res 2019;43:8410–25. https://doi.org/10.1002/er.4839.
[48] Safarian S, Aramoun F. Energy and exergy assessments of modified Organic Rankine Cycles (ORCs). Energy Rep 2015;1:1–7. https://doi.org/10.1016/j.egyr.2014.10.003.

5.3. Cascaded dual-loop organic Rankine cycle with alkanes and low global warming potential refrigerants as working fluids

Abbas WKA, Vrabec J. Cascaded dual-loop organic Rankine cycle with alkanes and low global warming potential refrigerants as working fluids. Energy Conversion and Management 2021;249:114843. DOI: 10.1016/J.ENCONMAN.2021.114843.

With permission of Elsevier reprinted from the journal Energy Conversion and Management (Copyright 2021).

In this paper, alkanes and 31 low-GWP refrigerants were selected as working fluids for the CORC system. Thermal and exergy efficiencies were used as criteria to evaluate the system performance. The working fluid selection was based on the environmental considerations (GWP $\leq$ 150). In addition, the relation between the thermo-physical properties and system performance was investigated. The obtained results underlined the dependence of thermal and exergy efficiencies on the critical temperature and molecular structure of working fluids. Moreover, a comparison between the regular ORC and the CORC system was performed with respect to thermal efficiency.

The author of this thesis selected the working fluids, operating conditions, simulation parameters and conducted the simulations with EBSILON®Professional. The author validated the results by comparison with literature references. The paper was written by the author of this thesis and was revised by Jadran Vrabec.

Energy Conversion and Management 249 (2021) 114843

Contents lists available at ScienceDirect

Energy Conversion and Management

journal homepage: www.elsevier.com/locate/enconman

Cascaded dual-loop organic Rankine cycle with alkanes and low global warming potential refrigerants as working fluids

Wameedh Khider Abbas Abbas [a], Jadran Vrabec [b,*]

[a] Thermodynamics and Energy Technology, University of Paderborn, Warburger Straße 100, 33098 Paderborn, Germany
[b] Thermodynamics and Process Engineering, Technical University of Berlin, Ernst-Reuter-Platz 1, 10587 Berlin, Germany

ARTICLE INFO

Keyword:
Cascaded dual-loop ORC
Low GWP refrigerants
Thermal efficiency
Critical temperature of working fluids

ABSTRACT

A cascaded dual-loop organic Rankine cycle (CD-ORC) consisting of a high-temperature ORC (HT-ORC) and a low-temperature ORC (LT-ORC) with a shared heat exchanger is studied. Thermal efficiency is investigated as a key indicator for system performance over a wide range of heat source temperature ranging from 170 °C to 330 °C. The relation between the thermal efficiency and the critical temperature of the working fluids is explored. For this purpose, six alkanes and 31 refrigerants with a low GWP (≤150) are considered as working fluids in the HT-ORC and the LT-ORC, respectively. Cyclohexane and cyclopentane are found to be suitable for the HT-ORC with a maximum thermal efficiency of 19.13% and 18.03%. The thermal efficiency of both loops is highly affected by the working fluids since it increases with the critical temperature. As a whole, the CD-ORC may achieve a total thermal efficiency of 25.24%, 24.88% and 24.60% when using the working fluid combinations cyclohexane-R1366mzz(Z), cyclohexane-R1233zd(E) or cyclohexane-butane. This indicates that low GWP refrigerants are well-suited for LT-ORC. Compared to regular ORC, CD-ORC systems may achieve a thermal efficiency that is better by around a quarter.

1. Introduction

The rise in population as well as urban and technology development was accompanied by a significantly increased demand for energy, which is met by fossil fuels as the primary energy source due to their availability and low cost. However, studies have analyzed the risks of using fossil fuels and their derivatives which entail extensive pollution and threaten environmental disasters in the future [1]. Pollution and increased carbon dioxide emissions were accompanied by climate change and unprecedented weather events. The IPCC reported on August 9, 2021 that the world will reach 1.5 °C of warming within the next twenty years. There is thus a growing need to find alternative fuels, clean power sources with less harmful emissions and impact on the environment [2,3].

A large body of literature has grown around the organic Rankine cycle (ORC) as a technology to generate power from low and medium temperature heat sources. The ORC is a sustainable technology for power generation because it can utilize heat from geothermal [4], solar [5], combined heat and power [6], biomass [7], waste heat from industrial processes [8,9] or other sources [10].

Many studies have investigated different ORC architectures to enhance system performance. It was shown that multi-loop ORC theoretically can achieve a better thermal efficiency and net power output than regular ORC systems. Moreover, they have the capacity to concurrently recover heat from different sources [11–18]. Multi-loop ORC consist of several ORC loops, where each loop operates under different conditions (temperature, pressure and mass flow rate). Generally, dual-loop ORC consist of a high-temperature loop (HT-ORC) and a low-temperature loop (LT-ORC). The HT-ORC (topping ORC) is driven by the main heat source, while the LT-ORC loop (bottoming ORC) employs residual heat from the HT-ORC and/or is driven by a secondary heat source. A dual-loop ORC may allow for a better temperature profile matching between the heat source and the working fluid in the power generating cycle, which improves thermal efficiency. The disadvantage of multi-loop systems is their higher cost since they require more components than regular ORC. Such systems are also characterized by more complexity in terms of devices, sensors and operational parameters that need to be orchestrated [19].

Ayachi et al. [20] made an exergetic optimization to examine regular and dual-loop ORC performance for heat source temperatures between 150 °C and 165 °C. The authors considered three low GWP refrigerants, i.e. R1234yf, butane and isobutene, and reported that the critical temperature of the working fluid is closely related to exergy efficiency.

* Corresponding author.
E-mail address: vrabec@tu-berlin.de (J. Vrabec).

https://doi.org/10.1016/j.enconman.2021.114843
Received 31 July 2021; Accepted 3 October 2021
0196-8904/© 2021 Elsevier Ltd. All rights reserved.

Nomenclature

C1	HT-ORC condenser [−]
C2	LT-ORC condenser [−]
HE1	HT-ORC heat exchanger [−]
HE2	LT-ORC heat exchanger [−]
GWP	Global warming potential [−]
G1	HT-ORC generator [−]
G2	LT-ORC generator [−]
LNG	Liquefied natural gas [−]
M0	Heating cycle pump [−]
M1	HT-ORC pump [−]
M2	LT-ORC pump [−]
M3	Cooling cycle pump [−]
c_p	Specific isobaric heat capacity [kJ/(kg K)]
$\dot{E}_{in}$	Exergy flow input [kW]
h	Specific enthalpy [kJ/kg]
$\dot{m}_{HC}$	Mass flow rate in heating cycle [kg/s]
$\dot{m}_{HT}$	Mass flow rate in HT-ORC [kg/s]
$\dot{m}_{LT}$	Mass flow rate in LT-ORC [kg/s]
M	Molar mass [g/mol]
p_c	Critical pressure [bar]
p_e	Evaporation pressure [bar]
$\dot{Q}$	Heat flow [kW]
s	Specific entropy [kJ/(kg K)]
T_c	Critical temperature [°C]
$\dot{W}_{net}$	Net power output [kW]
$\dot{W}_P$	Pump power [kW]
$\dot{W}_T$	Turbine power output [kW]
$\eta_{ex,HT}$	Exergy efficiency of HT-ORC [%]
η_t	Turbine efficiency [%]
η_{th}	Thermal efficiency [%]

Kosmadakis et al. [21] tested 33 refrigerants to select a suitable working fluid for the HT cycle of a dual-loop ORC, where the operating temperature is between 130 °C and 140 °C. They discussed the performance of selected refrigerants together with their environmental issues and found that low GWP refrigerants may allow for good power output and thermal efficiency.

Preissinger et al. [22] studied a dual-loop ORC system driven by a wood pellet heater and considered 35 working fluids to examine system performance. The authors presented a relationship between the system performance and the thermophysical properties (critical temperature, critical pressure and molar mass) of the working fluids. They reported that the overall thermal efficiency is affected more by the LT-ORC working fluid than by the HT-ORC working fluid.

A study of a dual-loop ORC for waste heat recovery from a catalytic membrane reactor with hydrocarbons and low GWP refrigerants as working fluids has been presented by Fouad [23]. The author showed that the highest thermal efficiency was achieved with heptane as a working fluid in the HT-ORC. He found that R1234ze(Z) is a suitable alternative for R245fa and reported a maximum overall thermal efficiency of 13.39%.

Shu et al. [24] proposed a dual-loop ORC and analyzed the impact of the working fluid and other parameters on system performance. The proposed system consists of a HT-ORC to recover waste heat from exhaust gas and a LT-ORC to recover the residual heat from the HT-ORC and engine coolant. The authors selected six low GWP refrigerants for the LT-ORC and reported that the highest net power output was achieved with R1234yf. On the other hand, the maximum thermal efficiency was obtained with butane.

Wang et al. [25] investigated sub- and supercritical dual-loop ORC to recover waste heat from internal combustion engines. They utilized four pairs of working fluids, including two low GWP refrigerants, i.e. R1234yf and R1233zd(E). The authors showed that these are the most appropriate for dual-loop ORC among the considered working fluids.

Emadi et al. [26] studied working fluid selection for a dual-loop ORC, where the HT-ORC recovers heat from a solid-oxide fuel cell, while the LT-ORC was driven by LNG cryogenic energy. They considered 17 low GWP refrigerants and hydrocarbons to investigate performance in terms of exergy efficiency and turbine power output. It was found that maximum exergy efficiency and power output are achieved with a combination of hydrocarbons.

Xia et al. [27] made a theoretical investigation on working fluids for dual-loop ORC by employing their normal boiling point as a selection criterion. The authors studied 27 candidate pairs to choose combinations for HT-ORC and LT-ORC to maximize performance. They found that the optimal combination is cyclohexane-butane for the HT-ORC and LT-ORC, respectively.

Xue et al. [28] analyzed a dual-loop ORC layout to recover waste heat from LNG cryogenic energy and a gas-steam combined cycle power plant by taking two refrigerants as working fluids in the HT-ORC and LT-ORC. They studied the influence of operational conditions, such as mass flow rate and turbine inlet pressure, on performance. It was found that the maximum thermal efficiency was 25.64%.

The exergetic optimization of dual-loop ORC for waste heat recovery was studied by Braimaikis et al. [19]. They employed seven low GWP working fluids (three refrigerants and four hydrocarbons) to investigate the exergy efficiency for a heat source temperature between 100 °C and 300 °C. The authors compared dual-loop ORC with regular ORC and reported that the exergy efficiency of dual-loop ORC improves by up to a quarter when using cyclopentane and butane in the HT-ORC and LT-ORC, respectively. They noted that the dual-loop ORC is appropriate when the difference between the critical temperature of the working fluids and the heat source temperature is small.

This literature overview outlines that the dual-loop ORC is a promising technology for power generation and efficient utilization of heat sources. It also demonstrates that low GWP refrigerants are advantageous working fluids for dual-loop ORC because of environmental and safety aspects. To improve dual-loop ORC technology, more studies are needed for further development, which was the goal of this work. It was attempted to fill some of the gaps with a simulative investigation of dual-loop ORC technology by looking at a wide range of heat source temperature. Despite many studies on refrigerants, there is a lack of work that examines low GWP (≤150) working fluids, especially zeotropic and azeotropic refrigerant mixtures. Several studies have considered refrigerants in ORC systems, but most have focused on specific groups only.

This paper considers six alkanes and 31 low GWP refrigerants as working fluids in the HT-ORC and LT-ORC, respectively. The selection criteria were based solely on environmental considerations, where the selected working fluids have a GWP value of up to 150 and zero or negligible ODP. The first goal was to estimate performance in terms of thermal efficiency over a wide range of heat source temperature by employing EBSILON@Professional as simulation software, resting on the most accurate equations of state for the thermophysical properties. The second goal was to investigate the correlation between critical temperature of the working fluid and thermal efficiency. The efficiency of a dual-loop ORC system is discussed by comparing with that of a regular ORC.

2. Working fluids

The selection of working fluids is a fundamental factor for ORC system design and performance. Many publications have demonstrated their vital role [37]. In case of dual-loop ORC, the working fluids in the HT-ORC and LT-ORC must match with each other and with the heat transfer fluid in the heating cycle. Several considerations have to be taken into account in this selection to satisfy the relevant requirements, including environmental friendliness, thermophysical characteristics, specific heat, heat transfer properties, chemical stability, material capability, safety, availability in the market and cost [40,41]. A considerable amount of literature deals with the impact of thermophysical properties on ORC system performance, including its relationship with the boiling point [29,30], molar mass [31,32], Jacob number [33,34] and critical temperature [35,36]. Most investigations have focused on the relationship between the thermal efficiency and the critical temperature. Song et al. [35] reported that working fluids with a higher critical temperature may achieve a better thermal efficiency. Barse and Mann [38] as well as Aljundi [39] also reported a strong relation between thermal efficiency and critical temperature of the working fluids, which rise together.

Vivian et al. [42] proposed that the optimum difference between the heat source temperature and the critical temperature of the working fluid is 35 °C, while Zhai et al. [43] showed that this difference varies between 35 °C and 50 °C. Braimakis et al. [19] found that a small gap between heat source temperature and critical temperature of the working fluid is favorable.

In this study, the thermal efficiency was investigated by considering different working fluids over a wide range of heat source temperature. 37 working fluids were examined to analyze the impact of their critical temperature on the thermal efficiency of the HT-ORC and the LT-ORC separately as well as overall system performance. The critical temperature of the selected working fluids varies from 85.60 °C to 295.59 °C, while the critical pressure varies between 24.83 bar and 55.79 bar.

2.1. Heating cycle

As a source, electric heaters were assumed so that a suitable heat transfer fluid is needed to transfer heat efficiently from the heating cycle (HC) to the HT-ORC. Therminol 66 was selected for this purpose due to its capability to operate over a wide range of temperature up to 345 °C. Therminol 66 has a low vapor pressure, good thermal stability and is

Table 1
Properties of working fluids considered in this work.

Substance	IUPAC name/Composition*	T_c [°C]	p_c [bar]	M [g/mol]	ODP	GWP	Refs.
Alkanes							
Octane	Octane	295.59	24.836	114.23	0	~20	[40,83]
Cyclohexane	Cyclohexane	280.45	40.805	84.159	0	~20	[40,85]
Heptane	Heptane	267.05	27.357	100.2	0	~20	[40,83]
Cyclopentane	Cyclopentane	238.57	45.828	70.133	0	~20	[40,86]
Hexane	Hexane	234.67	30.441	86.175	0	~20	[40,83]
R601	Pentane	196.55	33.675	72.149	0	~20	[40,83]
HFO							
R1366mzz(Z)	(Z)-1,1,1,4,4,4-Hexaflouro-2-butene	171.35	29.03	164.06	0	9	[83,96]
R1233zd(E)	*trans*-1-chloro-3,3,3-trifluoro-1-propene	166.45	36.237	130.5	0	4.5	[87,96]
R1234ze(Z)	*cis*-1,3,3,3-Tetrafluoropropene	150.12	35.306	114.04	0	7	[89,96]
R1234ze(E)	*trans*-1,3,3,3-Tetrafluoropropene	109.26	36.349	114.04	0	7	[92,96]
R1243zf	3,3,3-Trifluoropropene	103.78	35.179	96.051	0	149	[83,96]
R1234yf	2,3,3,3-Tetrafluoroprop-1-ene	94.7	33.822	114.04	0	4	[95,96]
HC							
R600	Butane	151.98	37.96	58.122	0	4	[88,96]
R600a	Isobutane	134.66	36.29	58.122	0	3	[88,96]
RE170	Dimethyl ether	127.23	53.368	46.068	0	3	[90,96]
Cyclopropane	Cyclopropane	125.15	55.797	42.081	0	~20	[40,83]
R290	Propane	96.74	42.512	44.096	0	3	[94,96]
R1270	Propylene	91.061	45.55	42.08	0	2	[83,96]
HFC							
R152a	1,1-Difluoroethane	113.26	45.168	66.051	0	124	[91,96]
R161	Fluoroethane	102.1	50.46	48.06	0	12	[93,96]
HC mixtures							
R510	0.88 RE170, 0.12 R600a	125.67	51.186	47.244	0	3	[83,97]
R441A	0.031 R170, 0.548 R290, 0.06 R600a, 0.361 R600	118.47	44.928	48.305	0	0	[83,96]
R436B	0.52 R290, 0.48 R600a	117.43	42.509	49.873	0	20	[83,97]
R436A	0.56 R290, 0.44 R600a	115.89	42.728	49.334	0	20	[83,97]
R432A	0.8 R1270, 0.2 RE170	97.256	47.564	42.821	0	16	[83,97]
R511A	0.95 R290, 0.05 RE170	96.977	42.879	44.19	0	9	[83,96]
R433A	0.3 R1270, 0.7 R290	94.416	43.454	43.471	0	20	[83,97]
HC/HFC mixtures							
R435A	0.8 RE170, 0.2 R152a	123.07	51.919	49.035	0	27	[83,96]
R429A	0.6 RE170, 0.1 R152a, 0.3 R600a	121.95	47.297	50.762	0	14	[83,96]
R430A	0.76 R152a, 0.24 R600a	107.2	40.891	63.957	0	110	[83,96]
R431A	0.71 R290, 0.29 R152a	89.591	42.069	48.8	0	53	[83,96]
HFC/HFO mixtures							
R444A	0.12 R32, 0.05 R152a, 0.83 R1234ze(E)	106.36	44.728	96.696	0	150	[83,96]
R451A	0.898 R1234yf, 0.102 R134a	94.364	34.43	112.69	0	149	[83,96]
R457A	0.18 R32, 0.12 R152a, 0.7 R1234yf	90.046	43.08	87.605	0	139	[83,96]
R459B	0.21 R32, 0.69 R1234yf, 0.10 R1234ze(E)	87.468	43.606	91.208	0	145	[83,96]
R454C	0.215 R32, 0.785 R1234yf	85.669	43.188	90.776	0	148	[83,96]
R455A	0.03 CO2, 0.215 R32, 0.755 R1234yf	85.609	46.538	87.453	0	145	[83,96]

*The composition is given in terms of the mass fraction.

non-corrosive to metals utilized in the construction of heating systems [44]. It was selected and recommended as a heat transfer fluid in ORC systems for different heat sources [45–47]. Its properties are listed in Table S1 in the supplementary material.

2.2. High-temperature cycle

Six alkanes were considered as working fluids for the HT-ORC cycle. They comprise four linear alkanes (pentane, hexane, heptane and octane) and two cyclic alkanes (cyclopentane and cyclohexane). The shorter four alkanes (methane, ethane, propane and butane) are not preferred in HT-ORC due to their low critical temperature. In addition, the working fluids for the HT-ORC were selected to satisfy operational requirements, being suitable with the heat source temperature [13,48–52]. The selected alkanes have the desired properties for working fluids in HT-ORC: thermal stability, material compatibility, appropriate critical temperature and pressure, low toxicity, zero ODP and low GWP. Moreover, alkanes exhibit a good performance and high efficiency in HT-ORC systems [52,53]. The critical temperature of these working fluids varies from 196.55 °C to 295.59 °C, while the critical pressure varies between 24.83 bar and 45.82 bar. The properties of the considered HT-ORC working fluids are listed in Table 1.

2.3. Low-temperature cycle

Global warming and ozone depletion are among the biggest challenges that the world faces. Several conventions and protocols emerged, such as the Montreal Protocol [54], Kyoto Protocol [55] and European regulations [56], to protect the ozone layer by eliminating or reducing the production of substances that are responsible for its depletion. The Montreal Protocol deals with excluding ozone-depleting refrigerants that contain either chlorine or bromine. In general, refrigerants can be classified according to their molecular composition into classes.

- Chlorofluorocarbons (CFC)

CFC refrigerants contain chlorine, fluorine and carbon atoms, such as R11, R12, R113, R114 or R115. These refrigerants were widely used in different applications due to their safety and thermodynamic properties. According to the Montreal Protocol, CFC refrigerants were phased out due to their high ODP and GWP values [57,58].

- Hydrochlorofluorocarbons (HCFC)

HCFC refrigerants contain hydrogen, chlorine, fluorine and carbon atoms, such as R22 or R123. These refrigerants are classified as having a medium to high GWP value and were introduced as substitutes for CFC due to thermodynamic similarity, intermediate ODP and somewhat lower GWP values. The Montreal Protocol was revised to phase out R22 by 2020 and all HCFC by 2030 [58].

- Hydrofluorocarbons (HFC)

HFC are the third generation of fluorine-based refrigerants and were introduced as transitional substitutes for CFC and HCFC. These refrigerants are classified as having zero ODP, but a significant GWP and were selected as alternatives for HCFC and CFC. Examples are R152a, R134a or R32 [59].

- Hydrofluoroolefins (HFO)

HFO contain hydrogen, fluorine and carbon atoms and represent the fourth generation of fluorine-based refrigerants, such as R1234yf, R1336zz(Z) or R1234ze(E). They are classified as environmentally friendly due to zero ODP and low GWP values so that they are a suitable alternative to CFC, HCFC and HFC refrigerants [60]. HFO are mildly flammable, may release hazardous substances, have a high price and require additional safety requirements [100,101]. The thermodynamic performance of HFO as working fluids in ORC systems is not well known. There is thus a need to evaluate favorable conditions (inlet temperature and pressure) under which a high thermal efficiency of ORC systems can be achieved [102].

- Hydrocarbons (HC)

HC are natural refrigerants, such as propane, propylene, butane or isobutane. These refrigerants are characterized by zero ODP, minimal GWP and low cost. HC refrigerants were introduced as alternatives for all existing fluorocarbon refrigerants that will phase out in the coming years. In addition, they are used as components in safety mixture fluids for small equipment applications [61].

- Refrigerant mixtures

Refrigerant mixtures are produced by blending pure refrigerants. They were introduced to provide fluids with a suitable thermodynamic behavior and to reduce undesired properties. Refrigerant mixtures may exhibit a good temperature profile match with heat transfer fluids in heat exchangers [62] and can be classified into:

Zeotropic mixtures, known as R5xx, contain two or more refrigerants species that have a different boiling point. This mixture type is characterized by a gliding condensation and evaporation temperature for a given pressure [63].

Azeotropic mixtures, known as R4xx, condensate and evaporate at a constant temperature for a given pressure so that they behave as pure refrigerants during phase change [64].

The implementation of European regulations on the environment and climate eliminated refrigerants with a high GWP, which includes R245fa and R134a, that are often used as working fluids in ORC systems [80]. Consequently, demand arose for alternatives of these eliminated refrigerants, which should have similar thermodynamic properties, good performance under different operational conditions and be environmentally friendly. Several studies suggested substitutes, such as HFO refrigerants [65], hydrocarbons, ammonia or carbon dioxide. Furthermore, refrigerant mixtures with tuned properties were proposed [66].

Lee et al. [67] presented two low GWP refrigerants, i.e. R455A and R454C, as suitable alternatives. Other studies have recommended synthetic refrigerants (R152a, R444A and R445A) for many applications as substitutes for high GWP refrigerants [68–70]. Xue et al. [71] and Sethi et al. [72] discussed that R600a and R455A can be considered as suitable for various applications due to desirable thermodynamic properties and lower GWP. Eyerer et al. [73] and Yang et al. [74] presented R1233zd(E) as an attractive alternative for R245fa in ORC systems. In addition, Molés et al. [75] and Yang et al. [76] assessed ORC system performance by utilizing R1336mzz(Z), R1234yf and R1233zd(E) as working fluids and alternatives for R245fa and R134a. The authors showed that such ORC systems could yield a higher thermal efficiency. Longo et al. [77] made a comparative study and showed that R1233zd(E) and R1234ze(Z) may lead to a similar or higher thermal efficiency than R245fa. Moreover, Bianchi et al. [78] laid out that R1234yf and R1234ze(E) are suitable substitutes for R134a in ORC systems. Devecioğlu et al. [79] considered a HFO/HFC mixture that showed an excellent performance. However, most research has focused on a specific group of refrigerants only. There is still a lack of investigations on other low GWP refrigerants, especially refrigerant mixtures, as working fluids in dual-loop ORC systems.

In this study, 31 refrigerants were considered as working fluids for the LT-ORC. All of them have a low GWP (≤150) and negligible ODP. These working fluids include six HFO (R1366mzz(Z), R1233zd(E), R1234ze(Z), R1234ze(E), R1234yf and R1243zf), six HC (R600a, R290, R600, RE170, cyclopropane and R1270), seven HC mixtures (R510A, R511A, R436A, R436B, R432A, R433A and R441A), four HC/HFC

mixtures (R429A, R430A, R431A and R435A), six HFC/HFO mixtures (R444A, R451A, R454C, R455A, R457A and R459B) and two HFC refrigerants (R152a and R161). Their critical temperature varies from 85.60 °C to 171.35 °C, while their critical pressure lies between 29.03 bar and 55.79 bar. The properties of the selected refrigerants are listed in Table1.

3. System description

The simulated system is based on an actual CD-ORC test rig, which is experimentally set up and tested at the University of Paderborn [81]. The present simulations consider the two main operational cycles, i.e. HT-ORC and LT-ORC. The heat source of the CD-ORC is given by electrical heaters because of their inherently simple regulation and control, together with less strict safety and hazard requirements. Furthermore, electrical heaters as a thermal equivalent are a source allowing for a wide range of temperature. Their maximum thermal power is 158 kW to supply the main cycles with the required heat. Both cycles consist of the four essential components, i.e. turbine, evaporator, condenser and pump. The simulation parameters and components were selected to be close to the actual CD-ORC test rig.

In the heating cycle (HC), the heat transfer fluid (Therminol 66) is heated up by the electrical heaters and transferred to the HT-ORC. The HT-ORC utilizes that heat directly, while the LT-ORC utilizes the residual heat from the HT-ORC. In the HT cycle, the low-pressure saturated working fluid liquid is compressed by the HT-ORC feed pump (M1) and then enters the evaporator (HE1) to be vaporized isobarically into a saturated or superheated state. The working fluid at high pressure and temperature is supplied to the turbine (HT-turbine) to generate mechanical power and then electrical power via the generator (G1). After expansion, the working fluid is still at a high temperature and the residual heat is used to drive the LT-ORC. The expanded working fluid enters the condenser (C1) to release its remaining residual heat in an isobaric process.

A similar thermodynamic process occurs in the LT-ORC. The working fluid absorbs the heat from the HT-ORC and evaporates in HE2. It expands across the turbine (LT-turbine) to yield mechanical power output. Subsequently, the working fluid releases residual heat in the second condenser (C2) and is converted into a saturated liquid. Finally, the working fluid is compressed by the LT-ORC pump (M2) to continue the thermodynamic cycle.

4. Thermodynamic analysis

Simulations were carried out with EBSILON@Professional [82] to investigate system performance under different operating conditions. Various assumptions were made to build the simulation setup of the CD-ORC system depicted in Fig. 1.

Process (1–2): In this process, the heat transfer fluid Therminol 66 enters the HE1 to heat up and carry thermal energy to the HT-ORC. The heat flow can be calculated by

$$\dot{Q}_{HC} = \dot{m}_{HC}.c_p.(T_2 - T_1) \tag{1}$$

where $\dot{Q}_{HC}$ is the heat flow of the HC cycle, $\dot{m}_{HC}$ the mass flow rate, c_p the isobaric heat capacity of Therminol 66 and T_1 and T_2 are its temperatures at the inlet and outlet of HE1, respectively. The heat flow in the HC cycle is equal to the heat flow driving the HT-ORC (3–4), leading to isobaric evaporation and superheating of the alkane in the HT-ORC. The heat flow absorbed by the alkane in the HT-ORC can be expressed as

$$\dot{Q}_{HT} = \dot{m}_{HT}.(h_4 - h_3) \tag{2}$$

where $\dot{m}_{HT}$ is the mass flow rate of the alkane in the HT-ORC, h_3 and h_4 are its enthalpies at the inlet and outlet of HE1.

Process (4–5) refers to the adiabatic expansion work of the HT-turbine. High pressure and temperature alkane enters and expands across the HT-turbine into a low pressure state. The HT-turbine power output is given by

$$\dot{W}_{T,HT} = \dot{m}_{HT}.(h_4 - h_5) \tag{3}$$

where h_4 and h_5 are the enthalpies at the inlet and outlet.

Process (6–7) refers to the isobaric condensation of the alkane in the HT-ORC, which releases residual heat in condenser C1 and can be calculated by

$$\dot{Q}_{C1} = \dot{m}_{HT}.(h_6 - h_7) \tag{4}$$

where h_6 and h_7 are the enthalpies at the inlet and outlet.

Process (7–3) is the compression with pump M1 that can be determined as

$$\dot{W}_{P,HT} = \dot{m}_{HT}.(h_3 - h_7) \tag{5}$$

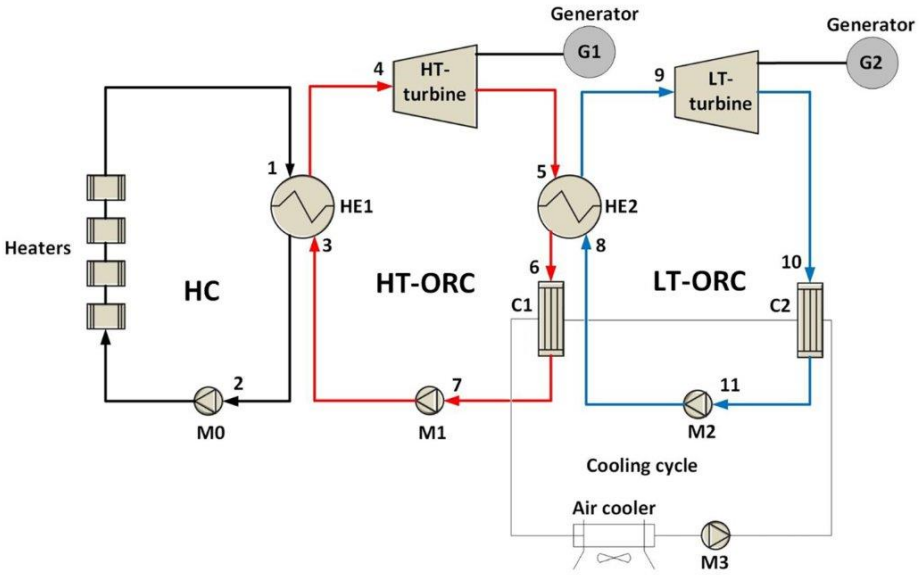

Fig. 1. Layout of the CD-ORC system investigated in the present work.

where h_7 and h_3 are the enthalpies at the inlet and outlet.

The thermal efficiency of the HT-ORC can be defined as the ratio of the net power output to the heat flow input to the HT-ORC

$$\eta_{th} = \frac{\dot{W}_{net,HT}}{\dot{Q}_{HT}} \tag{6}$$

where $\dot{W}_{net,HT} = \dot{W}_{T,HT} - \dot{W}_{P,HT}$.

Process (5–6): The heat flow from the HT-ORC is transferred to the LT-ORC via HE2 and is equal to that absorbed by the working fluid in the LT-ORC in process (8–9)

$$\dot{Q}_{LT} = \dot{m}_{LT}.(h_9 - h_8) \tag{7}$$

where $\dot{m}_{LT}$is the mass flow rate of the refrigerant in the LT-ORC, h_8 and h_9 are its enthalpies at the inlet and outlet.

Process (9–10) refers to the refrigerant expansion across the LT-ORC turbine and the power output is given by

$$\dot{W}_{T,LT} = \dot{m}_{LT}.(h_9 - h_{10}) \tag{8}$$

where h_9 and h_{10} are the enthalpies at the inlet and outlet.

Process (10–11) is the isobaric residual heat discharge of the refrigerant in the LT-ORC condenser C2

$$\dot{Q}_{C2} = \dot{m}_{LT}.(h_{10} - h_{11}) \tag{9}$$

where h_{10} and h_{11} are the enthalpies at the inlet and outlet.

Process (8–11): After condensation, the refrigerant is compressed adiabatically by the pump M2. The pump work in the LT-ORC is

$$\dot{W}_{P,LT} = \dot{m}_{LT}.(h_8 - h_{11}) \tag{10}$$

where h_{11} and h_8 are the enthalpies at the inlet and outlet.

The thermal efficiency of the LT-ORC can be defined as the ratio of the net power output to the heat flow input to the LT-ORC

$$\eta_{th} = \frac{\dot{W}_{net,LT}}{\dot{Q}_{LT}} \tag{11}$$

where $\dot{W}_{net,LT} = \dot{W}_{T,LT} - \dot{W}_{P,LT}$.

The total thermal efficiency of the CD-ORC is

$$\eta_{th,total} = \frac{\dot{W}_{net,total}}{\dot{Q}_{HC}} \tag{12}$$

where $\dot{W}_{net,total} = \dot{W}_{net,HT} + \dot{W}_{net,LT}$.

The exergy flow input can be calculated as

$$\dot{E}_{in} = \dot{m}_{HT}[(h_4 - h_3) - T_0(s_4 - s_3)] \tag{13}$$

where T_0 is the ambient temperature, h_3 and h_4 are working fluid enthalpies at the inlet and outlet of HE1, respectively, while s_3 and s_4 are the corresponding entropies.

The exergy efficiency of the HT-ORC can be calculated as

$$\eta_{ex,HT} = \frac{\dot{W}_{net,HT}}{\dot{E}_{in}} \tag{14}$$

Finally, the total exergy efficiency of the CD-ORC system can be calculated as

$$\eta_{ex,total} = \frac{\dot{W}_{net,total}}{\dot{E}_{in}} \tag{15}$$

5. Assumptions

The CD-ORC process was simulated with the software EBSILON@-Professional and the underlying thermophysical properties of the working fluids were supplied by REFPROP 10 [83] that rests on the most accurate equations of state as recommended by the National Institute of Science and Technology. The system was driven by heat from electrical heaters with a maximum heat flow of 158 kW. Evaporators and condensers of the CD-ORC system were assumed to be counter-current heat exchangers with a saturated or superheated outlet. It was operated under steady-state conditions in a steady flow process, neglecting potential and kinetic energy changes. Heat loss and pressure drop in pipelines and components as well as friction losses were neglected, except for turbine and pump efficiencies. The turbine inlet temperature was assumed to be lower than the critical temperature of the working fluid to avoid critical conditions. Isentropic efficiency of turbines and pumps in the HT-ORC and LT-ORC was set to 75% and the minimum pinch point temperature difference in evaporators and condensers was set to 5 °C. The minimum condensation temperatures were specified to be 50 °C and 35 °C in the HT-ORC and the LT-ORC, respectively. These assumptions and simulation parameters are listed in Table 2.

6. System validation

Due to the lack of work on CD-ORC systems (under the same operating conditions and the same working fluids), the present HT-ORC simulation was validated against literature data of a regular ORC system. The HT-ORC thermal efficiency was compared with results of Uusitalo et al. [84], where cyclohexane, cyclopentane, octane, heptane, hexane and pentane were considered as working fluids. To validate the present simulations, input parameters and conditions were the same as those in Ref. [84]: condensation temperature of 50 °C, η_t=0.75, no recuperator and a small degree of superheating were set for all working fluids in the HT-ORC and a maximum evaporation pressure ($p_e/p_c = 0.9$) was used to keep the working fluid below critical conditions. Moreover, the inlet state of the LT-ORC (heat flow and turbine inlet temperature) was compared with our previous experimental work using propane and butane as working fluids in the LT-ORC [81,98]. The thermal efficiency of butane was also compared with the study of Uusitalo et al. [84] at a turbine inlet temperature of 100 °C. The system behavior corresponded with the thermodynamic analysis of the thermal efficiency of the regular ORC system by using the same working fluids as in Refs. [52,53]. A comparison of the present work with these references is made in Table 3. Based on the good agreement with literature work, the present simulation model can be assumed to be validated.

7. Results and discussion

CD-ORC system performance in terms of thermal efficiency was simulated by adopting alkanes and low GWP refrigerants as working fluids. The first goal was to estimate the HT-ORC performance by employing cyclic and linear alkanes. The second goal was to simulate and analyze the entire CD-ORC and its overall system performance by

Table 2
Assumptions and operational conditions.

Parameter	value
Isentropic efficiency of turbines	75%
Mechanical efficiency of turbines	98%
Isentropic efficiency of pumps	75%
Mechanical efficiency of pumps	98%
Electric efficiency of pumps	85%
Efficiency of generators	90%
Power factor of generators	85%
Motor efficiency of pumps	85%
Minimum condensation temperature (HT-ORC)	50 °C
Minimum condensation temperature (LT-ORC)	35 °C
Minimum condensation pressure	1 bar
Mass flow rate of the HT-ORC	0.120–0.165 kg/s
Mass flow rate of the LT-ORC	0.05–0.10 kg/s
Minimum PPTD in evaporators	5 °C
Minimum PPTD in condensers	5 °C

Table 3
Comparison with the work by Uusitalo et al. [84].

Working fluid	Thermal efficiency [%]		Difference
	This work	Ref. [84]	
Cyclohexane	19.13	18.70	0.43
Cyclopentane	18.03	17.78	0.25
Octane	17.22	17.04	0.18
Heptane	16.23	16.52	0.29
Hexane	15.21	15.69	0.48
Pentane	13.92	14.08	0.16

utilizing low GWP refrigerants in the LT-ORC. A comparison between the regular ORC and the CD-ORC was made. This includes a study on the relationship between the critical temperature of the working fluid and the thermal efficiency as well as the effect of the HT-ORC on the LT-ORC. In addition, light is shed on the effectiveness of the CD-ORC for increasing the total thermal efficiency.

7.1. Thermal efficiency of the HT-ORC

A wide range of heat source temperature in increments of 10 °C was explored to study the thermal efficiency of the HT-ORC. Simulations were carried out by adopting cyclopentane, cyclohexane, pentane, hexane, heptane and octane as working fluids. The maximum applied heat source temperature was limited such that the HT-turbine inlet temperature was lower than the critical temperature of the given working fluid to avoid critical conditions. Consequently, the heat source temperature was in the range of 170–270 °C for cyclopentane, 170–320 °C for cyclohexane, 170–250 °C for pentane, 170–270 °C for hexane, 170–300 °C for heptane and 170–330 °C for octane.

Fig. 2 shows the thermal efficiency of the HT-ORC for this variation. As expected, an increasing trend of the thermal efficiency with heat source temperature was found for all working fluids. Simulation data indicate that cyclohexane has the most pronounced increase of thermal efficiency, while pentane has the lowest. The thermal efficiency increased from 11.53% to 19.13% for cyclohexane, from 11.28% to 18.03% for cyclopentane, from 9.52% to 17.22% for octane, from 8.83% to 16.22% for heptane, from 8.45% to 15.21% for hexane and from 7.95% to 13.92% for pentane. The main reason for that increasing trend is that the absorbed heat from the heating cycle and the net power output increase with rising heat source temperature. However, the net power output outweighs the increasing rate of the absorbed heat so that the thermal efficiency increases gradually with heat source temperature. Generally, a higher critical temperature is suitable for bringing the turbine inlet temperature to a high level, which may allow for an increase of the enthalpy difference across the turbine and leads to higher net power output and thermal efficiency. In addition, a higher critical temperature allows for a better use of the heat source. At a higher temperature, the heat flow carries a larger share of exergy, which is an indicator of the quality of energy.

The results show that the cyclic alkanes allow for a better thermal efficiency than the linear alkanes. Cyclic alkanes exhibit higher evaporation temperature levels, which leads to a suitable temperature match between heat source and working fluid to enhance the heat transfer between the heating cycle and the HT-ORC. Moreover, there is a direct correlation between thermal efficiency and critical temperature of the

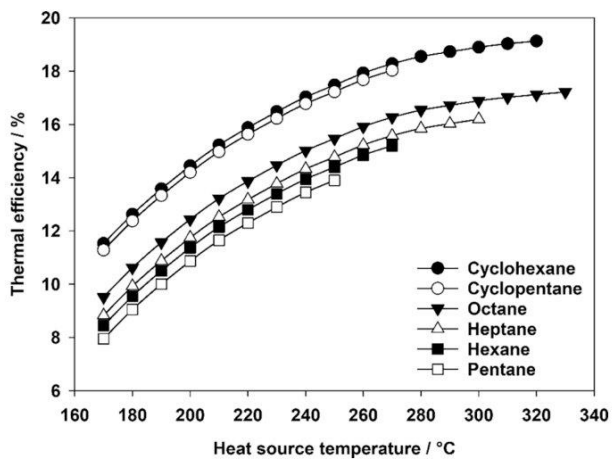

Fig. 2. Thermal efficiency of the HT-ORC as a function of heat source temperature for varying working fluids.

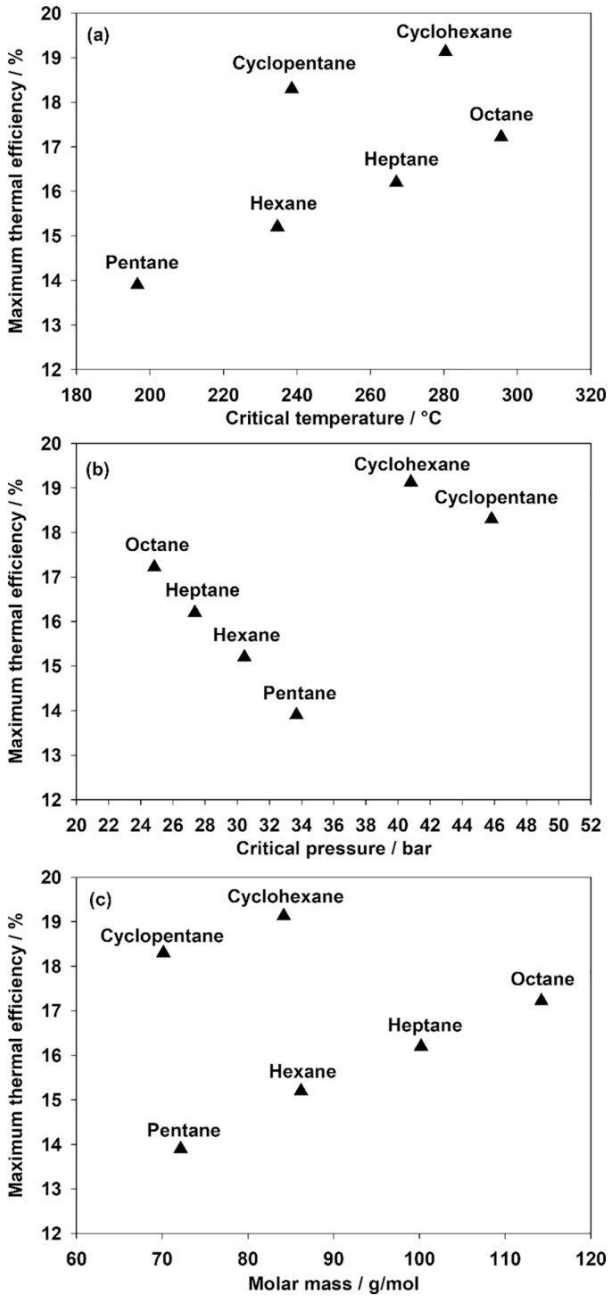

Fig. 3. Relation of the maximum thermal efficiency with (a) critical temperature, (b) critical pressure and (c) molar mass of the working fluid.

working fluid in each group. It can be seen that the thermal efficiency rises with the critical temperature of the working fluid. Fig. 3 depicts the relation between the thermophysical properties of working fluids and the maximum thermal efficiency of the HT-ORC. In each working fluid group (linear and cyclic alkanes), the thermal efficiency increases with rising critical temperature and molar mass. In contrast, it falls with increasing critical pressure in each working fluid group.

These results correspond to the findings of Shu et al. [52] and Liu et al. [53]. These authors investigated the thermal efficiency by employing cyclohexane, cyclopentane, octane, heptane, hexane and pentane as working fluids. They reported that the thermal efficiency of cyclohexane and cyclopentane is superior to that of linear alkanes. Uusitalo et al. [84] also showed that cyclic alkanes may achieve a higher thermal efficiency than linear alkanes.

7.2. Exergy flow analysis

Exergy indicates the quality of energy and defines the maximum achievable work during a process that brings the system into equilibrium with its environment [99]. An analysis was undertaken to determine the exergy flow input at the maximum applied heat source temperature, where each working fluid achieved its maximum thermal efficiency. Fig. 4(a) depicts the variation of exergy flow input with the maximum heat source temperature of the HT-ORC. The highest exergy flow input was 49.16 kW at a heat source temperature of 330 °C when using octane as working fluid, while the lowest exergy flow input was 36.92 kW at a heat source temperature of 250 °C when using pentane as a working fluid. In other words, the exergy flow input directly depends on the critical temperature of the working fluid. It also depends on the state of the system, the environment temperature and the temperature difference between the highest (the outlet of HE1) and lowest temperature (the inlet of HE1) as well as the mass flow rate of the working fluid. The inlet temperature of HE1 was constant for all working fluids, but the outlet state was limited by the critical temperature of the working fluid so that octane was capable to absorb the highest exergy flow input.

Fig. 4(b) depicts the variation of exergy efficiency of the HT-ORC at the maximum heat source temperature, where each working fluid achieved its maximum thermal efficiency. The highest exergy efficiency was 43.02% at a heat source temperature of 320 °C when using cyclohexane as a working fluid, while the lowest exergy efficiency was 31.58% at a heat source temperature of 250 °C when using pentane as a working fluid. In analogy to the thermal efficiency calculations, there is a direct correlation between exergetic efficiency and critical temperature of the working fluid in each group.

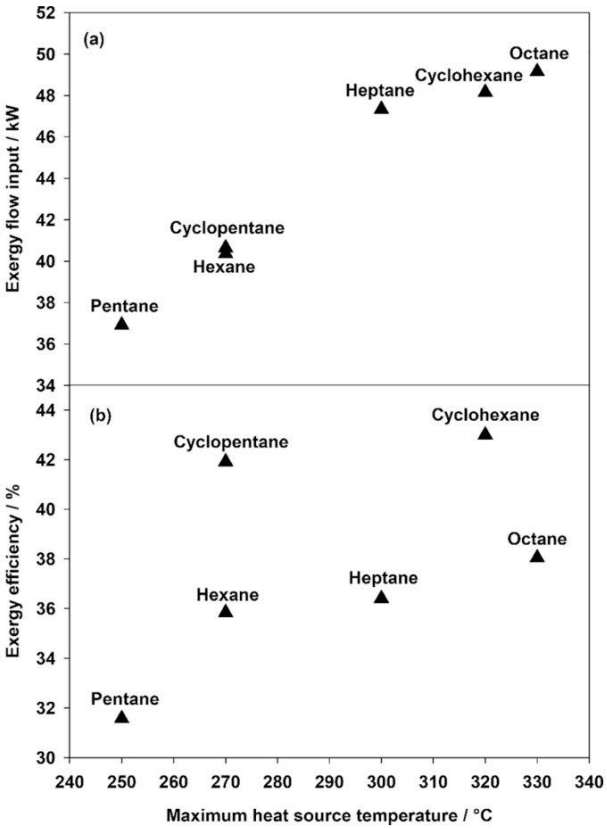

Fig. 4. Variation of (a) exergy flow input and (b) exergy efficiency at the maximum heat source temperature.

7.3. Thermal efficiency of the LT-ORC

The thermal efficiency of the LT-ORC was simulated for a wide heat source temperature range and only its maximum value is shown in Figs. 5(a)–8(a). Throughout, maximum thermal efficiency was achieved at the highest heat source temperature. The thermal efficiency was determined for all HT-ORC and LT-ORC working fluid combinations.

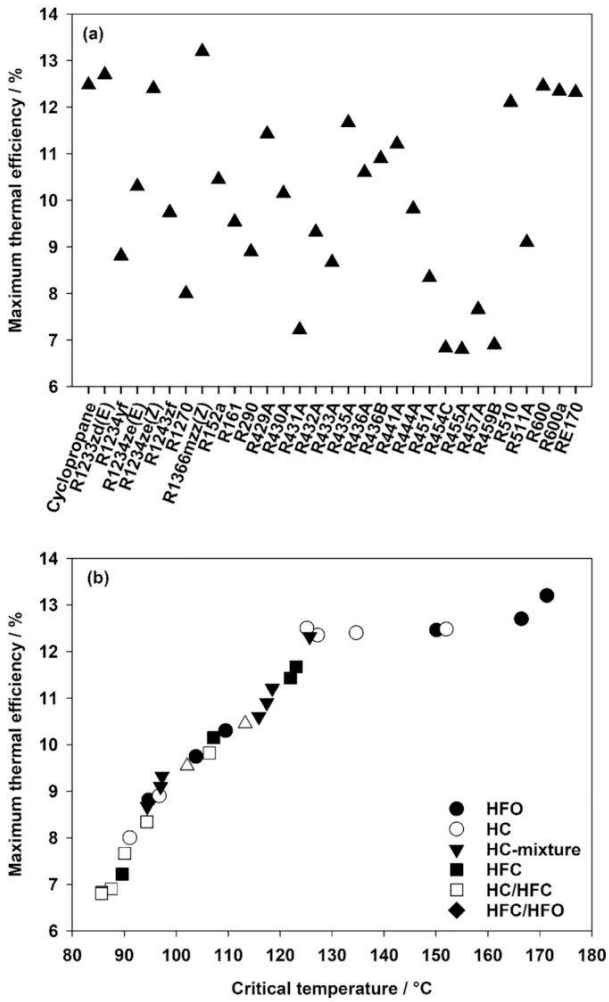

Fig. 5. (a) Variation of the LT-ORC maximum thermal efficiency by using cyclohexane as a working fluid in the HT-ORC and (b) relation between maximum thermal efficiency and critical temperature of the working fluid in the LT-ORC.

Figs. 5(b)–8(b) depict the variation of maximum thermal efficiency with critical temperature, where the LT-ORC working fluids are grouped.

Fig. 5(a) shows the maximum thermal efficiency of the LT-ORC when cyclohexane is used as a working fluid in the HT-ORC. The results represent data for a wide range of the heat source temperature from 170 °C to 330 °C. In general, it can be seen that there is a relation between the critical temperature of the working fluid and the efficiency, as shown in Fig. 5(b). Working fluids with a higher critical temperature in the range from 171.35 °C to 102.10 °C achieved a thermal efficiency from 13.20% to 9.32%, while refrigerants with a lower critical temperature in the range from 97.25 °C to 85.60 °C had a thermal efficiency from 9.54% to 6.81%. The LT-ORC has the highest thermal efficiency of 13.20% with R1366mzz(Z), followed by R1233zd(E) 12.70%, cyclopropane 12.50%, butane 12.48% and R1234ze(Z) 12.40%. The lowest thermal efficiency was 7.66%, 7.22%, 6.90%, 6.83% and 6.80% for R457A, R431A, R459B, R454C and R455A in the LT-ORC, respectively. Among the LT-ORC working fluids, the HC and HFO yield a higher thermal efficiency in the range from 13.20% to 8.02% compared to the other refrigerant groups.

Fig. 6(a) illustrates the LT-ORC thermal efficiency when using cyclopentane in the HT-ORC and varying refrigerants in the LT-ORC. The system was investigated for a heat source temperature range from 170 °C to 270 °C and the results also indicate that the thermal efficiency increases with the critical temperature for all refrigerants in the LT-ORC. The thermal efficiency of R1366mzz(Z), R1233zd(E), cyclopropane, butane and R1234ze(Z) is the highest. In contrast, lower thermal efficiency was achieved by R457A, R431A, R459B, R454C and R455A. Pure refrigerants, namely HFO, HC and HFC, achieved a thermal efficiency ranging from 7.45% to 11.86%, 6.77% to 11.58% and 8.32% to 8.85%, respectively. Moreover, a thermal efficiency from 7.12% to 10.65%, 6.11% to 9.87% and 5.70% to 8.65% was reached with HC, HC/HFC and HFC/HFO mixtures. Fig. 6(b) shows the increase of thermal efficiency with the critical temperature of the refrigerants.

Fig. 7(a) depicts the thermal efficiency of the LT-ORC by employing octane as a working fluid in the HT-ORC. The system was investigated for a heat source temperature range from 170 °C to 330 °C. The highest thermal efficiency was 13.40%, 13.22%, 13.20%, 13.11% and 13.08% for R1366mzz(Z), R1233zd(E), cyclopropane, butane and R1234ze(Z), respectively. In contrast, lower thermal efficiencies of 7.87%, 7.34%, 7.15%, 7.05% and 7.01% were found for R457A, R431A, R459B, R454C and R455A. Fig. 7(b) indicates that the pure refrigerant groups, namely HFO, HC and HFC, exhibit a thermal efficiency ranging from 9.11% to 13.40%, 8.10% to 13.11% and 9.75% to 10.78%. Thermal efficiency ranged from 9.03% to 12.22%, 7.34% to 11.98% and 7.01% to 10.02%

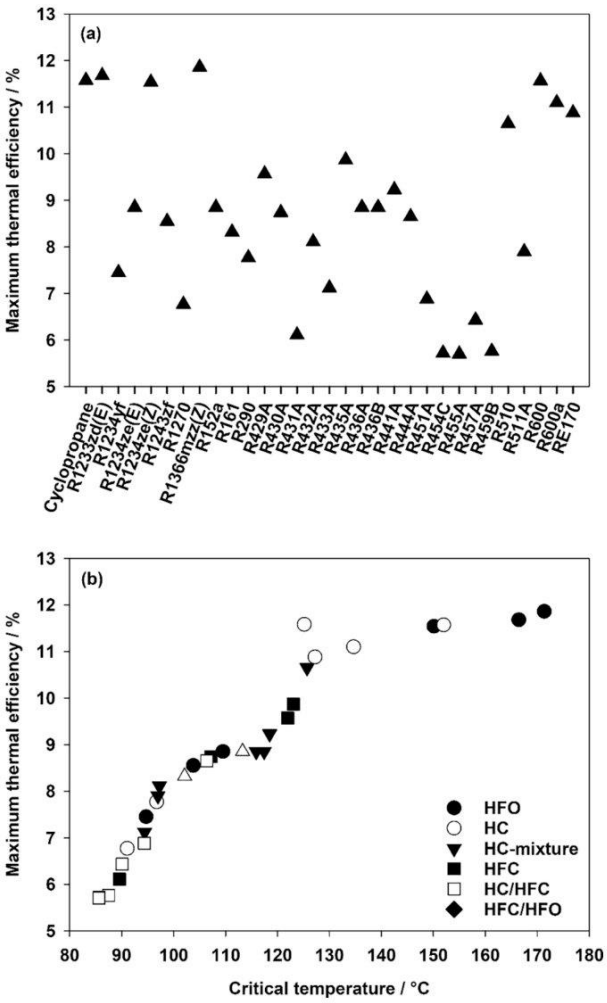

Fig. 6. (a) Variation of the LT-ORC maximum thermal efficiency by using cyclopentane as a working fluid in the HT-ORC and (b) relation between maximum thermal efficiency and critical temperature of the working fluid in the LT-ORC.

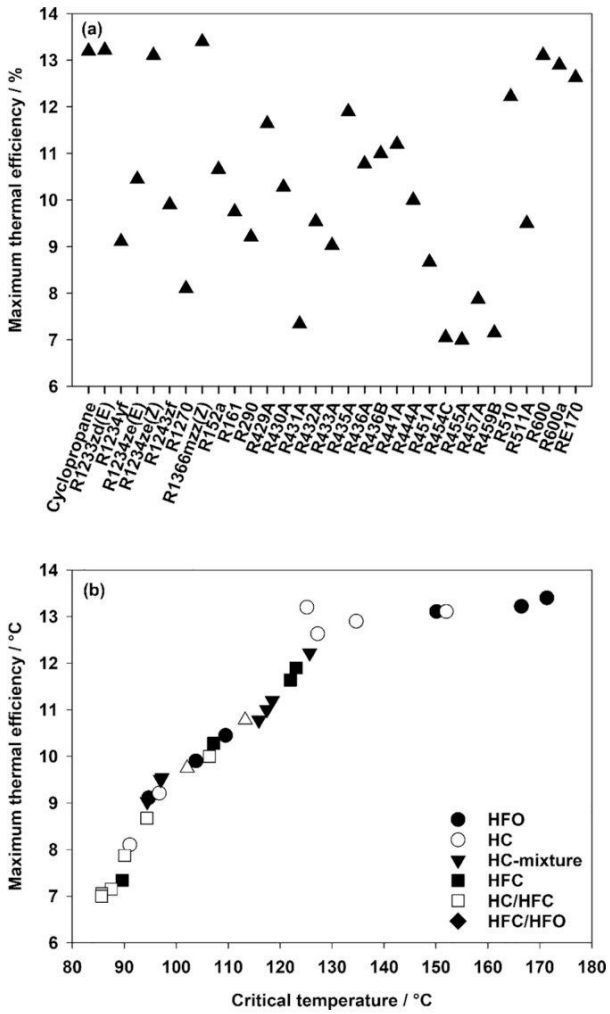

Fig. 7. (a) Variation of the LT-ORC maximum thermal efficiency by using octane as a working fluid in the HT-ORC and (b) relation between maximum thermal efficiency and critical temperature of the working fluid in the LT-ORC.

for HC, HC/HFC and HFC/HFO mixtures.

Fig. 8(a) illustrates the variation of the LT-ORC thermal efficiency when using heptane in the HT-ORC. The system was investigated for a heat source temperature range from 170 °C to 300 °C. The highest thermal efficiency was 12.20%, 12.00%, 11.98%, 11.95% and 11.90% by using R1366mzz(Z), R1233zd(E), cyclopropane, butane and R1234ze (Z), respectively. A thermal efficiency of 7.55%, 7.02%, 6.77%, 6.60% and 6.55% was found for R457A, R431A, R459B, R454C and R455A. Fig. 8(b) shows the increase of thermal efficiency with rising critical temperature of the refrigerants. The pure refrigerant groups, namely HFO, HC and HFC, exhibit a thermal efficiency ranging from 8.23% to 12.20%, 7.71% to 11.95% and 8.64% to 9.70%. Thermal efficiency ranged from 8.10% to 11.02%, 7.02% to 10.45% and 6.55% to 9.12% for HC, HC/HFC and HFC/HFO mixtures.

Hexane and pentane as working fluids in the HT-ORC lead to a further reduced thermal efficiency so that they are not described here in detail. The according results are depicted in Figs. S1 and S2 of the supplementary material.

The present data clearly indicate that pure fluids are preferred over refrigerant mixtures in any of the considered scenarios.

Fig. 9 summarizes the variation of the LT-ORC thermal efficiency for all working fluid combinations. It can be seen that the highest thermal efficiency of the LT-ORC was achieved with octane as a working fluid in the HT-ORC, while the lowest thermal efficiency was achieved with pentane as a working fluid in the HT-ORC. The figure demonstrates the effect of the working fluids' critical temperature on the thermal efficiency not only for the HT-ORC but also for the LT-ORC. For example, butane achieved a thermal efficiency of 13.11% when octane (with the highest critical temperature) was used as a working fluid in the HT-ORC. In comparison, butane achieved a thermal efficiency of only 8.80% when using pentane (with the lowest critical temperature) as a working fluid in the HT-ORC. Since the outlet of the HT-ORC turbine is the heat source of the LT-ORC, working fluids with a high critical temperature in the HT-ORC lead to an increase of the LT-ORC thermal efficiency.

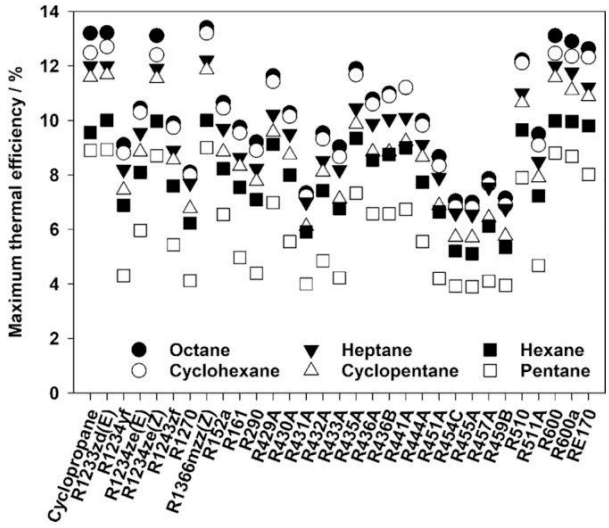

Fig. 9. Maximum thermal efficiency of the LT-ORC by utilizing cyclohexane, cyclopentane, octane, heptane, hexane and pentane as a working fluid in the HT-ORC.

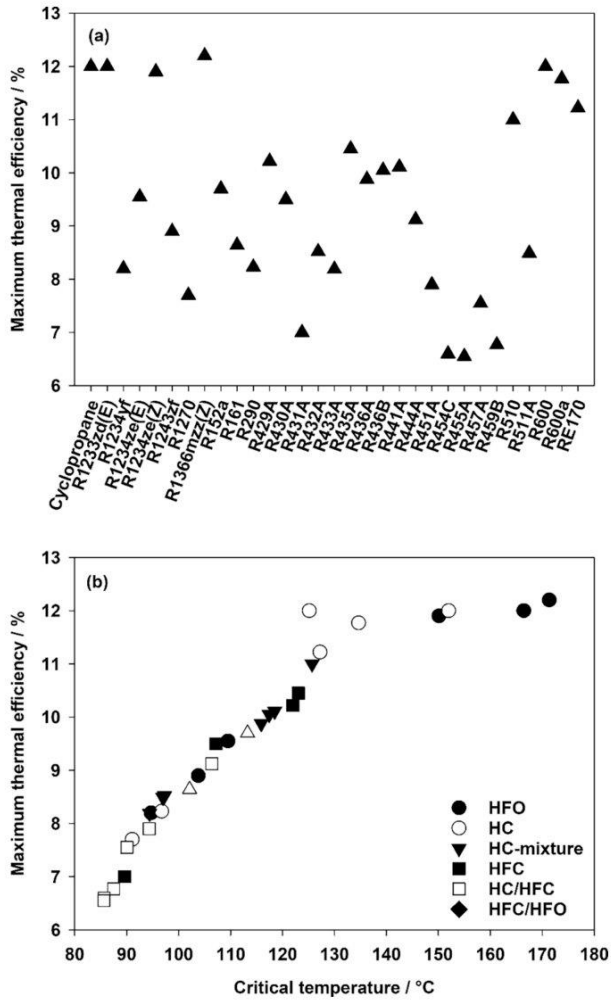

Fig. 8. (a) Variation of the LT-ORC maximum thermal efficiency by using heptane as a working fluid in the HT-ORC and (b) relation between maximum thermal efficiency and critical temperature of the working fluid in the LT-ORC.

It can be seen that the thermal efficiency of the LT-ORC is also highly affected by the critical temperature of the refrigerant. This can be explained by the fact that refrigerants with a high critical temperature allow for a higher turbine inlet temperature than refrigerants with a lower critical temperature. Moreover, a high critical temperature allows for a high evaporation temperature, which leads to an increase of thermal efficiency and an increase of the enthalpy difference across the turbine. Generally, a high critical temperature enhances the utilization of heat source temperature and is more suitable for temperature matching between the heat source and the working fluids. The effect of the critical temperature of alkanes acts not only on the HT-ORC, but on the LT-ORC as well.

Fig. 10 shows the total thermal efficiency of the CD-ORC for all working fluid combinations. The term (x-y) refers to x and y as working fluids in the HT-ORC and the LT-ORC, respectively. The results indicate that the highest total thermal efficiency of 25.24% was achieved by the combination (cyclohexane-R1366mzz(Z)) as working fluids in the CD-ORC system. In contrast, the lowest total thermal efficiency of 15.58% was obtained by employing the combination (pentane-R455A). A very high total thermal efficiency of 24.88%, 24.60%, 24.44% and 24.11% was also achieved by employing the combinations (cyclohexane-R1233zd(E)), (cyclohexane-butane), (cyclohexane-R1234ze(Z)) and (cyclohexane-isobutane), respectively.

7.4. Improvement of thermal efficiency

The total thermal efficiency of the CD-ORC was compared to that of a regular ORC under six conditions to analyze the percentage by which the thermal efficiency increased. This analysis is based on a comparison of

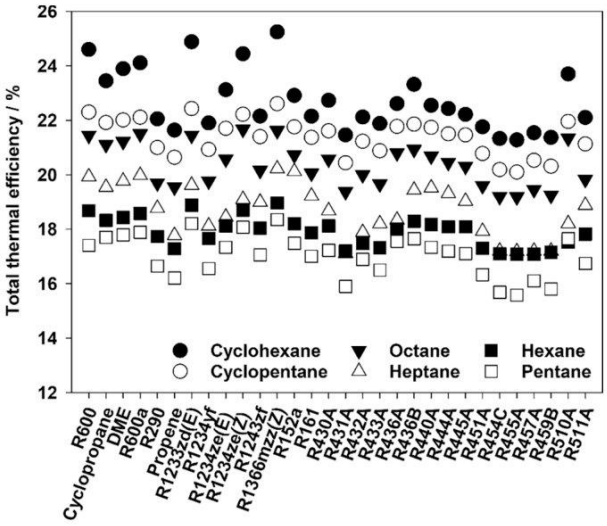

Fig. 10. Total thermal efficiency of the CD-ORC system.

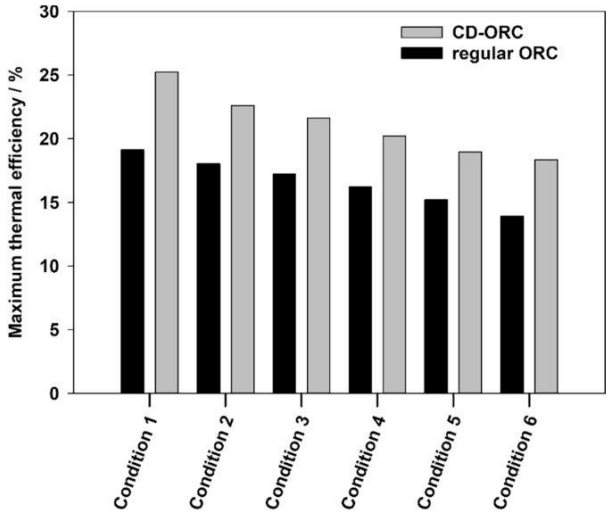

Fig. 11. Comparison of the thermal efficiency of CD-ORC and regular ORC under different operating conditions.

the highest thermal efficiency of the HT-ORC by adopting alkanes as a working fluid and the highest thermal efficiency of the CD-ORC system by adopting a combination of (alkane-R1366mzz(Z)). The combination (alkane-R1366mzz(Z)) was selected under all conditions because the CD-ORC always reached its highest total thermal efficiency by using R1366mzz(Z) in the LT-ORC. The combinations (cyclohexane-R1366mzz(Z)), (cyclopentane-R1366mzz(Z)), (octane-R1366mzz(Z)), (heptane-R1366mzz(Z)), (hexane-R1366mzz(Z)) and (pentane-R1366mzz(Z)) were used as working fluids under conditions (1) to (6) in the HT-ORC and LT-ORC of the CD-ORC system. The heat source temperature and the working fluids are listed in Table 4. Fig. 11 shows a comparison of the thermal efficiency of regular and CD-ORC under these conditions. The CD-ORC with the combination (cyclohexane-R1366mzz (Z) may enhance the thermal efficiency by a quarter, compared to the regular ORC (with cyclohexane as working fluid) at the maximum applied heat source temperature under condition (1). The comparison also shows the rise of the thermal efficiency under conditions (2) to (6), respectively. The results indicate that the thermal efficiency of the CD-ORC is higher than that of regular ORC, which is evidence of a more efficient utilization of the heat source. The addition of the LT-ORC in the CD-ORC led to more turbine power output and a higher thermal efficiency.

Table 4
Different conditions for comparison of the thermal efficiency of regular ORC and CD-ORC.

Condition (1)	
Heat source temperature	320 °C
Regular ORC working fluid	Cyclohexane
CD-ORC working fluids	Cyclohexane-R1366mzz(Z)
Condition (2)	
Heat source temperature	270 °C
Regular ORC working fluid	Cyclopentane
CD-ORC working fluids	Cyclopentane-R1366mzz(Z)
Condition (3)	
Heat source temperature	330 °C
Regular ORC working fluid	Octane
CD-ORC working fluids	Octane-R1366mzz(Z)
Condition (4)	
Heat source temperature	300 °C
Regular ORC working fluid	Heptane
CD-ORC working fluids	Heptane-R1366mzz(Z)
Condition (5)	
Heat source temperature	270 °C
Regular ORC working fluid	Hexane
CD-ORC working fluids	Hexane-R1366mzz(Z)
Condition (6)	
Heat source temperature	250 °C
Regular ORC working fluid	Pentane
CD-ORC working fluids	Pentane-R1366mzz(Z)

7.5. Improvement of exergy efficiency

This section focuses on the analysis of the total exergy efficiency that can be achieved with the CD-ORC system. The results indicate that the highest total exergy efficiency of 56.23% was achieved by the combination (cyclohexane-R1366mzz(Z)) as working fluids in the CD-ORC system. A very high total exergy efficiency of 54.85%, 54.23%, 53.54% and 53.14% was also achieved with the combinations (cyclohexane-R1233zd(E)), (cyclohexane-butane), (cyclohexane-R1234ze(Z)) and (cyclohexane-isobutane), respectively. By comparing the results of the total exergy efficiency of CD-ORC with that of the HT-ORC, the expected increase of the total exergy efficiency due to the increase of the net power output can be noticed. The results of exergy efficiency agree with the analysis of Braimakis et al. [19], who reported that the exergy efficiency may improve using a dual-loop ORC.

8. Conclusions

Alkanes and low GWP refrigerants were considered to investigate the thermal efficiency of the CD-ORC system. Simulations with EBSILON@Professional were carried out for a wide range of heat source temperature. The relation between the thermal efficiency and the critical temperature of the working fluids was analyzed. In the HT-ORC, the thermal efficiency is highly affected by the critical temperature, molecular mass and critical pressure. The results confirm that cyclic alkanes may achieve a higher thermal efficiency than linear alkanes. Thus, the thermal efficiency of alkanes rises with the critical temperature within the same group. Among the HT-ORC working fluids, cyclohexane provided the best thermal efficiency of 19.13%, while pentane achieved the worst thermal efficiency of 13.92%. The LT-ORC analysis with respect to the thermal efficiency was carried out by employing low GWP refrigerants as working fluids. Refrigerants with a high critical temperature are superior to other refrigerants. Relatively, R1366mzz(Z), R1233zde(E), cyclopropane, butane and R1234ze(Z) showed the highest thermal efficiency in the LT-ORC and refrigerant mixtures were found to

be less suitable. The CD-ORC system achieved a total thermal efficiency of 25.24%, 24.88%, 24.60%, 24.44% and 24.11% by utilizing the combinations (cyclohexane-R1366mzz(Z)), (cyclohexane-R1233zd(E)), (cyclohexane-butane), (cyclohexane-R1234ze(Z)) and (cyclohexane-isobutane), respectively. The CD-ORC system with a heat source temperature in the range from 170 °C to 330 °C exhibited a favorable performance when using refrigerants with a high critical temperature. Compared to the regular ORC, the CD-ORC system may lead to an increase of the thermal efficiency by up to a quarter. The results indicate that HFO refrigerants (namely R1366mzz(Z), R1233zd(E) and R1234ze (Z)) and HC refrigerants (namely butane, cyclopropane and isobutane) may be good alternatives for the refrigerants that are excluded by environmental regulations. Future work will include testing low GWP refrigerants as working fluids in CD-ORC systems practically, since our department has a CD-ORC test rig. Emphasis will also be placed on the simulation of environmentally friendly refrigerants under different conditions as working fluids in ORC as an alternative to excluded refrigerants.

Author contribution

Wameedh Khider Abbas Abbas has developed the simulation workflow, carried out the simulations, analyzed the results and wrote the manuscript. Jadran Vrabec initiated the project, supported this research and contributed to the manuscript's revision.

Declaration of Competing Interest

The authors declare that they have no known competing financial interests or personal relationships that could have appeared to influence the work reported in this paper.

Acknowledgements

We gratefully acknowledge the German Academic Exchange Service (DAAD) for financial support and the help provided by Dr. Gerhard Herres, University of Paderborn. The authors thank Dr. Antti Uusitalo, Lappeenranta University of Technology for providing data for the validation of the present simulation work.

Appendix A. Supplementary data

Supplementary data to this article can be found online at https://doi.org/10.1016/j.enconman.2021.114843.

References

[1] Prabhakaran SPS, Swaminathan G, Joshi VV. Thermogravimetric analysis of hazardous waste: Pet-coke, by kinetic models and Artificial neural network modelling. Fuel 2021;287:119470. https://doi.org/10.1016/j.fuel.2020.119470.
[2] Prabhakaran SPS, Swaminathan G, Joshi VV. Environmental Technology & Innovation Energy conservation – A novel approach of co-combustion of paint sludge and Australian lignite by principal component analysis, response surface methodology and artificial neural network modeling. Environ Technol Innov 2020;20:101061. https://doi.org/10.1016/j.eti.2020.101061.
[3] Jacob GA, Prabhakaran SPS, Swaminathan G, Joseyphus RJ. Thermal kinetic analysis of mustard biomass with equiatomic iron–nickel catalyst and its predictive modelling. Chemosphere 2022;286:131901. https://doi.org/10.1016/j.chemosphere.2021.131901.
[4] Liu X, Wang X, Zhang C. Sensitivity analysis of system parameters on the performance of the Organic Rankine Cycle system for binary-cycle geothermal power plants. Appl Therm Eng 2014;71:175–83. https://doi.org/10.1016/j.applthermaleng.2014.06.048.
[5] Wang M, Wang J, Zhao Y, Zhao P, Dai Y. Thermodynamic analysis and optimization of a solar-driven regenerative organic Rankine cycle (ORC) based on flat-plate solar collectors. Appl Therm Eng 2013;50:816–25. https://doi.org/10.1016/j.applthermaleng.2012.08.013.
[6] Farrokhi M, Noie SH, Akbarzadeh AA. Preliminary experimental investigation of a natural gas-fired ORC-based micro-CHP system for residential buildings. Appl Therm Eng 2014;69:221–9. https://doi.org/10.1016/j.applthermaleng.2013.11.060.
[7] Huang Y, McIlveen-Wright DR, Rezvani S, Huang MJ, Wang YD, Roskilly AP, et al. Comparative techno-economic analysis of biomass fuelled combined heat and power for commercial buildings. Appl Energy 2013;112:518–25. https://doi.org/10.1016/j.apenergy.2013.03.078.
[8] Dolz V, Novella R, García A, Sánchez J. HD Diesel engine equipped with a bottoming Rankine cycle as a waste heat recovery system. Part 1: Study and analysis of the waste heat energy. Appl Therm Eng 2012;36:269–78. https://doi.org/10.1016/j.applthermaleng.2011.10.025.
[9] Kwak DH, Binns M, Kim J-K. Integrated design and optimization of technologies for utilizing low grade heat in process industries. Appl Energy 2014;131:307–22. https://doi.org/10.1016/j.apenergy.2014.06.037.
[10] M.A. Al-Weshahi, A. Anderson, G. Tian, Organic Rankine Cycle recovering stage heat from MSF desalination distillate water, Appl. Energy 130 (2014) 738–747. doi.org/10.1016/j.apenergy.2014.02.038.
[11] Mehrpooya M, Ashouri M, Mohammadi A. Thermoeconomic analysis and optimization of a regenerative two-stage organic Rankine cycle coupled with liquefied natural gas and solar energy. Energy 2017;126:899–914. https://doi.org/10.1016/j.energy.2017.03.064.
[12] G. Shu, G. Yu, H. Tian, H. Wei, X. Liang, Z. Huang, Multi-approach evaluations of a cascade-Organic Rankine Cycle (C-ORC) system driven by diesel engine waste heat: Part A – Thermodynamic evaluations, Energy Convers. Manag. 108 (2016) 579–595. doi.org/10.1016/j.enconman.2015.10.084.
[13] Chen T, Zhuge W, Zhang Y, Zhang L. A novel cascade organic Rankine cycle (ORC) system for waste heat recovery of truck diesel engines. Energy Convers Manag 2017;138:210–23. https://doi.org/10.1016/j.enconman.2017.01.056.
[14] Yang F, Cho H, Zhang H, Zhang J. Thermoeconomic multi-objective optimization of a dual loop organic Rankine cycle (ORC) for CNG engine waste heat recovery. Appl Energy 2017;205:1100–18. https://doi.org/10.1016/j.apenergy.2017.08.127.
[15] Lim T, Choi Y, Hwang D. Optimal working fluids and economic estimation for both double stage organic Rankine cycle and added double stage organic Rankine cycle used for waste heat recovery from liquefied natural gas fueled ships. Energy Convers Manag 2021;242:114323. https://doi.org/10.1016/j.enconman.2021.114323.
[16] Yun E, Park H, Yoon SY, Kim KC. Dual parallel organic Rankine cycle (ORC) system for high efficiency waste heat recovery in marine application. J Mech Sci Technol 2015;29:2509–15. https://doi.org/10.1007/s12206-015-0548-5.
[17] Sung T, Kim KC. Thermodynamic analysis of a novel dual-loop organic Rankine cycle for engine waste heat and LNG cold. Appl Therm Eng 2016;100:1031–41. https://doi.org/10.1016/j.applthermaleng.2016.02.102.
[18] Ntavou E, Kosmadakis G, Manolakos D, Papadakis G, Papantonis D. Experimental testing of a small-scale two stage Organic Rankine Cycle engine operating at low temperature. Energy 2017;141:869–79. https://doi.org/10.1016/j.energy.2017.09.127.
[19] Braimakis K, Karellas S. Exergetic optimization of double stage Organic Rankine Cycle (ORC). Energy 2018;149:296–313. https://doi.org/10.1016/j.energy.2018.02.044.
[20] Ayachi F, Boulawz Ksayer E, Zoughaib A, Neveu P. ORC optimization for medium grade heat recovery. Energy 2014;68:47–56. https://doi.org/10.1016/j.energy.2014.01.066.
[21] Kosmadakis G, Manolakos D, Kyritsis S, Papadakis G. Comparative thermodynamic study of refrigerants to select the best for use in the high-temperature stage of a two-stage organic Rankine cycle for RO desalination. Desalinaion 2009;243:74–94. https://doi.org/10.1016/j.desal.2008.04.016.
[22] Preißinger M, Heberle F, Brüggemann D. Thermodynamic analysis of double-stage biomass fired Organic Rankine Cycle for micro-cogeneration. Int J Energy Res 2012;36:944–52. https://doi.org/10.1002/er.1952.
[23] Fouad WA. A combined heat, hydrogen and power tri-generation system based on the use of catalytic membrane reactors with a dual-loop organic Rankine cycle. Energy Convers Manag 2020;222:113255. https://doi.org/10.1016/j.enconman.2020.113255.
[24] Shu G, Liu L, Tian H, Wei H, Yu G. Parametric and working fluid analysis of a dual-loop organic Rankine cycle (DORC) used in engine waste heat recovery. Appl Energy 2014;113:1188–98. https://doi.org/10.1016/j.apenergy.2013.08.027.
[25] Wang E, Yu Z, Zhang H, Yang F. A regenerative supercritical-subcritical dual-loop organic Rankine cycle system for energy recovery from the waste heat of internal combustion engines. Appl Energy 2017;190:574–90. https://doi.org/10.1016/j.apenergy.2016.12.122.
[26] Emadi MA, Chitgar N, Oyewunmi OA, Markides CN. Working-fluid selection and thermoeconomic optimisation of a combined cycle cogeneration dual-loop organic Rankine cycle (ORC) system for solid oxide fuel cell (SOFC) waste-heat recovery. Appl Energy 2020;261:114384. https://doi.org/10.1016/j.apenergy.2019.114384.
[27] Xia XX, Wang ZQ, Zhou NJ, Hu YH, Zhang JP, Chen Y. Working fluid selection of dual-loop organic Rankine cycle using multi-objective optimization and improved grey relational analysis. Appl Therm Eng 2020;171:115028. https://doi.org/10.1016/j.applthermaleng.2020.115028.
[28] Xue X, Guo C, Du X, Yang L, Yang Y. Thermodynamic analysis and optimization of a two-stage organic Rankine cycle for liquefied natural gas cryogenic exergy recovery. Energy 2015;83:778–87. https://doi.org/10.1016/j.energy.2015.02.088.
[29] Kuo C, Hsu S, Chang K, Wang C. Analysis of a 50 kW organic Rankine cycle system. Energy 2011;36:5877–85. https://doi.org/10.1016/j.energy.2011.08.035.

[30] Mago PJ, Chamra LM, Somayaji C. Performance analysis of different working fluids for use in organic Rankine cycles. Proc Inst Mech Eng Part A J Power Energy 2007;221:255–64. https://doi.org/10.1243/09576509JPE372.
[31] Stijepovic MZ, Linke P, Papadopoulos AI, Grujic AS. On the role of working fluid properties in Organic Rankine Cycle performance. Appl Therm Eng 2012;36: 406–13. https://doi.org/10.1016/j.applthermaleng.2011.10.057.
[32] Jung D, Park S, Min K. Selection of appropriate working fluids for Rankine cycles used for recovery of heat from exhaust gases of ICE in heavy-duty series hybrid electric vehicles. Appl Therm Eng 2015;81:338–45. https://doi.org/10.1016/j.applthermaleng.2015.02.002.
[33] Wang D, Ling X, Peng H, Liu L, Tao LL. Efficiency and optimal performance evaluation of organic Rankine cycle for low grade waste heat power generation. Energy 2013;50:343–52. https://doi.org/10.1016/j.energy.2012.11.010.
[34] He C, Liu C, Zhou M, Xie H, Xu X, Wu S, et al. A new selection principle of working fluids for subcritical organic Rankine cycle coupling with different heat sources. Energy 2014;68:283–91. https://doi.org/10.1016/j.energy.2014.02.050.
[35] Song C, Gu M, Miao Z, Liu C, Xu J. Effect of fluid dryness and critical temperature on trans-critical organic Rankine cycle. Energy 2019;174:97–109. https://doi.org/10.1016/j.energy.2019.02.171.
[36] Xu J, Yu C. Critical temperature criterion for selection of working fluids for subcritical pressure Organic Rankine cycles. Energy 2014;74:719–33. https://doi.org/10.1016/j.energy.2014.07.038.
[37] Lai NA, Wendland M, Fischer J. Working fluids for high-temperature organic Rankine cycles. Energy 2011;36:199–211. https://doi.org/10.1016/j.energy.2010.10.051.
[38] Barse KA, Mann MD. Maximizing ORC performance with optimal match of working fluid with system design. Appl Therm Eng 2016;100:11–9. https://doi.org/10.1016/j.applthermaleng.2016.01.167.
[39] Aljundi IH. Effect of dry hydrocarbons and critical point temperature on the efficiencies of organic Rankine cycle. Renew Energy 2011;36:1196–202. https://doi.org/10.1016/j.renene.2010.09.022.
[40] Zhai H, Shi L, An Q. Influence of working fluid properties on system performance and screen evaluation indicators for geothermal ORC (organic Rankine cycle) system. Energy 2014;74:2–11. https://doi.org/10.1016/j.energy.2013.12.030.
[41] Saleh B, Koglbauer G, Wendland M, Fischer J. Working fluids for low-temperature organic Rankine cycles. Energy 2007;32:1210–21. https://doi.org/10.1016/j.energy.2006.07.001.
[42] Vivian J, Manente G, Lazzaretto A. A general framework to select working fluid and configuration of ORCs for low-to-medium temperature heat sources. Appl Energy 2015;156:727–46. https://doi.org/10.1016/j.apenergy.2015.07.005.
[43] Zhai H, An Q, Shi L. Analysis of the quantitative correlation between the heat source temperature and the critical temperature of the optimal pure working fluid for subcritical organic Rankine cycles. Appl Therm Eng 2016;99:383–91. https://doi.org/10.1016/j.applthermaleng.2016.01.058.
[44] Eastman chemical company. Product data sheet Therminol 66. Website address: http://www.eastman.com/pages/products/therminol66.asp; accessed on 09th May 2021.
[45] Sterrer R, Schidler S, Schwandt O, Franz P, Hammerschmid A. Theoretical analysis of the combination of CSP with a biomass CHP-plant using ORC-technology in Central Europe. Energy Procedia 2014;49:1218–27. https://doi.org/10.1016/j.egypro.2014.03.131.
[46] Bianchi M, Branchini L, De Pascale A, Melino F, Orlandini V, Peretto A, et al. Techno-Economic Analysis of ORC in Gas Compression Stations Taking into Account Actual Operating Conditions. Energy Procedia 2017;129:543–50. https://doi.org/10.1016/j.egypro.2017.09.182.
[47] Tafone A, Borri E, Comodi G, Van Den Broek M, Romagnoli A. Preliminary assessment of waste heat recovery solution (ORC) to enhance the performance of Liquid Air Energy Storage system. Energy Procedia 2017;142:3609–16. https://doi.org/10.1016/j.egypro.2017.12.252.
[48] Song J, Song Y, Gu C. Thermodynamic analysis and performance optimization of an Organic Rankine Cycle (ORC) waste heat recovery system for marine diesel engines. Energy 2015;82:976–85. https://doi.org/10.1016/j.energy.2015.01.108.
[49] Tourkov K, Schaefer L. Performance evaluation of a PVT/ORC (photovoltaic thermal/organic Rankine cycle) system with optimization of the ORC and evaluation of several PV (photovoltaic) materials. Energy 2015;82:839–49. https://doi.org/10.1016/j.energy.2015.01.094.
[50] Siddiqi MA, Atakan B. Alkanes as fluids in Rankine cycles in comparison to water, benzene and toluene. Energy 2012;45:256–63. https://doi.org/10.1016/j.energy.2012.06.005.
[51] Tchanche BF, Papadakis G, Lambrinos G, Frangoudakis A. Fluid selection for a low-temperature solar organic Rankine cycle. Appl Therm Eng 2009;29:2468–76. https://doi.org/10.1016/j.applthermaleng.2008.12.025.
[52] Shu G, Li X, Tian H, Liang X, Wei H, Wang X. Alkanes as working fluids for high-temperature exhaust heat recovery of diesel engine using organic Rankine cycle. Appl Energy 2014;119:204–17. https://doi.org/10.1016/j.apenergy.2013.12.056.
[53] Liu P, Shu G, Tian H, Wang X, Yu Z. Alkanes based two-stage expansion with interheating Organic Rankine cycle for multi-waste heat recovery of truck diesel engine. Energy 2018;147:337–50. https://doi.org/10.1016/j.energy.2017.12.109.
[54] United Nations. Montreal Protocol on Substances That Deplete the Ozone Layer. Ozone Secretariat, New York, NY, USA: United Nations Environment Program; 1987.
[55] Occhipinti Z, Verona R. Kyoto Protocol (KP). In: Leal FW, Azul AM, Brandli L, Özuyar PG, Wall T, editors. Climate Action. Encyclopedia of the UN Sustainable Development Goals. Cham: Springer; 2020. https://doi.org/10.1007/978-3-319-95885-9_23.
[56] European Parliament. Regulation (EU) No 517/2017 of the European parliament and of the council of 16 april 2014 on fluorinated greenhouse gases and repealing regulation (EC) No 842/2006. Council of the European Union 2014.
[57] Kopko WL. Beyond CFCs: Extending the search for new refrigerants. Int J Refrig 1990;13:79–85. https://doi.org/10.1016/0140-7007(90)90005-H.
[58] Wang H, Zhao L, Cao R, Zeng W. Refrigerant alternative and optimization under the constraint of the greenhouse gas emissions reduction target. J Clean Prod 2021;296:126580. https://doi.org/10.1016/j.jclepro.2021.126580.
[59] Sánchez D, Cabello R, Llopis R, Arauzo I, Catalán-gil J, Torrella E. Energy performance evaluation of R1234yf, R1234ze(E), R600a, R290 and R152a as low-GWP R134a alternatives. Int J Refrig 2020;74:269–82. https://doi.org/10.1016/j.ijrefrig.2016.09.020.
[60] Albà CG, Vega LF, Llovell F. A consistent thermodynamic molecular model of n-hydrofluoroolefins and blends for refrigeration applications. Int J Refrig 2020; 113:145–55. https://doi.org/10.1016/j.ijrefrig.2020.01.008.
[61] Mota-Babiloni A, Makhnatch P. Predictions of European refrigerants place on the market following F-gas regulation restrictions. Int J Refrig 2021;127:101–10. https://doi.org/10.1016/j.ijrefrig.2021.03.005.
[62] Xiao B, Chang H, He L, Zhao S, Shu S. Annual performance analysis of an air source heat pump water heater using a new eco-friendly refrigerant mixture as an alternative to R134a. Renew Energy 2020;147:2013–23. https://doi.org/10.1016/j.renene.2019.09.143.
[63] Dai B, Liu S, Li H, Sun Z, Song M, Yang Q, et al. Energetic performance of transcritical CO2 refrigeration cycles with mechanical subcooling using zeotropic mixture as refrigerant. Energy 2018;150:205–21. https://doi.org/10.1016/j.energy.2018.02.111.
[64] Morrison G, McLinden MO. Azeotropy in refrigerant mixtures. Int J Refrig 1993; 16:129–38. https://doi.org/10.1016/0140-7007(93)90069-K.
[65] Vaitkus L, Dagilis V. Analysis of alternatives to high GWP refrigerants for eutectic refrigerating systems. Int J Refrig 2017;76:160–9. https://doi.org/10.1016/j.ijrefrig.2017.01.024.
[66] Li Z, Shen B, Gluesenkamp KR. Multi-objective optimization of low-GWP mixture composition and heat exchanger circuitry configuration for improved system performance and reduced refrigerant flammability. Int J Refrig 2021;126:133–42. https://doi.org/10.1016/j.ijrefrig.2021.01.003.
[67] B.-M. Lee, H.-H. Gook, S.-B. Lee, Y.-W. Lee, D.-H. Park, N.-H. Kim, Condensation heat transfer and pressure drop of low GWP R-404A alternative refrigerants (R-448A, R-449A, R-455A, R-454C) in a 5.6 mm inner diameter horizontal smooth tube, Int. J. Refrig. 128 (2021) 71-82. 10.1016/j.ijrefrig.2020.12.025.
[68] Schulze C, Raabe G, Tegethoff WJ, Koehler J. Transient evaluation of a city bus air conditioning system with R-445A as drop-in – From the molecules to the system. Int J Therm Sci 2015;96:355–61. https://doi.org/10.1016/j.ijthermalsci.2015.01.033.
[69] Devecioğlu AG, Oruç V. An analysis on the comparison of low-GWP refrigerants to alternatively use in mobile air-conditioning systems. Therm Sci Eng Prog 2017; 1:1–5. https://doi.org/10.1016/j.tsep.2017.02.002.
[70] Li G, Eisele M, Lee H, Hwang Y, Radermacher R. Experimental investigation of energy and exergy performance of secondary loop automotive air-conditioning systems using low-GWP (global warming potential) refrigerants. Energy 2014;68: 819–31. https://doi.org/10.1016/j.energy.2014.01.018.
[71] M. Xue, N. Kojima, L. Zhou, T. Machimura, A. Tokai, Dynamic analysis of global warming impact of the household refrigerator sector in Japan from 1952 to 2030, J. Clean. Prod. 145 (2017) 172–179. 10.1016/j.jclepro.2017.01.059.
[72] Sethi A, Pottker G, Motta SY. Experimental evaluation and field trial of low global warming potential R404A replacements for commercial refrigeration. Sci Tech Built Environ 2016;22:1175–84. https://doi.org/10.1080/23744731.2016.1209032.
[73] Eyerer S, Wieland C, Vandersickel A, Spliethoff H. Experimental study of an ORC (Organic Rankine Cycle) and analysis of R1233zd-E as a drop-in replacement for R245fa for low temperature heat utilization. Energy 2016;103:660–71. https://doi.org/10.1016/j.energy.2016.03.034.
[74] Yang J, Sun Z, Yu B, Chen J. Experimental comparison and optimization guidance of R1233zd(E) as a drop-in replacement to R245fa for organic Rankine cycle application. Appl Therm Eng 2018;141:10–9. https://doi.org/10.1016/j.applthermaleng.2018.05.105.
[75] Molés F, Navarro-Esbrí J, Peris B, Mota-Babiloni A, Mateu-Royo C. R1234yf and R1234ze as alternatives to R134a in Organic Rankine Cycles for low temperature heat sources. Energy Procedia 2017;142:1192–8. https://doi.org/10.1016/j.egypro.2017.12.380.
[76] Yang J, Ye Z, Yu B, Ouyang H, Chen J. Simultaneous experimental comparison of low-GWP refrigerants as drop-in replacements to R245fa for Organic Rankine cycle application: R1234ze(Z), R1233zd(E), and R1336mzz(E). Energy 2019;173: 721–31. https://doi.org/10.1016/j.energy.2019.02.054.
[77] Longo GA, Mancin S, Righetti G, Zilio C, Brown JS. Assessment of the low-GWP refrigerants R600a, R1234ze(Z) and R1233zd(E) for heat pump and organic Rankine cycle applications. Appl Therm Eng 2020;167:114804. https://doi.org/10.1016/j.applthermaleng.2019.114804.
[78] Bianchi M, Branchini L, De Pascale A, Melino F, Ottaviano S, Peretto A, et al. Replacement of R134a with low-GWP fluids in a kW-size reciprocating piston expander: Performance prediction and design optimization. Energy 2020;206: 118174. https://doi.org/10.1016/j.energy.2020.118174.

[79] Devecioğlu AG, Oruç V. Characteristics of Some New Generation Refrigerants with Low GWP. Energy Procedia 2015;75:1452–7. https://doi.org/10.1016/j.egypro.2015.07.258.
[80] Park B-S, Usman M, Imran M, Pesyridis A. Review of Organic Rankine Cycle experimental data trends. Energy Convers Manag 2018;173:679–91. https://doi.org/10.1016/j.enconman.2018.07.097.
[81] Dubberke FH, Linnemann M, Abbas WK, Baumhögger E, Priebe K-P, Roedder M, et al. Experimental setup of a cascaded two-stage organic Rankine cycle. Appl Therm Eng 2018;131:958–64. https://doi.org/10.1016/j.applthermaleng.2017.11.137.
[82] STEAG Energy Services GmbH: EBSILON Professional, URL: http://www.steag-systemtechnologies.com/ebsi-lon_professional.html, assessed on 16.05.2021.
[83] Lemmon EW, Huber ML, McLinden MO. Reference fluid thermodynamic and transport properties (REFPROP), version 10.0, in NIST Standard Reference Database 23. Gaithersburg, MD: National Institute of Standard and Technology; 2007.
[84] Uusitalo A, Honkatukia J, Turunen-Saaresti T, Grönman A. Thermodynamic evaluation on the effect of working fluid type and fluids critical properties on design and performance of Organic Rankine Cycles. J Clean Prod 2018;188:253–63. https://doi.org/10.1016/j.jclepro.2018.03.228.
[85] Zhou Y, Liu J, Penoncello SG, Lemmon EW. An equation of state for the thermodynamic properties of cyclohexane. J Phys Chem Ref Data 2014;43:043105. https://doi.org/10.1063/1.4900538.
[86] Gedanitz H, Davila MJ, Lemmon EW. Speed of sound measurements and a fundamental equation of state for cyclopentane. J Chem Eng Data 2015;60:1331–7. https://doi.org/10.1021/je5010164.
[87] Mondéjar ME, Mclinden MO, Lemmon EW. Thermodynamic properties of trans-1-chloro-3,3,3-trifluoropropene (R1233zd(E)): vapor pressure, (p, ρ, T) behavior, and speed of sound measurements, and equation of state. J Chem Eng Data 2015;60:2477–89. https://doi.org/10.1021/acs.jced.5b00348.
[88] Bücker D, Wagner W. Reference equations of state for the thermodynamic properties of fluid phase n-butane and isobutane. J Phys Chem Ref Data 2006;35:929–1019. https://doi.org/10.1063/1.1901687.
[89] Akasaka R, Lemmon EW. Fundamental equations of state for cis-1,3,3,3-tetrafluoropropene [R-1234ze(Z)] and 3,3,3-trifluoropropene (R-1243zf). J Chem Eng Data 2019;64:4679–91. https://doi.org/10.1021/acs.jced.9b00007.
[90] Wu J, Zhou Y, Lemmon EW. An equation of state for the thermodynamic properties of dimethyl ether. J Phys Chem Ref Data 2011;40:023104. https://doi.org/10.1063/1.3582533.
[91] Outcalt SL, McLinden MO. A modified Benedict-Webb-Rubin equation of state for the thermodynamic properties of R152a (1,1-difluoroethane). J Phys Chem Ref Data 1996;25:605–36. https://doi.org/10.1063/1.555979.
[92] Thol M, Lemmon EW. Equation of State for the Thermodynamic Properties of trans-1,3,3,3-Tetrafluoropropene [R-1234ze(E)]. Int J Thermophys 2016;37:28. https://doi.org/10.1007/s10765-016-2040-6.
[93] Qi H, Fang D, Gao K, Meng X, Wu J. Compressed liquid densities and Helmholtz energy equation of state for fluoroethane (R161). Int J Thermophys 2016;37:37–55. https://doi.org/10.1007/s10765-016-2061-1.
[94] Lemmon EW, McLinden MO, Wagner W. Thermodynamic properties of propane. III. A reference equation of state for temperatures from the melting line to 650 K and pressures up to 1000 Mpa. J Chem Eng Data 2009;54:3141–80. https://doi.org/10.1021/je900217v.
[95] Richter M, McLinden MO, Lemmon EW. Thermodynamic properties of 2,3,3,3-tetrafluoroprop-1-ene (R1234yf): Vapor pressure and p – ρ – T Measurements and an Equation of State. J Chem Eng Data 2011;56:3254–64. https://doi.org/10.1021/je200369m.
[96] S. Solmon, D. Qin, M. Manning, M. Marquis, M.M.B Tiguor, H.L. Miller, Z. Chen, Climate Change 2007: The Physical Science Basis. Contribution of Working Group I to the Fourth Assessment Report of the Intergovernmental Panel on Climate Change, Cambridge University Press, Cambridge, United Kingdom and New York, NY, USA, p 996.
[97] J.M. Calm, G.C. Hourahan, Physical, safety, and environmental data for current and alternative refrigerants, Proceedings of the 23rd IIR International Congress of Refrigeration: Prague, Czech Republic, August 21-26, 2011.
[98] Abbas WKA, Linnemann M, Baumhögger E, Vrabec J. Experimental study of two cascaded organic Rankine cycles with varying working fluids. Energy Convers Manag 2021;230:113818. https://doi.org/10.1016/j.enconman.2020.113818.
[99] Safarian S, Aramoun F. Energy and exergy assessments of modified Organic Rankine Cycles (ORCs). Energy Rep 2015;1:1–7. https://doi.org/10.1016/j.egyr.2014.10.003.
[100] Liu W, Meinel D, Wieland C, Spliethoff H. Investigation of hydro fluoroolefins as potential working fluids in organic Rankine cycle for geothermal power generation. Energy 2014;67:106–16. https://doi.org/10.1016/j.energy.2013.11.081.
[101] Giuffrida A. A theoretical study on the performance of a scroll expander in an organic Rankine cycle with hydrofluoroolefins (HFOs) in place of R245fa. Energy 2018;161:1172–80. https://doi.org/10.1016/j.energy.2018.07.146.
[102] Ciconkov R. Refrigerants: There is still no vision for sustainable solutions. Int J Refrig 2018;86:441–8. https://doi.org/10.1016/j.ijrefrig.2017.12.006.

5.4. Experimental investigation of organic Rankine cycle performance using alkanes or hexamethyldisiloxane as a working fluid

Abbas W K A, Baumhögger E, Vrabec J. Experimental investigation of organic Rankine cycle performance using alkanes or hexamethyldisiloxane as a working fluid. Energy Conversion and Management: X 2022;15;100244. DOI: 10.1016/J.ECMX.2022.100244.

With permission of Elsevier reprinted from the journal Energy Conversion and Management X (Copyright 2022).

The HT-ORC in the CORC system was tested as a regular ORC unit over a wide range of heat source temperature and turbine inlet pressure. MM, cyclopentane, pentane and butane were selected as working fluids. In addition, the system performance in terms of thermal and exergy efficiencies was investigated for various values of superheating degree and pressure ratio. Exergy loss measurement was performed for the main components at the highest heat source temperature. The results indicated the positive effect of large heat source temperature and pressure ratio. The results showed that the superheating degree should be within a certain range. Moreover, the relationship between system performance and thermo-physical properties, such as critical temperature and critical pressure, was studied.

The author of this thesis selected the working fluids, operating conditions and conducted the experiments. Elmar Baumhögger supported the experiments. This paper was written by the author of this thesis and was revised by Jadran Vrabec.

Energy Conversion and Management: X 15 (2022) 100244

Contents lists available at ScienceDirect

Energy Conversion and Management: X

journal homepage: www.sciencedirect.com/journal/energy-conversion-and-management-x

Experimental investigation of organic Rankine cycle performance using alkanes or hexamethyldisiloxane as a working fluid

Wameedh Khider Abbas Abbas [a], Elmar Baumhögger [a], Jadran Vrabec [b,*]

[a] Thermodynamics and Energy Technology, University of Paderborn, Warburger Straße 100, 33098 Paderborn, Germany
[b] Thermodynamics and Process Engineering, Technical University of Berlin, Ernst-Reuter-Platz 1, 10587 Berlin, Germany

ARTICLE INFO

Keywords:
Thermal efficiency
Exergy efficiency
Heat source temperature
Working fluid
Alkane
Siloxane

ABSTRACT

An experimental investigation of the organic Rankine cycle (ORC) is carried out using butane, pentane, cyclopentane or hexamethyldisiloxane as a working fluid. Thermal and exergy efficiencies are used to assess system performance over a wide range of heat source temperature, turbine inlet pressure and superheating degree. The results indicate that both of these efficiencies increase with rising heat source temperature and turbine inlet pressure. Under the present experimental conditions, without using an optimized turbine, the highest thermal efficiency and exergy efficiency are 8.0% and 25.2%, respectively. The results show that hexamethyldisiloxane is a better working fluid than the alkanes under all studied experimental conditions. Moreover, it is found that a small superheating degree may be beneficial. Exergy loss analysis indicates that most of the loss occurs in the evaporator and that a working fluid with a high critical temperature is advantageous for ORC systems driven by a heating cycle with a heat transfer fluid.

Introduction

Power supply is at the core of modern societies and it is clear that the demand for more is poised to further increase in the decades to come due to population growth and development. While the large majority of electrical energy stems from fossil sources, the associated release of carbon dioxide is not sustainable. Now, it is widely accepted that traditional energy conversion processes must be curbed and alternatives are urgently needed [1,2]. One option that can yield clean, eco-friendly power is the organic Rankine cycle (ORC). This technology can be driven by any heat source, such as geothermal, biomass, solar-thermal or industrial waste heat, utilizing various temperature levels [3].

Currently, there are more than 2700 ORC projects with power generation units ranging from a few kilowatts to several dozen megawatts and the total capacity is above 4 GW. Since 2016, the ORC market has witnessed a significant growth, as more than 850 units were added with a capacity of about 1.18 GW. The total capacity can be divided into geothermal (77.4 %), waste heat recovery (11.6 %) and biomass (10.1 %), while other applications have a minor percentage: waste-to-energy (0.7 %), solar (0.2 %) and remote (0.03 %) [4,5].

Since the emergence of ORC technology, many studies have experimentally tested its efficiency and studied different operating conditions, architectures and heat sources. Most of the published experiments were based on small-scale ORC or prototypes [6]. Park et al. [7] presented a comprehensive review of experimental investigations from 2009 until 2018. They reported that R245fa, R123 and R134a were the most widely employed working fluids and that the majority of published works examined ORC systems with a turbine power output below 10 kW. The investigated ORC systems were thus on a small scale and the applied heat source temperature was either constant or varied over a small range.

In the subsequent short review of experimental works from 2018 until today, we also found that most researchers have studied small-scale ORC with a turbine power output between 1 and 50 kW. It was focused on system performance in terms of thermal, exergy and turbine efficiencies as well as heat characteristics. The thermal efficiency is usually considered as the most suitable indicator because it is the ratio between the net power output and the heat flow rate supplied to the evaporator.

Mascuch et al. [8] carried out an experimental study on a kilowatt-scale biomass-fired ORC utilizing hexamethyldisiloxane (MM) as a working fluid with a turbine inlet temperature of 192 °C. The authors showed that the isentropic efficiency of the turbine was between 28% and 52%, which led to a low thermal efficiency of 2.5%. Feng et al. [9] considered R245fa as a working fluid and explored the performance of basic and regenerative ORC. The maximum thermal efficiency was 5.5%

* Corresponding author.
E-mail addresses: jadran.vrabec@upb.de, vrabec@tu-berlin.de (J. Vrabec).

https://doi.org/10.1016/j.ecmx.2022.100244
Received 6 March 2022; Received in revised form 23 May 2022; Accepted 4 June 2022
Available online 7 June 2022
2590-1745/© 2022 The Authors. Published by Elsevier Ltd. This is an open access article under the CC BY-NC-ND license (http://creativecommons.org/licenses/by-nc-nd/4.0/).

Nomenclature

c_p	Specific isobaric heat capacity [kJ/(kg K)]
$\dot{E}^{in}$	Exergy flow input [kW]
h	Specific enthalpy [kJ/kg]
$\dot{I}$	Exergy flow loss [kW]
$\dot{m}$	Mass flow rate in ORC [kg/s]
$\dot{m}_{HC}$	Mass flow rate in heating cycle [kg/s]
M	Molar mass [g/mol]
p_c	Critical pressure [bar]
$\dot{Q}$	Heat flow [kW]
$\dot{Q}_{HC}$	Heat flow in heating cycle [kW]
s	Specific entropy [kJ/(kg K)]
T_c	Critical temperature [°C]
$\dot{W}_{net}$	Net power output [kW]
$\dot{W}_P$	Pump power [kW]
$\dot{W}_T$	Turbine power output [kW]

Acronyms

GWP	Global warming potential [–]
HC	Heating cycle [–]
HE	Heat exchanger [–]
HT	High-temperature [–]
LT	Low-temperature [–]
ODP	Ozone depletion potential [–]
TIP	Turbine inlet pressure [bar]

Greek symbols

η_{ex}	Exergy efficiency [%]
η_T	Isentropic turbine efficiency [%]
η_{th}	Thermal efficiency [%]

Subscripts and superscripts

1–2	Process from state 1 to state 2
C	Condenser
G	Generator
M0	Heating cycle pump
M1	ORC pump
M2	Cooling cycle pump

and it was found that the evaporator was critical with respect to exergy loss, indicating that system performance can be improved by decreasing the temperature difference between the heat source and the turbine inlet. Gao et al. [10] investigated a R290-based ORC experimentally by varying evaporation pressure and pressure drop, achieving a maximum thermal efficiency of 6.78%. Wang et al. [11] studied a 1 kW-scale ORC with R290 as a working fluid in the context of cold energy utilization. System performance was evaluated at a heat source temperature in the range of 20–55 °C and the maximum thermal efficiency was 6.49%. Araya et al. [12] experimentally compared R1233zd(E) and R245fa as working fluids with respect to system performance. They reported that the highest thermal efficiency was 5.0% when utilizing R1233zd(E) at a heat source temperature of 85.7 °C. Kaczmarzyk et al. [13] presented an experimental investigation on a small-scale ORC system which uses a biomass boiler as a heat source. They utilized a radial-flow turbine as expander device and recorded an isentropic turbine efficiency in the range from 52% to 71%, leading to a maximum thermal efficiency of 6.5%. İpek et al. [14] investigated the performance of a low-temperature ORC system to recover heat from a gas turbine using R134a as a working fluid. They found that the heat source temperature in the range 86–88 °C was optimal to reach maximum system performance in terms of thermal efficiency, expansion ratio and turbine power output. The highest achieved thermal efficiency was 6.84% at a heat source temperature of 86.5 °C. Wu et al. [15] studied system performance in terms of thermal and exergy efficiencies and exergy loss using R245fa as a working fluid. They reported that the highest thermal and exergy efficiencies were 2.54% and 8.09%, respectively. The authors also found that most of the exergy loss occurred in the evaporator (58.38%). Fatigati et al. [6] followed an experimental approach to evaluate turbine power output and thermal efficiency of a small-scale ORC for different flow rates of R245fa working fluid. Their system generated a turbine power output in the range of 200–500 W, while the thermal efficiency was 4–6%. The authors pointed out that the low thermal efficiency was due to the poor efficiency of the turbine, which underlines that the latter is a crucial parameter for ORC system performance. Qui and Entchev [16] carried out an experimental study with a micro-combined heat and power ORC system using R1223zd(E) and n-pentane as a working fluid. The thermal efficiency of both working fluids was tested at a turbine inlet temperature of 135–136 °C and a pressure ratio of 3.65, leading to a maximum thermal efficiency of 5.6% and 5.3%, respectively. Carraro et al. [17] investigated the performance of a biomass-fired micro-ORC system using R245fa as a working fluid that had its maximum performance for a heat source temperature of 150 °C. They reported that the electrical efficiency (ratio of net electric power to absorbed heat flow) and turbine efficiency were 7.4% and 57%, respectively. Qiu et al. [18] tested an ORC-based micro-combined heat and power unit for residential applications. They selected pentane as a working fluid to study turbine power output and cycle efficiency. Their simulation results showed that their system may reach a cycle efficiency of 10%, which was higher than the experimental results.

Table 1
Overview of recent experimental studies of the ORC.

Ref.	Working fluid	Source temperature	η_{th}[%]	η_T[%]
[8]	MM	192 °C	2.5%	28%-52%
[9]	R245fa	77–108 °C	5.5%	
[10]	R290	n.a	6.7%	
[11]	R290	20–55 °C	6.49%	
[12]	R1223zd(E) & R245fa	85.7 °C	5.0%	
[13]	HFE7100	n.a	6.5%	52–71%
[14]	R134a	86–88 °C	6.84%	
[15]	R245fa	120 °C	2.54%	
[6]	R245fa	70–110 °C	4–6%	
[16]	R1223zd(E) & n-pentane	135–136 °C	5.6–5.3%	
[17]	R245fa	120–155 °C	7.4%	57%

The present literature review confirms that ORC systems with a turbine power of up to 15 kW are characterized by a low thermal efficiency, which in turn is attributed to the poor turbine efficiency at this power scale. Most research focused on specific working fluids and the measurements were done at a specific heat source temperature or over a narrow range. Rather few parameters were varied in a given work. Studies dealing with alkanes and siloxanes as working fluids are very limited. As far as the authors are aware, there is no experimental study that tests and compares the performance of several alkanes and a siloxane over a wide range of operating conditions. Table 1 gives a summary of the present literature review.

Generally, there is a gap between theoretical and practical work looking at ORC system performance. The reason is that theoretical studies depend on calculations with simulation programs to assess different working fluids and varying operating conditions. However, most of these theoretical studies assumed parameters at optimal values that require well-designed components that are different to be put in

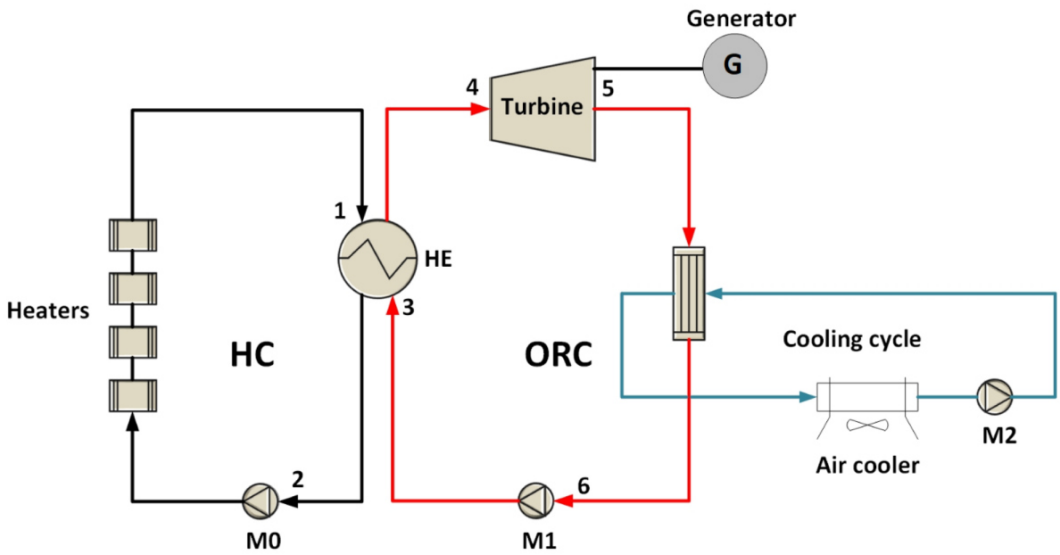

Fig. 1. Layout of the investigated ORC test rig in the present work.

practice [19,20].

The novelty of this work is that the performance of a ORC system is studied experimentally in terms of thermal and exergy efficiencies using four working fluids over a wide range of heat source temperature, turbine inlet pressure and superheating degree. Turbine efficiency, enthalpy drop across the turbine and exergy loss are investigated as well. It attempts to fill this gap with an experimental investigation of ORC system technology over a wide range of operating conditions, where butane, pentane, cyclopentane and MM were employed as a working fluid.

Materials and methods

ORC test rig

The present test rig facility is a part of the cascaded two-ORC system (CORC) that was designed and built at the University of Paderborn. It formed the basis for several studies. The first one dealt with the installation of the system and explained its main components and operation process, outlining a preliminary test using two working fluids [22]. The second investigation looked at CORC operation with varying working fluids, where thermal efficiency, heat transfer properties and pinch point temperature difference were assessed [25]. The third paper described a simulation study of the same system considering alkanes and 31 low-GWP refrigerants [26].

The CORC consists of two cascaded ORC, namely the high-temperature cycle (HT-ORC) and the low-temperature cycle (LT-ORC). Each cycle consists of the main components of an ORC system, i.e. pump, evaporator, turbine and condenser. According to the design of the test rig, the HT-ORC can operate as a regular ORC system because it contains all main components and is directly connected to the heat source.

The ORC test rig has three main cycles, i.e. heating cycle that acts as the source, power generation cycle and cooling cycle. The process diagram and the front view of the ORC test rig are shown in Fig. 1. The system was connected to the heating cycle with a thermal power of up to 158 kW. The maximum applicable temperature was specified to be 300 °C to avoid thermal decomposition of the heat transfer fluid (Therminol 66) in the heating cycle. The ORC test rig provided a stable and controlled mass flow rate of working fluid and heat source temperature. To mitigate safety issues, the system was equipped with fast-acting controllers and valves. The system components were designed and selected to improve operating flexibility and allow for the utilization of a wide range of working fluids. Furthermore, the ORC test rig components were sized to meet demanding conditions in terms of heat source temperature, vapor pressure, mass flow rate of the working fluid, environmental and safety aspects. Consequently, the turbine was not optimized for a specific working fluid or operating conditions. The flexible design of the present ORC test rig makes it suitable for testing a large number of working fluids over a wide range of conditions. The maximum operating temperature of the system is 300 °C so that it may recover heat from several source types, such as biomass or waste heat, which can be found e.g. in cement or aluminium industries. Moreover, the ORC system is an assembly of heat exchangers, pumps and condensers that are readily available in the market such that it can be converted into a practical application quite straightforwardly. The ORC cycle and its main components are shown in Fig. 2. Tables 2 and 3 list the basic components and measuring devices of the ORC test rig.

ORC cycle

The present ORC consisted of a progressive cavity pump (M1), a plate heat exchanger acting as an evaporator (HE), a radial turbine as an expander (T), a six-pole synchronous generator (G) and a plate heat exchanger as a condenser (C). The pump pressurized the working fluid in the liquid state and delivered it to the evaporator (process 6–3), where it was preheated, evaporated and superheated (process 3–4). Then, the working fluid expanded through the turbine to generate power (process 4–5). After expansion, the working fluid was cooled down and liquified in the condenser by discharging heat to the ambient via the cooling cycle (process 5–6).

Heating cycle

Four flow heaters represented the heat source with a maximum thermal power of 158 kW. The electrical heaters consisted of three standard heating rods and one thyristor-controlled heating rod for specifying the heat source temperature. Electrical heaters are inherently simple to control and can be easily adjusted, which allows for the investigation of a wide range of heat source temperatures. Moreover, electrical heaters may reach a high temperature level with low operational risk and reduce the uncertainty of heat flow input. Therminol 66 was used as a heat transfer fluid due to its good thermal stability, low

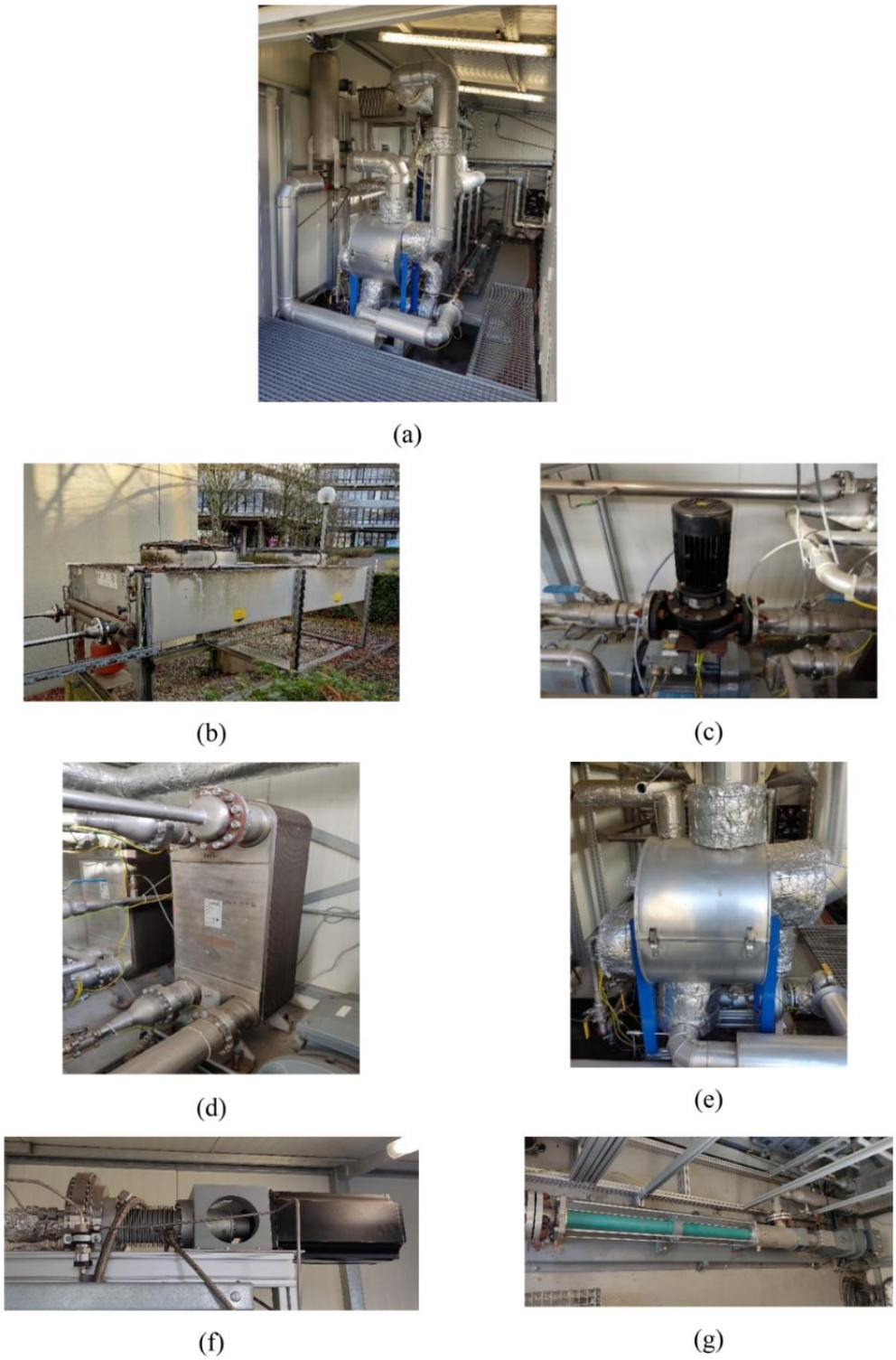

Fig. 2. (a) The ORC test rig was in a container due to safety considerations, (b) air cooler, (c) pump M2, (d) condenser C, (e) heat exchanger HE, (f) turbine T and generator G, (g) pump M0.

vapor pressure and non-corrosiveness to the components of the heating cycle. The heat transfer fluid was supplied by Fragol [27]. During the process, Therminol 66 was heated up by the electrical heaters and circulated through the heating cycle via a radial flow pump (M0) to deliver the driving heat flow to the working fluid via the heat exchanger.

Table 2
Main components of the ORC system considered in the present work.

Component	Type	Range	Refs.
M0	Radial flow	Up to: 350 °C, 1250 m^3/h	[21]
Flow heaters	GC heat D01-00508	0 – 158 kW	[22]
M1	NETZSCH NEMO	−20 – 200 °C	[23]
HE	Plate & Shell	−20 – 280 °C, 0 – 60 bar	[24]
C	Plate heat exchanger	Max. 25 bar	[22]
T	Radial flow	Up to 325 °C	[22]
G	6-pole servomotor	Up to 15 kW	[22]

Table 3
Measuring devices of the ORC test rig.

Variable	Sensor type	Range	Uncertainty
p (HC)	Jumo	0–6 bar	±0.5%
T_1, T_2 (HC)	Pt 1000	−40 to 380 °C	±0.1%
$\dot{m}_{HC}$ (HC)	Pressure difference	0–25 bar	±0.1%
T_3, T_4	Pt 1000	−40 to 380 °C	±0.1%
T_5, T_6	Pt 1000	−40 to 250 °C	±0.1%
p_3, p_4	APT	0–60 bar	±0.5%
p_5, p_6	APT	0–16 bar	±0.5%
$\dot{m}$	Pressure difference	0–100 bar	≤0.065%

Cooling cycle

The role of the cooling cycle of the ORC system was to dissipate the residual heat after the expansion process. The cooling cycle was located outside of the test laboratory and consisted of an air cooler connected to a condenser in the form of a plate heat exchanger. The working fluid in the cooling cycle was a binary ethylene–glycol/water mixture that was circulated with a pump (M2). The residual heat flow after expansion was absorbed by the liquid ethylene–glycol/water mixture and rejected to the ambient via the air cooler.

Working fluid selection

The selection of the working fluid is of key importance for the performance and is the first step of designing an ORC system. It should address several considerations, including thermodynamic properties, thermal stability, material compatibility, inertness with respect to the employed materials, heat transfer characteristics, specific heat, cost, safety aspects and environmental considerations (GWP and ODP) [28,29]. The working fluids selected in this work have a low GWP and zero ODP. MM is environmentally friendly and does not harm the ozone layer, while the alkanes have a GWP of about 20 and zero ODP.

Alkanes have been introduced as working fluids due to environmental aspects and their desirable critical temperature, which allows for a wide range of heat source temperatures. Consequently, butane and pentane are utilized in some commercial ORC systems [30]. Siloxanes have been introduced as a working fluid of ORC systems with a high heat source temperature. Wang et al. [31] measured the thermal stability of siloxanes and reported that they are appropriate working fluids for high-temperature ORC systems. In this context, a noticeable number of studies investigated the effect of different working fluid groups on ORC system performance. Li et al. [32] reported that alkanes are suitable for high-temperature waste heat recovery as well. The authors recommended working fluids with a high critical temperature for high heat source temperatures due to the high turbine inlet temperature that can be imposed during the expansion process. Uusitalo et al. [33] evaluated the impact of the critical properties of working fluids on ORC performance for alkanes and siloxanes. Their results indicated that there is a strong relationship between the thermal efficiency of the system and the critical properties of the working fluid. Loni et al. [34] presented a review of solar-driven ORC systems. They found that butane is the best option for low-temperature ORC units, while MM may be suitable for high-temperature ORC systems due to its high critical temperature, good thermal stability and thermodynamic performance. Sorgulu et al. [35] reported energy and exergy analyses of an ORC system that was integrated with drying and combustion subsystems using MM as a working fluid. Their results indicated that the energy and exergy efficiencies were 29.45% and 28.05%, respectively. Bahrami et al. [36] presented a review of low-GWP working fluids for ORC applications and pointed out that alkanes allow for a good thermodynamic performance. Pili et al. [37] reported a multi-objective optimization of an ORC system utilizing three working fluids. Their results indicated that pentane is the best option for their ORC among the selected working fluids in terms of net power output. The exergetic optimization of two-stage ORC for waste heat recovery was investigated by Braimaikis et al. [38]. They considered four alkanes and three refrigerants to explore the exergy efficiency for a heat source temperature between 100 °C and 300 °C. They reported that their system achieved the highest exergy efficiency when utilizing cyclopentane and butane in the high-temperature ORC and the low-temperature ORC, respectively.

Table 4
Working fluids and their properties.

Working fluid	T_c (°C)	p_c (bar)	M (g/mol)	GWP	ODP	Refs.
MM	245.55	19.311	162.38	Very low	0	[51]
Cyclopentane	238.57	45.828	70.133	~20	0	[46,50]
Pentane	196.55	33.675	72.149	~20	0	[46,49]
Butane	151.98	37.96	58.122	4	0	[46,48]

There is a growing body of literature that deals with the relationship between ORC system performance and the thermophysical properties of working fluids. The selection of working fluids with a high critical temperature may allow for a good thermal efficiency in low- and high-temperature ORC systems [39]. Aljundi [40] and Barse et al. [41] showed a correlation between thermal efficiency and the critical temperature of the working fluid. Braimakis et al. [38] reported that a small difference between the heat source temperature and the critical temperature of the working fluid is advantageous. In this context, Vivian et al. [42] reported that a difference of 35 °C between the heat source temperature and the critical temperature of the working fluid is optimal, while Zhai et al. [43] proposed that this difference should vary between 35 °C and 50 °C.

The objective of this work was to provide practical data on the performance of a ORC using alkanes and MM as working fluids and under different conditions, including heat source temperature, turbine inlet pressure (TIP), superheating degree and pressure ratio. The relationship between system performance and critical properties of the working fluids was studied as well. The critical temperature of the four working fluids varies from 151.98 °C to 245.55 °C, while the critical pressure varies from 19.311 bar to 45.828 bar. Table 4 lists the properties of the selected working fluids.

Thermodynamic analysis

To evaluate the experimentally measured data, the ORC system was modelled on the basis of the first and second laws of thermodynamics. Thereby, it was assumed to be in a steady state and heat losses in the components were neglected. Furthermore, it was assumed that no significant pressure drop occurs in the condenser, heat exchangers or pipes and that the turbine does not exchange heat with the ambient.

For the evaluation of the measured quantities of this experimental study, working fluid properties were calculated with the REFPROP 10.0 [44] database, which rests on the most accurate equations of state, i.e the ones by Bücker et al. [45] for butane, Span et al. [46] for pentane, Gedanitz et al. [47] for cyclopentane and Thol et al. [48] for MM.

Process (1–2): Therminol 66 is heated by electrical heaters to transfer the heat flow $\dot{Q}_{HC}$[kW] to the working fluid of the ORC via the heat

exchanger HE. The heat flow [kW] can be calculated by [22]

$$\dot{Q}_{HC} = \dot{m}_{HC} c_p (T_2 - T_1) \tag{1}$$

where $\dot{m}_{HC}$ [kg/s] the mass flow rate of Therminol 66, c_p [kJ/(kg K)] its specific isobaric heat capacity and T_1 and T_2 [°C] are the inlet and outlet temperatures of the heat exchanger, respectively. The heat flow delivered by the heating cycle drives the ORC (3–4) and evaporates the working fluid. The heat flow [kW] absorbed by the working fluid is [22]

$$\dot{Q} = \dot{m}(h_4 - h_3) \tag{2}$$

where $\dot{m}$ is the mass flow rate of the working fluid in the ORC, h_3 and h_4 [kJ/kg] are its enthalpies at the inlet and outlet of the heat exchanger HE.

Process (4–5) represents the expansion of the working fluid through the turbine, where the power output [kW] is given by [11]

$$\dot{W}_T = \dot{m}(h_4 - h_5) \tag{3}$$

where h_4 and h_5 are the enthalpies at the inlet and outlet of the turbine.

Process (5–6) refers to the condensation process of the working fluid which rejectes heat in condenser C and can be calculated by [49]

$$\dot{Q}_C = \dot{m}(h_5 - h_6) \tag{4}$$

where h_5 and h_6 are the enthalpies at the inlet and outlet of the condenser.

Process (6–3) represents the compression with pump M1 and the associated power [kW] can be determined as [11]

$$\dot{W}_P = \dot{m}\,(h_3 - h_6) \tag{5}$$

where h_6 and h_3 are the enthalpies at the inlet and outlet of the pump.

The thermal efficiency [%] of the ORC can be defined as the ratio of the net power output [kW] to the heat flow input to the ORC [49]

$$\eta_{th} = \frac{\dot{W}_{net}}{\dot{Q}_{HC}} \tag{6}$$

where

$$\dot{W}_{net} = \dot{W}_T - \dot{W}_P \tag{7}$$

The exergy efficiency [%] of the ORC is expressed as the ratio of net power output to exergy flow input [kW] [38]

$$\eta_{ex} = \frac{\dot{W}_{net}}{\dot{E}^{in}} \tag{8}$$

Therein, $\dot{E}^{in}$[kW] is the exergy flow from the heat source, which was calculated by [38]

$$\dot{E}^{in} = \dot{m}_{HC}[(h_{in} - h_0) - T_0(s_{in} - s_0)] \tag{9}$$

where subscript 0 refers to ambient conditions, s_{in} and s_0 [kJ/(kg K)] are the corresponding entropies, while the subscript *in* refers to the inlet condition of Therminol 66.

The isentropic turbine efficiency [%] can be calculated by [11]

$$\eta_T = \frac{h_4 - h_5}{h_4 - h_{5s}} \tag{10}$$

where h_{5s} is the enthalpy of the working fluid at the outlet of a hypothetical isentropic turbine.

The exergy loss of component i [kW] can be calculated by [19]

$$\dot{I}_i = \dot{E}_i^{in} - \dot{E}_i^{out} \tag{11}$$

where $\dot{E}_i^{in}$ is the exergy flow into component i and $\dot{E}_i^{out}$ is the exergy flow at the outlet of component i.

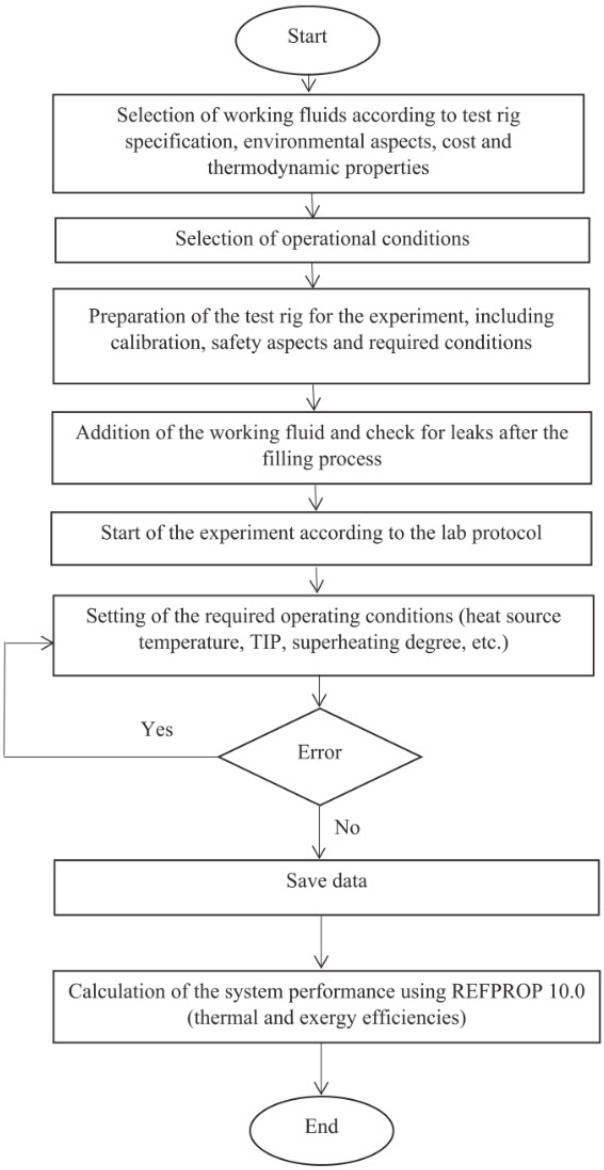

Fig. 3. Procedure of the experimental work.

The exergy loss percentage [%] of each component was calculated by [40]

$$X_i = \frac{\dot{I}_i}{\dot{I}_{total}} \tag{12}$$

where $\dot{I}_{total}$ is the total exergy loss [kW] in the system.

All measurements that we inserted in to Eqs. (1) to (12) to evaluate the ORC process were average values of temperature and pressure at each state point.

Parameters and operational conditions of the experiments

Heat source temperature, TIP and superheating degree were employed as parameters to investigate system performance. Thermal efficiency indicates the use of the heat source and the fraction of heat flow input that is converted into turbine power output. Therefore, it is linked to the available heat flow, which is related to heat exchanger

Table 5
Parameters and operational conditions.

Parameter	Range
Effects of heat source analysis	
Heat source temperature	80–280 °C
Mass flow rate (ORC)	0.08–0.12 kg/s
Ambient pressure	1.013 bar
Ambient temperature	5–25 °C
Mass flow rate (HC)	0.42–0.55 kg/s
Effects of turbine inlet pressure	
Turbine inlet pressure	10–44 bar
Mass flow rate (ORC)	0.09–0.14 kg/s
Mass flow rate (HC)	0.37–0.56 kg/s
Effects of superheating degree	
Superheating degree	1–18 °C
Mass flow rate (ORC)	0.08–0.12 kg/s
Mass flow rate (HC)	0.45–0.55 kg/s

performance. On the other hand, exergy analysis (exergy efficiency and exergy loss) addresses maximum power that can theoretically be generated by bringing the system into equilibrium with its surrounding and clarifies the exergy loss in different components of the ORC system [50]. Moreover, the turbine efficiency and enthalpy drop across the turbine were calculated because these two factors have a direct impact on the design of the turbine and the thermal efficiency of the system.

First, the performance of the ORC in terms of turbine power output, thermal efficiency and exergy efficiency was investigated over a wide range of heat source temperature. Experiments were carried out by using either butane, pentane, cyclopentane or MM as a working fluid. To avoid critical conditions, the maximum applied heat source temperature was restricted by the operating temperature of the heat exchanger and it was ensured that the turbine inlet temperature was below the critical temperature of the working fluid. Consequently, the heat source temperature was in the range of 80–180 °C for butane, 130–230 °C for pentane, 180–280 °C for cyclopentane and 180–280 °C for MM.

Measurements were carried out according to the experimental procedure shown in the flow chart in Fig. 3. Initially, the electric heaters were turned on to bring the heat transfer fluid to the targeted heat source temperature. Then, the mass flow of Therminol 66 was gradually raised and pump M1 was switched on to transfer the working fluid to the evaporator (HE) to absorb heat from the heating cycle. When the measuring point was changed, the electric heating power was gradually increased to raise the heat source temperature by an increment of 10 °C and the mass flow rates of Therminol 66 and the working fluid were adjusted. When the required parameters were reached, it has waited for sampling until the operation point was stable. The measured data were stored automatically with a personal computer.

Second, the heat source temperature was kept constant at the maximum applicable temperature for each working fluid, while the TIP was varied from 28 bar to 36 bar for butane, 24 bar to 32 bar for pentane, 36 bar to 44 bar for cyclopentane and 10 bar to 18 bar for MM. Third, system performance was investigated by applying a varying superheating degree between 1 °C and 18 °C. The TIP was varied by changing the rotational speed of the pump M1. Each time the rotational speed of the pump was raised, the mass flow of the heating cycle and the heat source temperature were adjusted to meet the required values.

The heat source temperature controllers were set to the required temperature and the TIP was gradually raised, with attention to other parameters like working fluid mass flow rate. The same superheating range was measured for all working fluids, ensuring that the heat source temperature did not reach critical states.

The operating conditions and basic parameters of these experiments are listed in Table 5. They are related to design aspects of various components and the thermophysical properties of the working fluids in the present ORC system.

Table 6
Comparison of present results with the literature.

Working fluid	Parameter [%]	Temperature [°C]	This work	Ref.	Difference
Pentane	η_{th}	136	5.38%	5.3 % [16]	0.08
Butane	η_{th}	180	5.4%	5.51% [26]	0.11

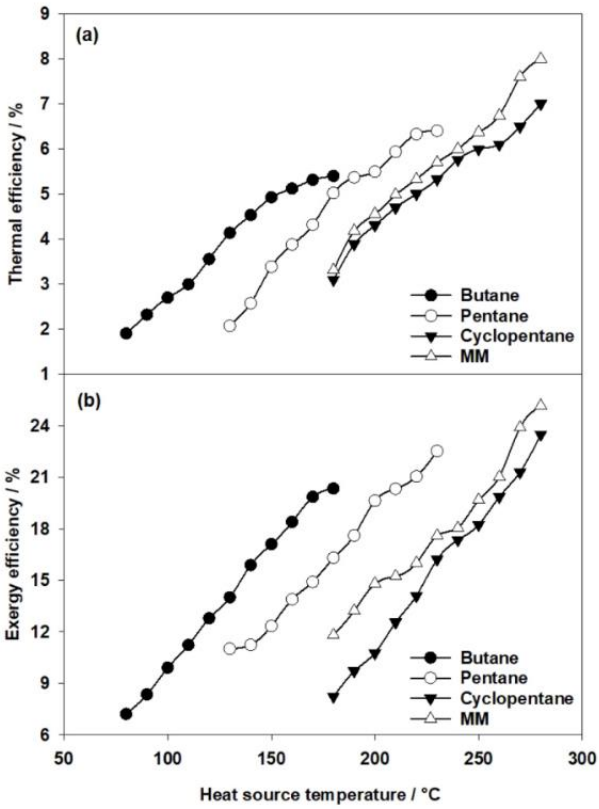

Fig. 4. Effect of heat source temperature on (a) thermal efficiency and (b) exergy efficiency for varying working fluids.

Uncertainties and validation

Thermodynamic calculations were based on REFPROP, which is a Helmholtz energy equation of state library provided by the National Institute of Standards and Technology, Boulder, CO. Typical uncertainties of the thermodynamic properties of the selected working fluids vary from 0.2% to 1% in terms of isobaric heat capacity, 0.1% to 1% in terms of speed of sound, 0.1% to 0.2% in terms of vapor pressure and 0.2% to 0.3% in terms of density [44]. The uncertainties are larger in the region around the critical point, which was avoided in this investigation.

The uncertainties of the measuring devices of the test rig are listed in Table 3. Due to the lack of experimental investigations on ORC systems with the same working fluids and the same operating conditions, the thermal efficiency of pentane was compared with Ref. [16] for a heat source temperature of 136 °C. The thermal efficiency of butane was compared with our simulation work [26] at the same heat source temperature. Present results are compared with literature data in Table 6.

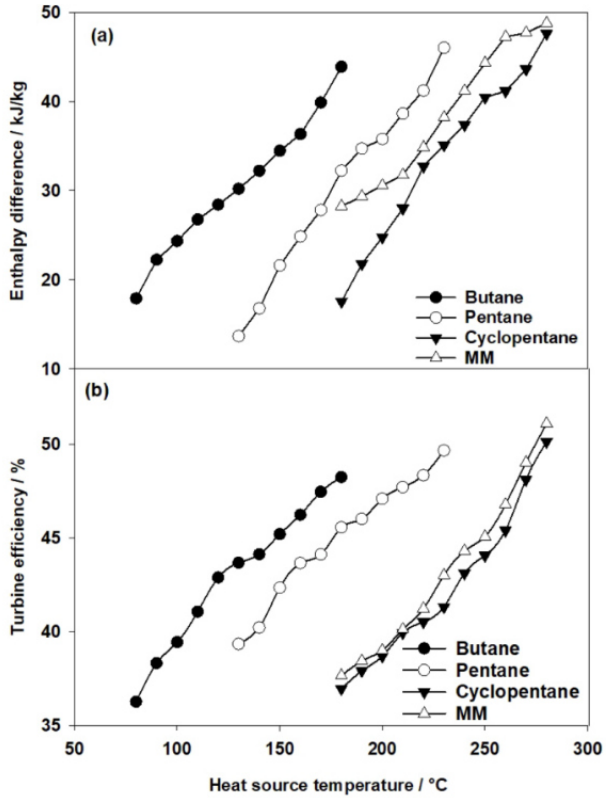

Fig. 5. (a) Enthalpy difference and (b) turbine efficiency as a function of heat source temperature for varying working fluids.

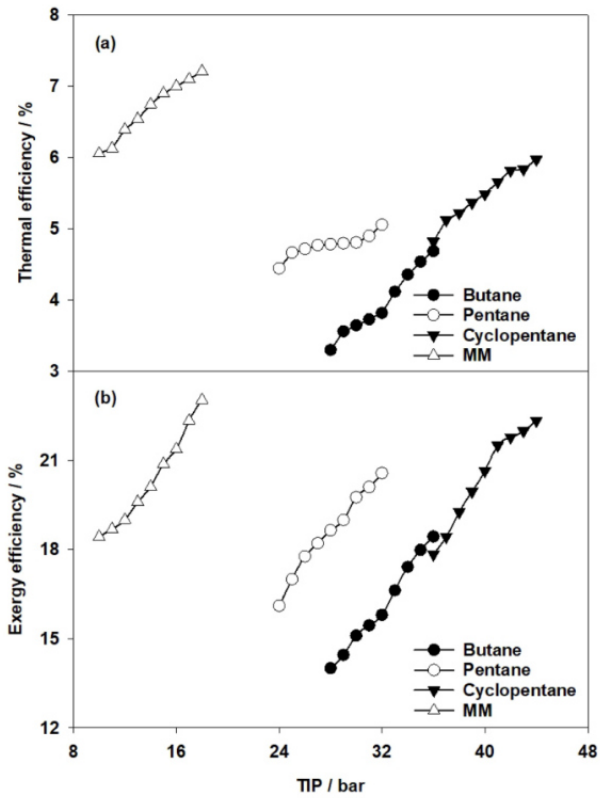

Fig. 6. Effect of turbine inlet pressure on (a) thermal efficiency and (b) exergy efficiency for varying working fluids.

Results and discussion

Heat source temperature

A system performance analysis was made to identify suitable operating conditions of the present ORC. The experiments were carried out adopting butane, pentane, cyclopentane or MM as a working fluid over a heat source temperature in increments of 10 °C. The heat source temperature was in the range of 80–180 °C for butane, 130–230 °C for pentane, 180–280 °C for cyclopentane and 180–280 °C for MM.

Fig. 4 (a) depicts the variation of thermal efficiency with heat source temperature. As expected, all working fluids showed an increasing thermal efficiency with rising heat source temperature. The most pronounced increase of thermal efficiency was found for MM, while it was lowest for butane. The thermal efficiency increased from 1.9% to 5.4% for butane, from 2.1% to 6.4% for pentane, from 3.1% to 6.9% for pentane and from 3.3% to 8.0% for MM. The main reason for the enhanced thermal efficiency is that the enthalpy drop across the turbine increases with rising heat source temperature, leading to more net power output. The increase of the heat source temperature led to an increase of the heat flow input from the heating cycle, but the increasing rate of net power output outweighed the rising rate of absorbed heat so that the thermal efficiency increased gradually. In addition, a higher heat source temperature in this test allowed for a better utilization of the heat source for each working fluid.

Fig. 4 (b) depicts the variation of exergy efficiency with heat source temperature. The higher the heat source temperature, the higher the exergy efficiency for all working fluids. The increasing trend of exergy efficiency is related to the increase of net power output rising with the heat source temperature. The highest achieved exergy efficiency was 20.3%, 22.5%, 23.5% and 25.2% by adopting butane, pentane, cyclopentane and MM, respectively.

As shown in Fig. 5 (a), the enthalpy difference across the turbine increased greatly upon temperature rise from 17.91 kJ/kg to 43.9 kJ/kg, from 13.7 kJ/kg to 46.0 kJ/kg, from 17.5 kJ/kg to 47.6 kJ/kg and from 28.3 kJ/kg to 48.8 kJ/kg by adopting butane, pentane, cyclopentane and MM, respectively. Fig. 5 (b) shows the variation of turbine efficiency with heat source temperature. The results indicate that the turbine efficiency increased with heat source temperature for all working fluids. The highest turbine efficiency was 48.2%, 49.6%, 50.1% and 51.1% for butane, pentane, cyclopentane and MM, respectively. Turbine efficiency and enthalpy difference are two important factors for evaluating the performance of the turbine and for the future design of a dedicated turbine.

Turbine inlet pressure

System performance was investigated for different TIP levels that were in the range of 28–36 bar for butane, 24–32 bar for pentane, 36–44 bar for cyclopentane and 10–18 bar for MM. The heat source temperature was kept constant at 180 °C for butane, 230 °C for pentane, 280 °C for cyclopentane and 280 °C for MM in these TIP variations. These heat source temperatures were selected because the system reached the highest thermal and exergy efficiencies under these conditions. The TIP was gradually increased for each working fluid by adjusting the rotation frequency of the pump M1. The inlet pressure was maintained below the critical pressure of the given working fluid to avoid supercritical conditions. Fig. 6 (a) shows the effect of the TIP on the thermal efficiency. When the TIP rises, the thermal efficiency increases rather slightly from 3.3% to 4.7%, from 4.4% to 5.1%, from 4.8% to 5.9% and from 6.1% to 7.2% by adopting butane, pentane, cyclopentane and MM as a working fluid, respectively. The increase of the TIP led to an increase of the

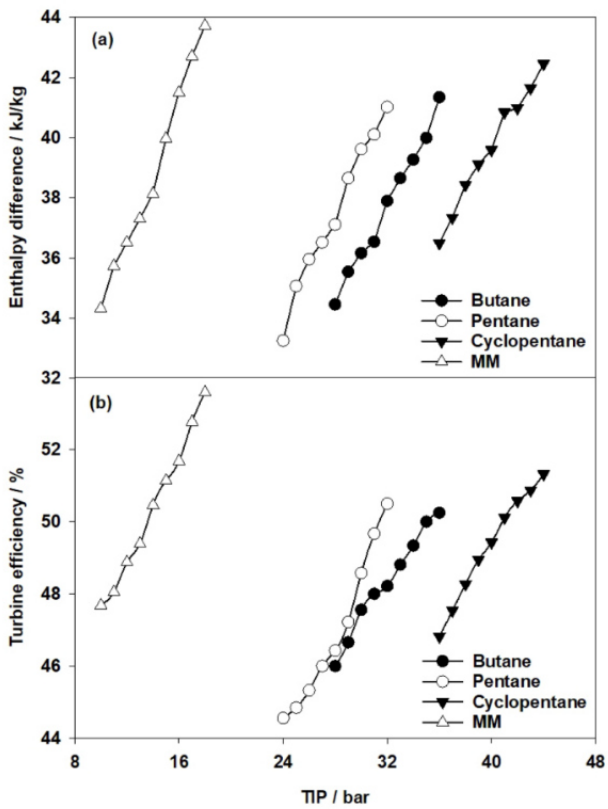

Fig. 7. Variation of (a) enthalpy difference and (b) turbine efficiency with turbine inlet pressure for varying working fluids.

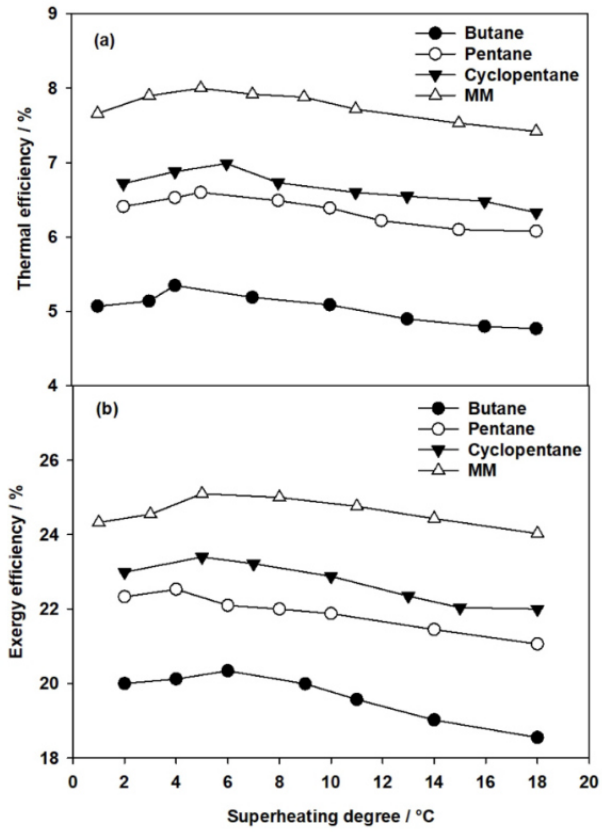

Fig. 8. (a) Thermal efficiency and (b) exergy efficiency as a function of superheating degree for varying working fluids.

pressure ratio between inlet and outlet. A rising pressure ratio is related to the enthalpy drop across the turbine and more net power is produced as shown in Fig. 7 (a). In other words, the increase of the TIP resulted in an increase of the ratio of net power output to heat flow input, i.e. a better thermal efficiency.

The variation of exergy efficiency with TIP is depicted in Fig. 6 (b). It can be seen that the exergy efficiency also rises with TIP. It increased from 14.0% to 18.4% for butane, from 16.1% to 20.6% for pentane, from 17.8% to 22.3% for cyclopentane and from 18.4% to 23.1% for MM. This exergy efficiency trend is expected due to the rising enthalpy drop across the turbine as shown in Fig. 7 (a). A higher TIP led to more net power output and better exergy efficiency. Increasing the TIP led to a better ratio of net power output to exergy flow input.

Fig. 7 shows the effect of the TIP on the enthalpy difference across the turbine and the turbine efficiency. As the TIP increased, the enthalpy difference increased from 34.5 kJ/kg to 41.3 kJ/kg, from 33.2 kJ/kg to 41.0 kJ/kg, from 36.4 kJ/kg to 42.4 kJ/kg and from 34.3 kJ/kg to 43.7 kJ/kg for butane, pentane, cyclopentane and MM, respectively. The maximum turbine efficiency was 50.2%, 50.6%, 51.3% and 53.5% adopting butane, pentane, cyclopentane and MM, respectively.

A higher TIP required more pump power, which reduced net power output. Moreover, increasing the TIP led to a rise of the absorbed heat from the heating cycle and reduced the thermal efficiency. Consequently, the thermal efficiency in the heat source temperature case (Fig. 4) is higher for all working fluids than in the TIP case (Fig.6). The same applies to the exergy efficiency.

Superheating degree

System performance was assessed for a varying superheating degree in the range of 1 °C to 18 °C. The heat source temperature was carefully increased together with the mass flow rate of Therminol 66 to reach a targeted superheating degree. In Fig. 8 (a), it can be seen that the thermal efficiency first increases slightly with superheating degree up to a maximum and then decreases slightly for all working fluids. The highest thermal efficiency was generally at a superheating degree between 3 °C and 6 °C. MM and pentane reached the highest thermal efficiency at a superheating degree of 5 °C, while cyclopentane and butane showed the highest thermal efficiency at 6 °C and 4 °C, respectively. A further increase of the superheating degree did not have a significant effect. With the rise of the superheating degree, the ratio of net power to absorbed heat flow increased until a certain superheating degree, then the effect was reversed and that ratio fell so that the thermal efficiency decreased. These results agree with the analysis of Uusitalo et al. [33] and our previous work [26]. Uusitalo et al. recommended a small superheating degree for regular ORC (without recuperator) to achieve a better performance and to control the heat transfer in the evaporator of the ORC system. A control of heat transfer may reduce the exergy loss in the evaporator and increase thermal and exergy efficiencies.

Fig. 8 (b) depicts the variation of exergy efficiency with superheating degree. The exergy efficiency also increases with superheating degree and then decreases. As shown in Fig. 8 (b), it reaches maximum values between 3 °C and 6 °C of superheating for all working fluids. At a superheating degree between 3 °C and 6 °C, the ratio of net power output to exergy flow input increases slightly. MM and cyclopentane reached the highest exergy efficiency at a superheating degree of 5 °C, while pentane and butane led to the highest exergy efficiency at 4 °C and 6 °C, respectively. These results agree with those of Zhou et al. [20], who found that a further increase of the superheating degree may lead to a slight decrease of the exergy efficiency. According to the impact of the

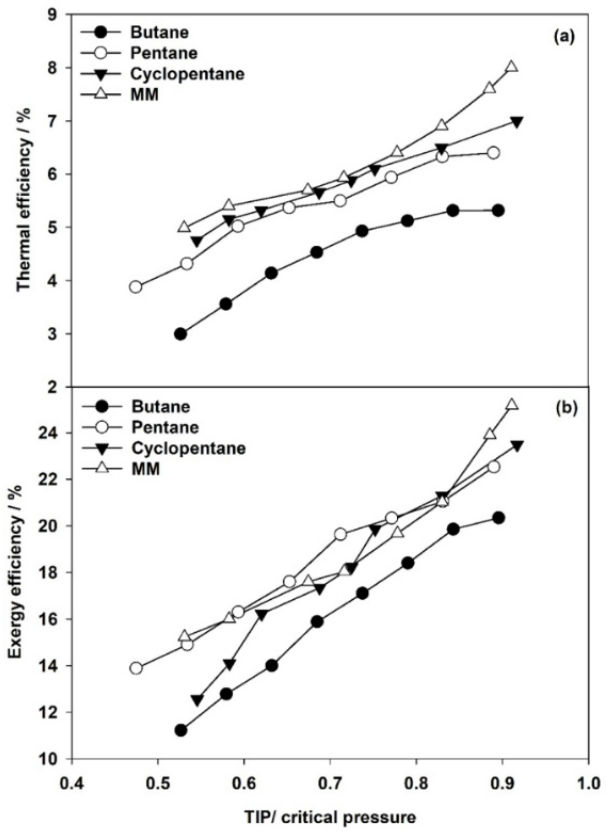

Fig. 9. Variation of (a) thermal efficiency and (b) exergy efficiency with pressure ratio for varying working fluids.

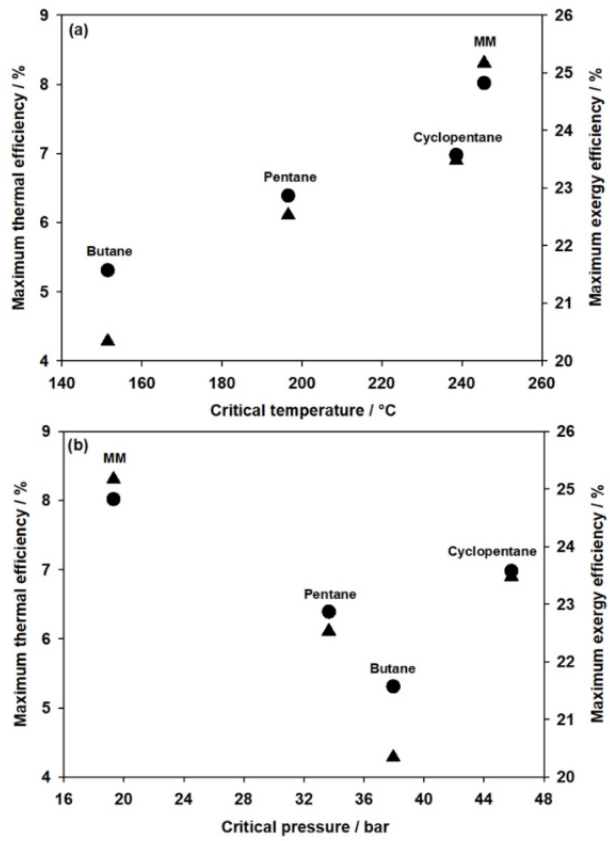

Fig. 10. Maximum thermal efficiency (bullets) and maximum exergy efficiency (triangles) over (a) critical temperature and (b) critical pressure for varying working fluids.

superheating degree on the system performance, it is clear that the superheating degree should be controlled to be in that limited range.

Pressure ratio

Fig. 9 shows the variation of system performance with the pressure ratio, which is given in the form of TIP divided by the critical pressure. The results indicate that both thermal end exergy efficiencies increase with the pressure ratio for all working fluids. It can be seen that MM reached the highest thermal and exergy efficiencies at a pressure ratio of 0.9, while cyclopentane, pentane and butane reached the highest thermal efficiency at a pressure ratio of 0.91, 0.88 and 0.89, respectively, which is rather close to the critical pressure of the given working fluid. The main reason is that the increase of the TIP led to an increase of the pressure difference between the inlet and outlet of the turbine and thus a large enthalpy difference, which raised the net power output and increased thermal and exergy efficiencies.

Critical properties

Fig. 10 (a) shows the relation between the critical properties of the working fluids and the thermal and exergy efficiencies. It can be seen that there is a clear relation between system performance and the critical temperature of the working fluid, where thermal and exergy efficiencies attained better values with increasing critical temperature. The higher the critical temperature of the working fluid, the higher the efficiencies. MM with the highest critical temperature achieved the best thermal and exergy efficiencies under all experimental conditions. The mean reason is that working fluids with a high critical temperature allow for a high turbine inlet temperature and evaporation temperature, which resulted in a large enthalpy difference across the turbine. In addition, the use of a working fluid with a high critical temperature may yield more turbine net power output and a better thermal efficiency. The relation between critical temperature and system performance as outlined in the present work agrees with the results and analyses in Refs. [33,51,52]. On the other hand, Fig. 10 (b) shows that there is no clear relationship between the critical pressure of the working fluid and system performance.

Exergy loss analysis

Exergy loss analysis is important to explore the dissipation of usable energy in the ORC components due to irreversibilities. Such an analysis was carried out for each component of the present ORC system under the operating conditions where the highest thermal and exergy efficiencies were reached. Fig. 11 shows that the highest exergy loss occurred in the evaporator (HE) due to the irreversibility during heat transfer between Therminol 66 and the working fluid. The percentage of exergy loss was 55.4%, 53.6%, 51.7% and 50.4% adopting butane, pentane, cyclopentane and MM, respectively. The results agree with the analyses of Li et al. [53] and Safarian et al. [54], who reported that the highest exergy loss occurs in the evaporator which represents the critical component of regular ORC systems. Other practical works [9,15] that looked at the exergy loss in ORC systems also found that the largest contribution is exerted in the evaporator. The exergy loss in the evaporator using butane or pentane with a heat source temperature in the range of 180–230 °C is higher than when using cyclopentane or MM with a heat source temperature of 280 °C. Working fluids with a high critical

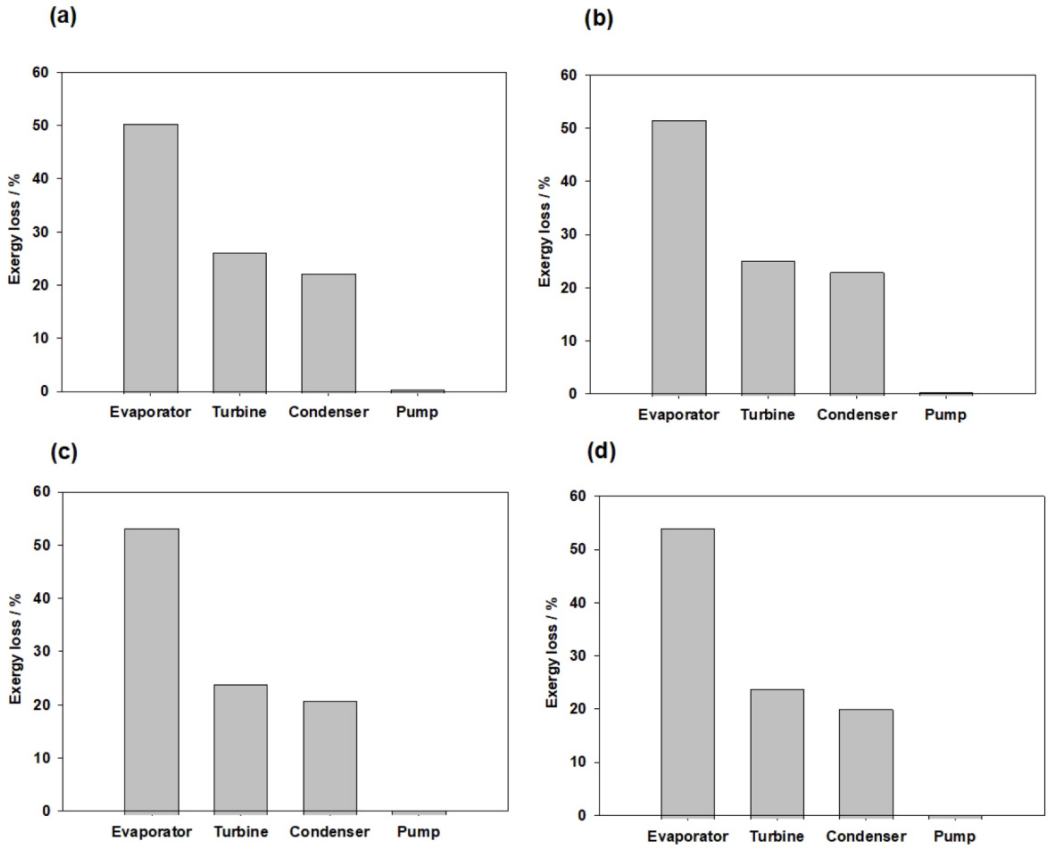

Fig. 11. Percentage of exergy loss in the main ORC components using (a) MM, (b) cyclopentane, (c) pentane and (d) butane as a working fluid.

temperature can provide a high turbine inlet temperature and evaporation temperature. Moreover, they allow for a better matching between the heating cycle and working fluid in the evaporator at higher temperatures. This explains the large exergy loss in the evaporator when adopting butane or pentane in comparison to cyclopentane or MM. In this context, butane for a heat source temperature of 180 °C had a larger difference between the heat source temperature and the turbine inlet temperature and more exergy loss in the evaporator, while MM had a smaller difference and less exergy loss.

The results attribute the low thermal efficiency to the poor turbine efficiency, as it generates less power output in relation to the available enthalpy difference. Using a turbine with a better efficiency would increase the thermal efficiency and performance of the ORC system. In general, the present ORC system may be effective for recovering heat from wide range of heat sources, especially since the market needs to introduce small units to recover heat from various sources.

Conclusions and outlook to future work

An ORC system was experimentally investigated utilizing electrical heaters as a heat source. System performance in terms of thermal efficiency and exergy efficiency was studied over a wide range of heat source temperature, turbine inlet pressure and superheating degree by using butane, pentane, cyclopentane or MM as a working fluid. The heat source temperature was in the range of 80–180 °C for butane, 130–230 °C for pentane, 180–280 °C for cyclopentane and 180–280 °C for MM. The turbine inlet pressure was in the range of 28–36 bar for butane, 24–32 bar for pentane, 36–44 bar for cyclopentane and 10–18 bar for MM. The maximum measured values of thermal efficiency and exergy efficiency were 8.0% and 25.2%, respectively, and were found for MM. The maximum turbine efficiency and enthalpy drop across the turbine were 53.5% and 48.8 kJ/kg adopting MM as a working fluid. With a superheating degree from 3 to 6 °C, all working fluids reached the highest thermal and exergy efficiencies. Moreover, a pressure ratio between 0.88 and 0.91 was optimal throughout. The results show that a small degree of superheating is efficient to increase system performance. An exergy loss analysis indicated that the highest exergy loss occurred in the evaporator due to the irreversibility during heat transfer from the heat source. In addition, it was confirmed that working fluids with a high critical temperature are more beneficial for ORC systems with a heating cycle.

This work aims to provide experimental data that can be employed to improve and optimize ORC systems. The low turbine efficiency during the present operations clearly indicates that a new dedicated turbine must be designed to enhance power output. Moreover, we are interested to experimentally investigate low-GWP refrigerants as working fluids. Future work will include the heat transfer properties of the system, i.e. pinch point temperature difference, heat recovery efficiency and heat exchanger performance.

Declaration of Competing Interest

The authors declare that they have no known competing financial interests or personal relationships that could have appeared to influence the work reported in this paper.

Acknowledgements

The authors acknowledge the financial support by the German Academic Exchange Service (DAAD). We thank Dr. Gerhard Herres, University of Paderborn who provided insight and expertise that greatly assisted the present work.

Author contribution

Wameedh Khider Abbas Abbas has written the manuscript, developed the cycle calculations, carried out the field tests and analyzed the results. He conducted the cycle tests and selected the working fluids together with the operational conditions. Elmar Baumhögger supported test operations. Jadran Vrabec initiated and supported the team over the entire time of the project and contributed to the manuscript's revision.

References

[1] Khan I, Hou F, Irfan M, Zakari A, Le HP. Does energy trilemma a driver of economic growth? the roles of energy use, population growth, and financial development. Renew Sustain Energy Rev 2021;146:111157. https://doi.org/10.1016/J.RSER.2021.111157.
[2] Majeed MT, Ozturk I, Samreen I, Luni T. Evaluating the asymmetric effects of nuclear energy on carbon emissions in Pakistan. Nucl Eng Technol 2022;54:1664–73. https://doi.org/10.1016/j.net.2021.11.021.
[3] Shi Y, Lin R, Wu X, Zhang Z, Sun P, Xie L, et al. Dual-mode fast DMC algorithm for the control of ORC based waste heat recovery system. Energy 2022;244:122664. https://doi.org/10.1016/j.energy.2021.122664.
[4] Wieland C, Dawo F, Schifflechner C, Astolfi M. Market Report on organic Rankine cycle power system: Recent development and outlook. In 6th International Seminar on ORC Power Systems, October 11-13, 2021, Munich, Germany. https://orc-world-map.org.
[5] Tartière T, Astolfi M. A world overview of the organic Rankine cycle market. Energy Procedia 2017;129:2–9. https://doi.org/10.1016/J.EGYPRO.2017.09.159.
[6] Fatigati F, Vittorini D, Di Bartolomeo M, Cipollone R. Experimental characterization of a small-scale solar Organic Rankine Cycle (ORC) based unit for domestic microcogeneration. Energy Convers Manage 2022;258:115493.
[7] Park BS, Usman M, Imran M, Pesyridis A. Review of Organic Rankine Cycle experimental data trends. Energy Convers Manage 2018;173:679–91. https://doi.org/10.1016/j.enconman.2018.07.097.
[8] Mascuch J, Novotny V, Vodicka V, Spale J, Zeleny Z. Experimental development of a kilowatt-scale biomass fired micro – CHP unit based on ORC with rotary vane expander. Renewable Energy 2020;147:2882–95. https://doi.org/10.1016/j.renene.2018.08.113.
[9] Feng Y, Wang X, Niaz H, Hung T, He Z, Jahan ZA, et al. Experimental comparison of the performance of basic and regenerative organic Rankine cycles. Energy Convers Manage 2020;223:113459. https://doi.org/10.1016/J.ENCONMAN.2020.113459.
[10] Gao W, Wu Z, Tian Z, Zhang Y. Experimental investigation on an R290-based organic Rankine cycle utilizing cold energy of liquid nitrogen. Appl Therm Eng 2022;202:117757. https://doi.org/10.1016/J.APPLTHERMALENG.2021.117757.
[11] Wang F, Gao W, Li G, Tian Z, Wang X. Experimental study on power generation plant of a 1 kW small-scale Organic Rankine Cycle system using R290. Energy Sci Eng 2022;10:740–51. https://doi.org/10.1002/ese3.1049.
[12] Araya S, Wemhoff AP, Jones GF, Fleischer AS. An experimental study of an Organic Rankine Cycle utilizing HCFO-1233zd(E) as a drop-in replacement for HFC-245fa for ultra-low-grade waste heat recovery. Appl Therm Eng 2020;180:115757. https://doi.org/10.1016/J.APPLTHERMALENG.2020.115757.
[13] Zygmunt Kaczmarczyk T. Experimental research of a small biomass organic Rankine cycle plant with multiple scroll expanders intended for domestic use. Energy Convers Manage 2021;244:114437.
[14] İpek O, Mohammedsalih MM, Gürel B, Kılıç B. Experimental investigation of low-temperature organic Rankine cycle using waste heat from gas turbine bearings for different conditions. Int J Environ Sci Technol 2022;19:1519–30. https://doi.org/10.1007/s13762-021-03172-x.
[15] Wu T, Wei X, Meng X, Ma X, Han J. Experimental study of operating load variation for organic Rankine cycle system based on radial inflow turbine. Appl Therm Eng 2020;166:114641. https://doi.org/10.1016/J.APPLTHERMALENG.2019.114641.
[16] Qiu K, Entchev E. A micro-CHP system with organic Rankine cycle using R1223zd (E) and n-Pentane as working fluids. Energy 2022;239:121826. https://doi.org/10.1016/J.ENERGY.2021.121826.
[17] Carraro G, Bori V, Lazzaretto A, Toniato G, Danieli P. Experimental investigation of an innovative biomass-fired micro-ORC system for cogeneration applications. Renewable Energy 2020;161:1226–43. https://doi.org/10.1016/J.RENENE.2020.07.012.
[18] Qiu K, Entchev E. Development of an organic Rankine cycle-based micro combined heat and power system for residential applications. Appl Energy 2020;275:115335. https://doi.org/10.1016/J.APENERGY.2020.115335.
[19] Linnemann M, Priebe KP, Heim A, Wolff C, Vrabec J. Experimental investigation of a cascaded organic Rankine cycle plant for the utilization of waste heat at high and low temperature levels. Energy Convers Manage 2020;205:112381. https://doi.org/10.1016/j.enconman.2019.112381.
[20] Zhou N, Wang X, Chen Z, Wang Z. Experimental study on Organic Rankine Cycle for waste heat recovery from low-temperature flue gas. Energy 2013;55:216–25. https://doi.org/10.1016/j.energy.2013.03.047.
[21] Allweiler GmbH. Product catalog Allweiler NTWH 25 200/10. Website address: https://www.allweiler.de/16550/Products/Product-Catalog/Centrifugal-Pumps/with-shaft-seal/Base-plate-design/ALLHEAT-NTWH/Product/awr_index_2017.aspx.; accessed on 20th April 2022.
[22] Dubberke F, Linnemann M, Abbas WK, Baumhögger E, Priebe KP, Roedder M, et al. Experimental setup of a cascaded two-stage organic Rankine cycle. Appl Therm Eng 2018;131:958–64. https://doi.org/10.1016/j.applthermaleng.2017.11.137.
[23] Netzsch Group. Products-and-accessories. NETZSCH NEMO. Website address: https://pumps-systems.netzsch.com/en/products-and-accessories/nemo-progressing-cavity-pumps.; accessed on 20th April 2022.
[24] Vahterus Company. Plate and shell heat exchangers. Website address: https://vahterus.com/technology/customised-pshe-solution/fully-welded-design. ; accessed on 20th April 2022.
[25] Abbas WKA, Linnemann M, Baumhögger E, Vrabec J. Experimental study of two cascaded organic Rankine cycles with varying working fluids. Energy Convers Manage 2021;230:113818. https://doi.org/10.1016/j.enconman.2020.113818.
[26] Abbas WKA, Vrabec J. Cascaded dual-loop organic Rankine cycle with alkanes and low global warming potential refrigerants as working fluids. Energy Convers Manage 2021;249:114843. https://doi.org/10.1016/J.ENCONMAN.2021.114843.
[27] Fragol company. Product data sheet Therminol 66. Website address: http://www.fragol.de.asp; accessed on 20th December 2021.
[28] Hu B, Guo J, Yang Y, Shao Y. Selection of working fluid for organic Rankine cycle used in low temperature geothermal power plant. Energy Rep 2022;8:179–86. https://doi.org/10.1016/j.egyr.2022.01.102.
[29] Wang S, Liu C, Zhang S, Li Q, Huo E. Multi-objective optimization and fluid selection of organic Rankine cycle (ORC) system based on economic-environmental-sustainable analysis. Energy Convers Manage 2022;254:115238. https://doi.org/10.1016/J.ENCONMAN.2022.115238.
[30] Dai X, Shi L, Qian W. Review of the working fluid thermal stability for organic Rankine cycles. J Therm Sci 2019;28:597–607. https://doi.org/10.1007/s11630-019-1119-3.
[31] Wang W, Dai X, Shi L. Influence of thermal stability on organic Rankine cycle systems using siloxanes as working fluids. Appl Therm Eng 2022;2022(200):117639. https://doi.org/10.1016/J.APPLTHERMALENG.2021.117639.
[32] Li Y, Li W, Gao X, Ling X. Thermodynamic analysis and optimization of organic Rankine cycles based on radial-inflow turbine design. Appl Therm Eng 2021;184:116277. https://doi.org/10.1016/J.APPLTHERMALENG.2020.116277.
[33] Uusitalo A, Honkatukia J, Turunen-Saaresti T, Grönman A. Thermodynamic evaluation on the effect of working fluid type and fluids critical properties on design and performance of Organic Rankine Cycles. J Cleaner Prod 2018;188:253–63. https://doi.org/10.1016/J.JCLEPRO.2018.03.228.
[34] Loni R, Mahian O, Markides CN, Bellos E, le Roux WG, Kasaeian A, et al. A review of solar-driven organic Rankine cycles: Recent challenges and future outlook. Renew Sustain Energy Rev 2021;150:111410. https://doi.org/10.1016/J.RSER.2021.111410.
[35] Sorgulu F, Akgul MB, Cebeci E, Yilmaz TO, Dincer I. A new experimentally developed integrated organic Rankine cycle plant. Appl Therm Eng 2021;187:116561. https://doi.org/10.1016/J.APPLTHERMALENG.2021.116561.
[36] Bahrami M, Pourfayaz F, Kasaeian A. Low global warming potential (GWP) working fluids (WFs) for Organic Rankine Cycle (ORC) applications. Energy Rep 2022;8:2976–88.
[37] Pili R, Bojer Jørgensen S, Haglind F. Multi-objective optimization of organic Rankine cycle systems considering their dynamic performance. Energy 2022;246:123345. https://doi.org/10.1016/J.ENERGY.2022.123345.
[38] Braimakis K, Karellas S. Exergetic optimization of double stage Organic Rankine Cycle (ORC). Energy 2018;149:296–313. https://doi.org/10.1016/j.energy.2018.02.044.
[39] Uusitalo A, Turunen-Saaresti T, Honkatukia J, Dhanasegaran R. Experimental study of small scale and high expansion ratio ORC for recovering high temperature waste heat. Energy 2020;208:118321. https://doi.org/10.1016/J.ENERGY.2020.118321.
[40] Aljundi IH. Effect of dry hydrocarbons and critical point temperature on the efficiencies of organic Rankine cycle. Renew Energy 2011;36:1196–202. https://doi.org/10.1016/j.renene.2010.09.022.
[41] Barse KA, Mann MD. Maximizing ORC performance with optimal match of working fluid with system design. Appl Therm Eng 2016;100:11–9. https://doi.org/10.1016/j.applthermaleng.2016.01.167.
[42] Vivian J, Manente G, Lazzaretto A. A general framework to select working fluid and configuration of ORCs for low-to-medium temperature heat sources. Appl Energy 2015;156:727–46. https://doi.org/10.1016/j.apenergy.2015.07.005.
[43] Zhai H, An Q, Shi L. Analysis of the quantitative correlation between the heat source temperature and the critical temperature of the optimal pure working fluid for subcritical organic Rankine cycles. Appl Therm Eng 2016;99:383–91. https://doi.org/10.1016/j.applthermaleng.2016.01.058.
[44] Lemmon EW, Huber ML, McLinden MO. Reference fluid thermodynamic and transport properties (REFPROP), version 10.0, in NIST Standard Reference Database 23. Gaithersburg, MD: National Institute of Standard and Technology; 2007.
[45] Bücker D, Wagner W. Reference equations of state for the thermodynamic properties of fluid phase n-butane and isobutane. J Phys Chem Ref Data 2006;35:929–1019. https://doi.org/10.1063/1.1901687.

[46] Span R, Wagner W. Equations of State for Technical Applications. II. Results for Nonpolar Fluids. In. Int J Thermophys 2003;24:41–109. https://doi.org/10.1023/A:1022310214958.
[47] Gedanitz H, Davila MJ, Lemmon EW. Speed of sound measurements and a fundamental equation of state for cyclopentane. J Chem Eng Data 2015;60:1331–7. https://doi.org/10.1021/je5010164.
[48] Thol M, Dubberke F, Rutkai G, Windmann T, Köster A, Span R, et al. Fundamental equation of state correlation for hexamethyldisiloxane based on experimental and molecular simulation data. Fluid Phase Equilib 2016;418:133–51. https://doi.org/10.1016/J.FLUID.2015.09.047.
[49] Zhang T, Liu L, Hao J, Zhu T, Cui G. Correlation analysis based multi-parameter optimization of the organic Rankine cycle for medium- and high-temperature waste heat recovery. Appl Therm Eng 2021;188:116626.
[50] Mahian O, Mirzaie MR, Kasaeian A, Mousavi SH. Exergy analysis in combined heat and power systems: A review. Energy Convers Manage 2020;226:113467. https://doi.org/10.1016/J.ENCONMAN.2020.113467.
[51] Shu G, Li X, Tian H, Liang X, Wie H, Wang X. Alkanes as working fluids for high-temperature exhaust heat recovery of diesel engine using organic Rankine cycle. Appl Energy 2014;119:204–17. https://doi.org/10.1016/j.apenergy.2013.12.056.
[52] Liu P, Shu G, Tian H, Wang X, Yu Z. Alkanes based two-stage expansion with interheating Organic Rankine cycle for multi-waste heat recovery of truck diesel engine. Energy 2018;147:337–50. https://doi.org/10.1016/j.energy.2017.12.109.
[53] Li W, Feng X, Yu LJ, Xu J. Effects of evaporating temperature and internal heat exchanger on organic Rankine cycle. Appl Therm Eng 2011;31:4014–23. https://doi.org/10.1016/J.APPLTHERMALENG.2011.08.003.
[54] Safarian S, Aramoun F. Energy and exergy assessments of modified Organic Rankine Cycles (ORCs). Energy Rep 2015;1:1–7. https://doi.org/10.1016/j.egyr.2014.10.003.

6. Summary and conclusions

Using the ORC system to generate power is a promising technology to meet the growing energy demand and reduce the adverse environmental effects of fossil fuels. Several architectures of the ORC have been developed and designed to enhance system performance and optimize the utilization of heat sources. One of these adopted architectures is the CORC system, which consists of two cycles instead of one for better utilization of heat flows from different sources. This type of architecture may increase thermal and exergy efficiencies, reducing the exergy loss, since the residual heat from the HT-ORC is used in the LT-ORC. The novelty of this work involves the investigation of system performance experimentally and by simulations choosing working fluids from different groups, namely low GWP refrigerants, alkanes and siloxanes. In this work, the fluid selection process was based on the thermodynamic properties and environmental considerations, including GWP and ODP values. Experimental and simulation work was carried out and based on the CORC test rig at the University of Paderborn. The results have been published in four papers.

6.1. Simulation results

The simulation process was based on the CORC test rig, using alkanes and low GWP refrigerants in the HT-ORC and LT-ORC, respectively. System performance was evaluated based on two criteria: thermal and exergy efficiencies over a wide heat source temperature range. In addition, the relationship between system performance and thermophysical properties of the working fluid, such as critical temperature, critical pressure, molar mass and molecular structure, was investigated. The results indicated that the maximum achieved thermal and exergy efficiencies were 25.2% and 54.8% by adopting cyclohexane and R1366mzz(Z) in HT-ORC and LT-ORC, respectively. Moreover, the results underlined the close relationship between thermophysical properties and system performance, as the thermal and exergy efficiencies increased with a rising critical temperature of the working fluid. On the other hand, the thermal and exergy efficiencies decreased with the rise of the critical pressure of the working fluid. The molecular structure shows a close relationship with thermal and exergy efficiencies, as cyclic alkanes achieved higher efficiencies than linear alkanes in the HT-ORC. The CORC system achieved an about 25% higher thermal efficiency than the regular ORC system represented by the HT-ORC. In the simulation process, 31 refrigerants were considered, and it was found that the thermal efficiency is strongly correlated with the critical temperature of the working fluid, where the thermal efficiency increased with the rise of the critical temperature of refrigerants. This is due to the fact that working fluids with a high critical temperature can

provide a high turbine inlet temperature, and thus the enthalpy difference across the turbine increases and the thermal efficiency rises. The results indicate that HFO refrigerants (namely R1366mzz(Z), R1233zd(E) and R1234ze(Z)) and HC refrigerants (namely butane, cyclopropane and isobutane) may be suitable candidates for CORC units.

6.2. Experimental results

Under various conditions, the system performance was practically tested using four working fluids: propane, butane, pentane and cyclopentane. The objective was to investigate the thermal and exergy efficiencies, turbine power output, turbine efficiency and enthalpy difference across the turbine. System efficiency was measured over a wide heat source temperature range, turbine inlet pressure and mass flow rate of the working fluid. The results indicated that the highest turbine power output and exergy efficiency were 4.92 kW and 20.2%, respectively. Thereby, the heat exchanger performance was tested, since the two cycles were connected with a common heat exchanger. Therefore, it was adequate to investigate the heat transfer between the HT-ORC and the LT-ORC in context with the PPTD. According to the heat transfer calculations between the two cycles, pentane was the best option among the selected working fluids in the LT-ORC.

The second section of the experimental work focused on testing the HT-ORC as a regular ORC system. The HT-ORC plays the most important role in the CORC system, as it presents the cycle that exploits the primary heat source and also is the heat source for the LT-ORC. The selected working fluids were butane, pentane, cyclopentane and MM. The purpose of the tests was to measure the thermal, exergy and turbine efficiencies over a wide range of heat source temperature, turbine inlet pressure, superheating degree and pressure ratio. Moreover, it was focused on studying the relationship between the thermodynamic properties of working fluids, system efficiency and exergy loss in the main components. The maximum achieved thermal and exergy efficiencies were 8.0% and 25.2%, respectively, and were obtained with MM as a working fluid. In addition, the maximum turbine efficiency was 53.5% and was also found for MM. The maximum exergy loss was identified to be in the evaporator due to the irreversibility during the heat transfer from the heat source. Moreover, it was found that a superheating degree between 3-6 °C is beneficial to reach the optimal thermal and exergy efficiencies. The results confirmed that working fluids with higher critical temperature are more appropriate for the HT-ORC. Generally, the simulations and experiments indicated that the CORC system is a promising and suitable technology to utilize heat sources, enhancing thermal and exergy efficiencies, and reducing exergy loss.

Bibliography

[1] Statista. Weltweiter Primärenergieverbrauch in den Jahren von 1980 bis 2021. Website address: https://www.statista.com; accessed on 6th January 2023.

[2] British Petrolium (BP). Statistical Review of World Energy 2022, 71st edition. Website address: https://www.bp.com/content/dam/bp/business-sites/en/global/corporate/pdfs/energy-economics/statistical-review/bp-stats-review-2022-full-report.pdf; accessed on 6th January 2023.

[3] World Economic Forum. The state of world's energy. Website address: https://www.weforum.org/agenda/2022/08/energy-charts-emissions-pandemic; accessed on 6th January 2023.

[4] British Petrolium (BP). Statistical Review of World Energy. Website address: https://www.bp.com/en/global/corporate/energy-economics/statistical-review-of-world-energy.html; accessed on 6th January 2023.

[5] Qian Z, Zhao Y, Shi Q, Zheng L, Wang S, Zhu J. Global value chains participation and CO2 emissions in RCEP countries. Journal of Cleaner Production 2022;332:130070.

[6] Mughal N, Arif A, Jain V, Chupradit S, Shabbir M S, Ramos-Meza C S, Zhanbayev R. The role of technological innovation in environmental pollution, energy consumption and sustainable economic growth: Evidence from South Asian economies. Energy Strategy Reviews 2022;39:100745.

[7] IPCC, 2021: Climate Change 2021: The Physical Science Basis. Contribution of Working Group I to the Sixth Assessment Report of the Intergovernmental Panel on Climate Change, Masson-Delmotte V, Zhai P, Pirani A, Connors S L, Péan, Berger S, Caud N, Chen Y, Goldfarb L, Gomis M I, Huang, Leitzell M K, Lonnoy E, Matthews J B R, Maycock T K, Waterfield T, Yelekçi O,Yu R, and Zhou B. Cambridge University Press, Cambridge, United Kingdom and New York, NY, USA.

[8] Abbas WKA, Linnemann M, Baumhögger E, Vrabec J. Experimental study of two cascaded organic Rankine cycles with varying working fluids. Energy Conversion and Management 2021;230:113818.

[9] Abbas WKA, Vrabec J. Cascaded dual-loop organic Rankine cycle with alkanes and low global warming potential refrigerants as working fluids. Energy Conversion and Management 2021;249:114843.

[10] Lecompte S, Huisseune H, van den Broek M, Vanslambrouck B, De Paepe M. Review of organic Rankine cycle (ORC) architectures for waste heat recovery. Renewable and Sustainable Energy Reviews 2015;47:448–461.

[11] Braimakis K, Karellas S. Exergetic optimization of double stage Organic Rankine Cycle (ORC), Energy 2018;149:296–313.

[12] Astolfi M. Technical options for Organic Rankine Cycle systems. Organic Rankine Cycle (ORC) Power Systems: Technologies and Applications 2017;67–89.

[13] Macchi E. Theoretical basis of the Organic Rankine Cycle. Organic Rankine Cycle (ORC) Power Systems: Technologies and Applications 2017;3–24.

[14] Bronicki LY, Schochet D N. Bottoming Organic Cycle for Gas Turbines. Proceedings of the ASME Turbo Expo 2005;5:79–86, Nevada, USA. ASME.

[15] Ainger A. Economy of steam engine. Quarterly journal of science, literature and art 1830;7:186–189. Website address: https://www.biodiversitylibrary.org/page/2430711#page/5/mode/1up. Accessed on 6th January 2023.

[16] Invernizzi C M. The Organic Rankine Cycle. In: Closed Power Cycles. Lecture Notes in Energy 2013;11:117–175. Springer, London.

[17] Colonna P, Casati E, Trapp C, Mathijssen T, Larjola J, Turunen-Saaresti T, Uusitalo A. Organic Rankine Cycle Power Systems: From the Concept to Current Technology, Applications, and an Outlook to the Future." ASME. J. Eng. Gas Turbines Power 2015;137:100801.

[18] Bronicki L Y. History of Organic Rankine Cycle systems. Organic Rankine Cycle (ORC) Power Systems: Technologies and Applications 2017;25–66.

[19] Knowledge Center on Organic Rankine Cycle technology. Website address: https://www.kcorc.org/en/science-technology/history; accessed on 6th January 2023.

[20] Di Pippo R. Geothermal power plants: Principles, applications, case studies and environmental impact 2015. Elsevier.

[21] Yamashita A. Power generation system by heat recovery from converter cooling water. The Sumitomo Search 1979, No. 25. May 1981.

[22] Wieland C, Dawo F, Schifflechner C, Astolfi M. Market report on orgnic Rankine cycle power systems: Recent development and outlook. In 6th International Seminar on ORC Power Systems 2021.

[23] Zhang J, Zhan, X, Zhang Z, Zhou P, Zhang Y,Yuan H. Performance improvement of ocean thermal energy conversion organic Rankine cycle under temperature glide effect. Energy 2022;246:123440.

[24] Astolfi M, Martelli E, Pierobon. Thermodynamic and technoeconomic optimization of Organic Rankine Cycle systems. Organic Rankine Cycle (ORC) Power Systems: Technologies and Applications 2017;173–249.

[25] Hossin K. Dynamic modelling and thermo-economic optimization of a small-scale hybrid solar/biomass organic rankine cycle power system. Doctoral thesis, Northumbria University, UK, 2017. Available online: https://nrl.northumbria.ac.uk/id/eprint/36243/1/hossin.khaled_phd.pdf. Accessed on 6th January 2023.

[26] Ji D, Cai H, Ye Z, Luo D, Wu G, Romagnoli A. Comparison between thermoelectric generator and organic Rankine cycle for low to medium temperature heat source: A Techno-economic analysis. Sustainable Energy Technologies and Assessments 2023;55:102914.

[27] Quoilin S. Sustainable Energy Conversion through the Use of Organic Rankine Cycles for Waste Heat Recovery and Solar Applications. Ph.D. Thesis, University of Liege, Liege, Belgium, 2011. Available online: https://hdl.handle.net/2268/96436. Accessed on 6th January 2023.

[28] Aeini E. Experimentelle und theoretische Untersuchungen an einem ORC-Prozess mit den Arbeitsfluiden R365mfc, R245fa und deren Gemische. Ph.D. Thesis, Gottfried Wilhelm Leibniz Universität Hannover, Germany, 2021. https://www.repo.uni-hannover.de/handle/123456789/11224. Accessed on 6th January 2023.

[29] Market research intellect. Organic Rankine Cycle (ORC) Systems Market Size and Forecast 2021. Report ID: 463194. Website address: https://www.marketresearchintellect.com/product/global-organic-rankine-cycle-orc-systems-market-size-and-forecast. Accessed on 6th January 2023.

[30] Tartière T, Astolfi M. A World Overview of the Organic Rankine Cycle Market. Energy Procedia 2017;129:2–9.

[31] Grand view research (GVR). Organic Rankine cycle market size, share & trends analysis report by application (Waste heat recovery, biomass, geothermal, solar thermal, oil gas, waste to energy), by region, and segment forecasts, 2022-2030. Report ID: GVR-4-68038-071-2. Website address: https://www.grandviewresearch.com/industry-analysis/organic-rankine-cycle-market. Accessed on 6th January 2023.

[32] Fan W, Han Z, Li P, Jia Y. Analysis of the thermodynamic performance of the organic Rankine cycle (ORC) based on the characteristic parameters of the working fluid and criterion for working fluid selection. Energy Conversion and Management 2020;211:112746.

[33] Özcan Z, Ekici Ö. A novel working fluid selection and waste heat recovery by an exergoeconomic approach for a geothermally sourced ORC system. Geothermics 2021;95:102151.

[34] Zhang X, Zhang Y, Wang J. New classification of dry and isentropic working fluids and a method used to determine their optimal or worst condensation temperature used in Organic Rankine Cycle. Energy 2020;201:117722.

[35] Györke G, Deiters U K, Groniewsky A, Lassu I, Imre, A R. Novel classification of pure working fluids for Organic Rankine Cycle. Energy 2018;145:288–300.

[36] Frutiger J, Andreasen J, Liu W, H, Fredrik Haglind, Abildskov J, Sin G. Working fluid selection for organic Rankine cycles – Impact of uncertainty of fluid properties. Energy 2016;109: 987-997.

[37] Shu G, Wang X, Tian H, Liu P, Jing D, Li X. Scan of working fluids based on dynamic response characters for Organic Rankine Cycle using for engine waste heat recovery. Energy 2017;133:609–620.

[38] Su W, Zhao L, Deng S. Simultaneous working fluids design and cycle optimization for Organic Rankine cycle using group contribution model. Applied Energy 2017;202:618–627.

[39] Uusitalo A, Honkatukia J, Turunen-Saaresti T, Grönman A. Thermodynamic evaluation on the effect of working fluid type and fluids critical properties on design and performance of Organic Rankine Cycles. Journal of Cleaner Production 2018;188:253–263.

[40] Mondejar M E, Andreasen J G, Regidor M, Riva S, Kontogeorgis G, Persico G, Haglind F. Prospects of the use of nanofluids as working fluids for organic Rankine cycle power systems. Energy Procedia 2017;129:160–167.

[41] Zhu J, Huang H. Performance analysis of a cascaded solar Organic Rankine Cycle with superheating. International Journal of Low-Carbon Technologies 2016;11:169–176.

[42] Arjunan P, Gnana Muthu J H, Somanasari Radha S L, Suryan A. Selection of working fluids for solar organic Rankine cycle-A review. International Journal of Energy Research 2022;46:20573–20599.

[43] Dogbe E S, Mandegari M, Görgens J F. Assessment of the thermodynamic performance improvement of a typical sugar mill through the integration of waste-heat recovery technologies. Applied Thermal Engineering 2019;158:113768.

[44] Safarian S, Aramoun F. Energy and exergy assessments of modified Organic Rankine Cycles (ORCs). Energy Reports 2015;1:1–7.

[45] He C, Liu C, Zhou M, Xie H, Xu X,Wu S, Li Y. A new selection principle of working fluids for subcritical organic Rankine cycle coupling with different heat sources, Energy 2014;68:283–291.

[46] Mago P J, Chamra L m, Somayaji C. Performance analysis of different working fluids for use in organic Rankine cycles, Proc. Inst. Mech. Eng. Part A J. Power Energy 2007; 221:255–264.

[47] Xu J, Yu C (2014). Critical temperature criterion for selection of working fluids for subcritical pressure Organic Rankine cycles. Energy 2016;74:719–733.

[48] Stijepovic M Z, Linke P, Papadopoulos A I, Grujic A S. On the role of working fluid properties in Organic Rankine Cycle performance, Appl. Therm. Eng. 2012;36:406–413.

[49] Aljundi I H. Effect of dry hydrocarbons and critical point temperature on the efficiencies of organic Rankine cycle, Renew. Energy 2011;201136:1196–1202.

[50] Barse K A, Mann M D. Maximizing ORC Performance with Optimal Match of Working Fluid with System Design, Appl. Therm. Eng. 2016;100:11–19.

[51] Song C, M. Gu, Z. Miao, C. Liu, J. Xu, Effect of fluid dryness and critical temperature on trans-critical organic Rankine cycle, Energy 2019;174:97–109.

[52] Zhai H, An Q, Shi L. Analysis of the quantitative correlation between the heat source temperature and the critical temperature of the optimal pure working fluid for subcritical organic Rankine cycles, Appl. Therm. Eng. 2016;99:383–391.

[53] Vivian J, Manente G, Lazzaretto A. A general framework to select working fluid and configuration of ORCs for low-to-medium temperature heat sources, Appl. Energy 2015;156:727–746.

[54] Chen H, Goswami D Y, Stefanakos E K. A review of thermodynamic cycles and working fluids for the conversion of low-grade heat. Renewable and Sustainable Energy Reviews 2010;14:3059–3067.

[55] Bianchi M, Branchini L, de Pascale A, Melino F, Orlandini V, Peretto A, Archetti D, Campana F, Ferrari T, Rossetti N. Techno-Economic Analysis of ORC in Gas Compression Stations Taking into Account Actual Operating Conditions. Energy Procedia 2017;129:543–550.

[56] IUPAC. Compendium of Chemical Terminology, 2nd ed. (the "Gold Book"). Compiled by Naught A D, Wilkinson A. Blackwell Scientific Publications, Oxford (1997). Online version, created by S. J. Chalk.

[57] March's Advanced Organic Chemistry, The Sixth Edition. Michael B S, Jerry M. John Wiley & Sons, 29.01.2007.

[58] Zakaria M , Bong C W, Vaezzadeh V. Fingerprinting of Petroleum Hydrocarbons in Malaysia Using Environmental Forensic Techniques: A 20-Year Field Data Review. Oil Spill Environmental Forensics Case Studies 2018, 345–372.

[59] Abbas W K A, Baumhögger E, Vrabec J. Experimental investigation of organic Rankine cycle performance using alkanes or hexamethyldisiloxane as a working fluid. Energy Conversion and Management: X 2022;15;100244.

[60] Zhai H, Shi L, An Q. Influence of working fluid properties on system performance and screen evaluation indicators for geothermal ORC (organic Rankine cycle) system. Energy 2014;74:2–11.

[61] Siddiqi A, Atakan B. Alkanes as fluids in Rankine cycles in comparison to water, benzene and toluene. Energy 2012;45:256–263.

[62] Lai N A, Wendland M, Fischer J. Working fluids for high-temperature organic Rankine cycles. Energy 2011;36:199–211.

[63] Quoilin S, Lemort V. Technological and Economical Survey of Organic Rankine Cycle Systems. European Conference on Economics and Management of Energy in Industry, Vilamoura, Portugal, April 2009.

[64] Shu G, Li X, Tian H, Liang X, Wei H, Wang X. Alkanes as working fluids for high-temperature exhaust heat recovery of diesel engine using organic Rankine cycle. Applied Energy 2014;119:204–217.

[65] Li Y, Li W, Gao X, Ling X. Thermodynamic analysis and optimization of organic Rankine cycles based on radial-inflow turbine design. Applied Thermal Engineering 2021;184:116277.

[66] Uusitalo A, Turunen-Saaresti T, Honkatukia J, Colonna P, Larjola J. Siloxanes as Working Fluids for Mini-ORC Systems Based on High-Speed Turbogenerator Technology. ASME. J. Eng. Gas Turbines Power 2013;135:042305.

[67] Han Z, Fina A, Camino G. Organosilicon Compounds as Polymer Fire Retardants. Polymer Green Flame Retardants 2014;389–418.

[68] Dubberke F. Thermophysical properties from experimental speed of sound measurements for working fluids in organic Rankine cycles, Paderborn, 2017.

[69] Fernández F J, Priet, M, Suárez I. Thermodynamic analysis of high-temperature regenerative organic Rankine cycles using siloxanes as working fluids. Energy 2011;36:5239–5249.

[70] Dai X, Shi L, Qian W. Review of the Working Fluid Thermal Stability for Organic Rankine Cycles. Journal of Thermal Science 2019;28:597–607.

[71] Loni R, Mahian O, Markides C N, Bellos E, le Roux, W G, Kasaeian A, Najafi G, Rajaee F. A review of solar-driven organic Rankine cycles: Recent challenges and future outlook. Renewable and Sustainable Energy Reviews 2021;150:111410.

[72] Sorgulu F, Akgul M B, Cebeci E, Yilmaz T O, Dincer I. A new experimentally developed integrated organic Rankine cycle plant. Applied Thermal Engineering 2021;187:116561.

[73] Calm J M. The next generation of refrigerants - Historical review, considerations, and outlook. International Journal of Refrigeration 2008;31:1123–1133.

[74] Edelmann F T, The life and legacy of Thomas Midgley J R, Papers and Proceedings of the Royal Society of Tasmania 2016;150:45-49.

[75] Uddin K, Saha B B. An Overview of Environment-Friendly Refrigerants for Domestic Air Conditioning Applications. Energies 2022;15:8082.

[76] United Nations. Montreal Protocol on Substances That Deplete the Ozone Layer. United Nations Environment Program, Ozone Secretariat, New York, NY, USA, 1987.

[77] Kuijpers L J M. Copenhagen 1992: a revision or a landmark?: Development in international agreements and regulations. International Journal of Refrigeration 1993;16:210–220.

[78] Occhipinti Z, Verona R. Kyoto Protocol (KP). In: Leal Filho W, Azul A M, Brandli L, Özuyar P G, Wall T. (eds) Climate Action. Encyclopedia of the UN Sustainable Development Goals 2020. Springer, Cham. Doi:10.1007/978-3-319-95885-9_23.

[79] Mota-Babiloni A, Makhnatch P. Predictions of European refrigerants place on the market following F-gas regulation restrictions. International Journal of Refrigeration 2021;127:101–110.

[80] Plummer L N, Busenberg E. Chlorofluorocarbons. In: Cook P G, Herczeg A L. Environmental Tracers in Subsurface Hydrology 2000. Springer, Boston, MA.

[81] Tsai W T. A review of environmental hazards and adsorption recovery of cleaning solvent hydrochlorofluorocarbons (HCFCs). Journal of Loss Prevention in the Process Industries 2002;15:147–157.

[82] Redhwan A A M, Azmi W H, Sharif M Z, Mamat R. Development of nanorefrigerants for various types of refrigerant based: A comprehensive review on performance. International Communications in Heat and Mass Transfer 2016;76:285–293.

[83] Katarkar A, Majumder , Bhaumik S. Effect of enhanced surfaces and materials in boiling heat transfer with HFO Refrigerants: A review. Materials Today: Proceedings 2020;26:2237–2241.

[84] Bayrakçi H C, Özgür A E. Energy and exergy analysis of vapor compression refrigeration system using pure hydrocarbon refrigerants. International Journal of Energy Research 2009;33:1070–1075.

[85] Cai D, Hao Z, Xu H, He G. Research on flammability of R290/R134a, R600a/R134a and R600a/R290 refrigerant mixtures. International Journal of Refrigeration 2022:137:53–61.

[86] Ebenezer S P. Refrigerant Mixtures, in Low-Temperature Technologies and Applications. London, United Kingdom: IntechOpen, 2021. Website address: https://www.intechopen.com/chapters/77985. Accessed on 6th January 2023.

[87] Wieland C, Schifflechner C, Dawo F, Astolfi M. The Organic Rankine Cycle Power Systems Market: Recent Developments and Future Perspectives. Applied Thermal Engineering 2023;224:119980.

[88] Gnutek Z, Bryszewska-Mazurek A. The thermodynamic analysis of multicycle ORC engine. Energy 2001; 26:1075–1082.

[89] Yun E, Park H, Yoon S Y, Kim K C. Dual parallel organic Rankine cycle (ORC) system for high efficiency waste heat recovery in marine application, J. Mech. Sci. Technol. 2015;29:2509–2515.

[90] Ayachi F, Boulawz Ksayer E, Zoughaib A, Neveu P, ORC optimization for medium grade heat recovery, Energy 2014;68:47–56.

[91] Chen T, Zhuge W, Zhang Y, Zhang L. A novel cascade organic Rankine cycle (ORC) system for waste heat recovery of truck diesel engines. Energy Conversion and Management 2017;138:210–223.

[92] Rashwan S S, Dincer I, Mohany A. Analysis and assessment of cascaded closed loop type organic Rankine cycle. Energy Conversion and Management 2019;184:416–426.

[93] White M T, Read M G, Sayma A I. Making the case for cascaded organic Rankine cycles for waste-heat recovery. Energy 2020;211:118912.

[94] White M T, Read M G, Sayma A I (2019). Comparison between single and cascaded organic Rankine cycle systems accounting for the effects of expansion volume ratio on expander performance. IOP Conference Series: Materials Science and Engineering 2019;604:012086.

[95] White M T, Read M G, Sayma AI. A comparison between cascaded and single stage ORC systems taken from the component perspective. In: 5th international seminar on ORC power systems2019;113:9-11 September, Athens, Greece.

[96] Kane M, Larrain D, Favrat D, Allani Y. Small hybrid solar power system. Energy 2003;28:1427-1443.

Appendix

A. Supplementary material for:

Experimental study of two cascaded organic Rankine cycle with varying working fluids

This supplementary provides information about the operating conditions that have been adopted to study the system performance. Moreover, it provides an uncertainty analysis of the experimental work.

Table A1: Basic parameters and operational conditions of the experimental work under condition 1 using cyclopentane as a working fluid.

Parameter	Range
Temperature of heat source	453 – 533 K
Mass flow rate (HC)	0.50 – 0.55 kg s^{-1}
Ambient temperature	278.15 – 288.15 K
Ambient pressure	0.1013 MPa
Mass flow rate (HT)	0.08 – 0.12 kg s^{-1}

Table A2: Basic parameters and operational conditions of the experimental work under condition 2 using cyclopentane as a working fluid.

Parameter	Range
Temperature of heat source	533 K
Mass flow rate (HC)	0.50 – 0.55 kg s^{-1}
Mass flow rate (HT)	0.12 – 0.15 kg s^{-1}
Ambient temperature	288.15 – 298.15 K
Ambient pressure	0.1013 MPa

Table A3: Basic parameters and operational conditions of the experimental work under condition 3.

Working fluid	Heat source temperature (K)	Mass flow rate (HC) kg/s	Mass flow rate (HT) kg/s	Mass flow rate (LT) kg/s	Ambient temperature (K)	Ambient pressure (bar)
Pentane	453-533	0.48-0.55	0.12	0.03-0.035	283.15-293.15	0.1013
Butane	453-533	0.48-0.55	0.12	0.03-0.035	281.15-288.15	0.1013
Propane	453-503	0.48-0.55	0.12	0.03-0.035	280.15-293.15	0.1013

Table A4: Basic parameters and operational conditions of the experimental work under condition 4.

Working fluid	Heat source temperature (K)	Mass flow rate (HC) kg/s	Mass flow rate (HT) kg/s	Mass flow rate (LT) kg/s	Ambient temperature (K)	Ambient pressure (bar)
Pentane	533	0.48-0.55	0.12	0.035-0.048	285.15-293.15	0.1013
Butane	533	0.48-0.55	0.12	0.035-0.048	283.15-288.15	0.1013
Propane	503	0.48-0.55	0.12	0.035-0.048	280.15-293.15	0.1013

Table A5: Uncertainties of the measuring devices implemented in the test rig.

Variable	Uncertainty
p (HC)	± 0.5%
T_1, T_2 (HC)	± 0.1%
$\dot{m}_{HC}$ (HC)	± 0.1%
T_3, T_4, T_5, T_6, T_7 (HT)	± 0.1%
p_3, p_4 (HT)	± 0.5%
p_5, p_6, p_7 (HT)	± 0.5%
$\dot{m}_{HT}$ (HT)	≤ 0.065 %
T_8, T_9 (LT)	± 0.1%
T_{10}, T_{11} (LT)	± 0.1%
p_8, p_9 (LT)	± 0.5%
p_{10}, p_{11} (LT)	± 0.5%
$\dot{m}_{LT}$ (LT)	≤ 0.065 %

Table A6: Uncertainties of the equations of state implemented in REFPROP.

Parameter	Uncertainty (%)	Reference
Density	0.01-0.5	[1-4]
Speed of sound	0.01-1	[1-4]
Isobaric heat capacity	0.2-1	[1-4]
Vapor pressure	0.02-0.5	[1-4]

References

[1] E.W. Lemmon, M.L. Huber, M.O. McLinden, Reference fluid thermodynamic and transport properties (REFPROP), version 10.0, in NIST Standard Reference Database 23. National Institute of Standard and Technology, Gaithersburg, MD, 2007.

[2] H. Gedanitz, M.J. Davila, E.W. Lemmon, Speed of sound measurements and a fundamental equation of state for cyclopentane, J. Chem. Eng. Data 60 (2015) 1331–1337. doi:10.1021/je5010164.

[3] E. W. Lemmon, M. O. McLinden, W. Wagner, Thermodynamic Properties of Propane. III. A Reference Equation of State for Temperatures from the Melting Line to 650 K and Pressures up to 1000 Mpa, J. Chem. Eng. Data 54 (2009), 3141–3180. doi:10.1021/je900217v.

[4] Bücker D, Wagner W. Reference equations of state for the thermodynamic properties of fluid phase n-butane and isobutane, J. Phys. Chem. Ref. Data 2006;35:929–1019. doi:10.1063/1.1901687.

B. Supplementary material for:

Cascaded dual-loop organic Rankine cycle with alkanes and low global warming potential refrigerants as working fluids

This supplementary material provides information about the LT-ORC maximum thermal efficiency by using hexane and pentane as a working fluid in the HT-ORC and the relation between maximum thermal efficiency and critical temperature of the working fluid in the LT-ORC. Moreover, it provides an uncertainty analysis of the simulations, the underlaying assumptions, exergy loss analysis and the properties of the heat transfer fluid Therminol 66.

B.1 Uncertainties analysis of simulation

Working fluid properties in the simulation software (Ebsilon@Professional) are based on REFPROP, which is a Helmholtz energy equation of state library. Typical uncertainties of the thermodynamic properties of the selected working fluids vary from 0.01% to 0.1% in terms of speed of sound, from 0.5% to 2% in terms of isobaric heat capacity and from 0.02% to 1% in terms of vapor pressure [1]. The uncertainties are larger for most of the selected working fluids in their critical region, but that range of states was avoided in this study.

B.2 Simulation assumption

In these simulations, the heat source temperature was set for each working fluid such that the turbine inlet temperature was below the critical temperature with a small superheating degree. A screw expander was assumed with an isentropic efficiency of 0.75, which is a common value [2]. The minimum condensation temperature in both cycles was between 35 °C and 50 °C, which is reasonable for most ORC systems and allows to validate the present results with those of reference [3]. No recuperator or internal heat exchanger was adopted in this investigation due the design of the CORC test rig [2]. The pinch point temperature difference in the heat exchangers and condensers was set to 5 °C following literature practice [4,5]. The maximum evaporation pressure was set to be lower than the critical pressure. The mechanical efficiency of turbines and pumps, efficiency and power factor of generators were assumed to be standard values as in most simulation and experimental works.

B.3 Exergy loss analysis

The exergy analysis was carried out for each component in the CORC in cases where the highest total exergy efficiency was reached. From Fig. B4, it can be seen that the highest exergy loss occurs in the evaporator due to the irreversibility during heat transfer. The exergy loss in the evaporator was 69.4%, 70.1%, 72.5% and 72.8% using the combinations cyclohexane-R1233zd(E), cyclohexane-butane, cyclohexane-R1234ze(Z) and cyclohexane-isobutane, respectively. These results agree with the analyses of Safarian et al. [6] and Li et al. [7]. Moreover, the evaporator represents the critical component in the CORC and has a more dominating effect on the system performance than the other components.

The exergy loss of the element i can be calculated as

$$Ii = E_i^{in} - E_i^{out}$$

where E_i^{in} is the exergy flow into element i and E_i^{out} is the outlet exergy of element i.

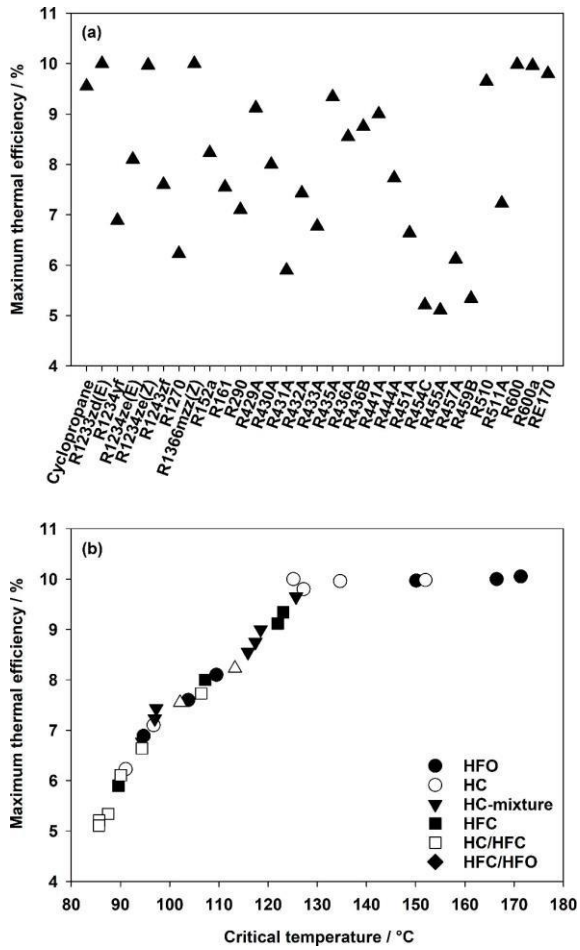

Fig. B1. (a) Variation of the LT-ORC maximum thermal efficiency by using hexane as a working fluid in the HT-ORC and (b) relation between maximum thermal efficiency and critical temperature of the working fluid in the LT-ORC.

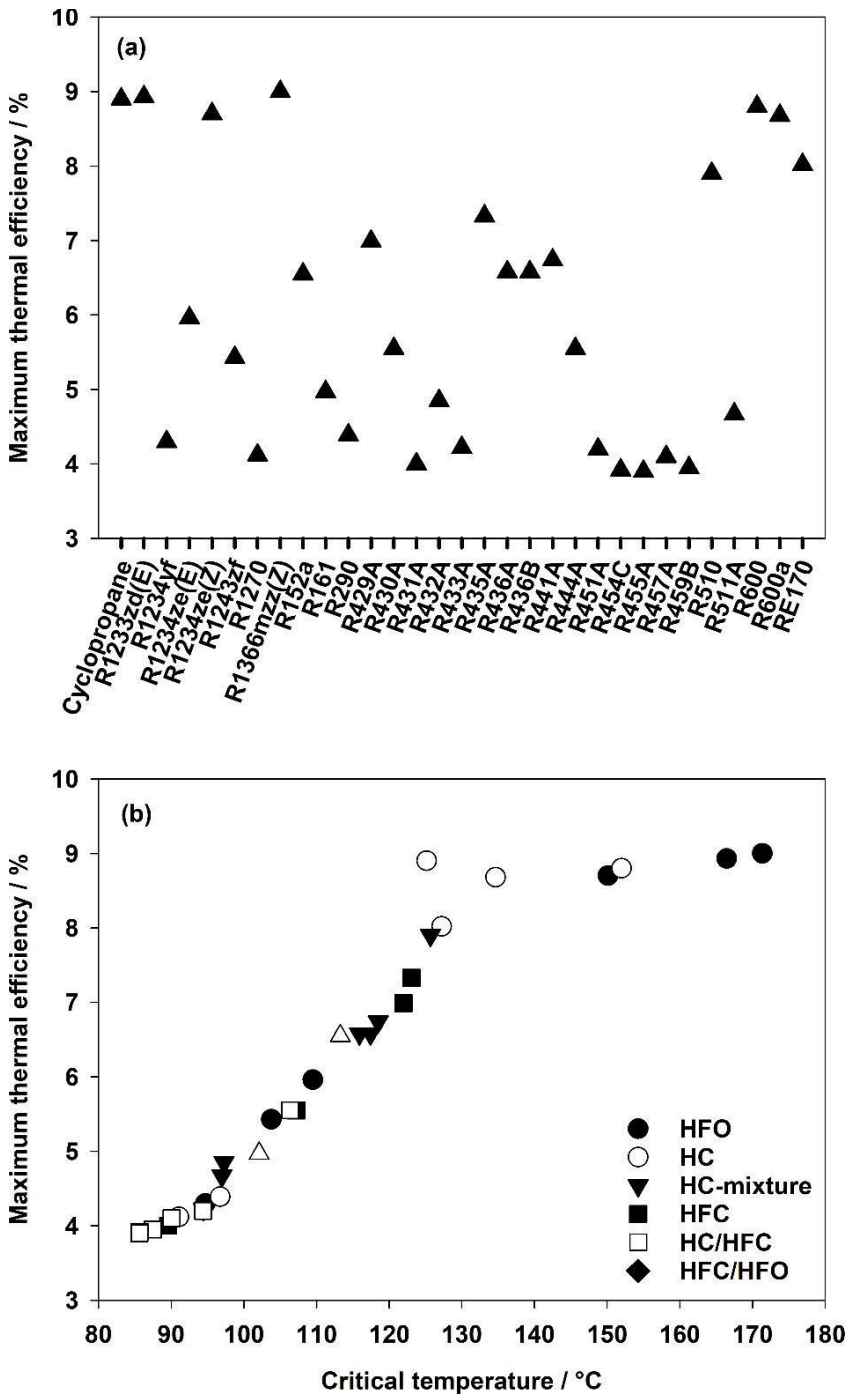

Fig. B2. (a) Variation of the LT-ORC maximum thermal efficiency by using pentane as a working fluid in the HT-ORC and (b) relation between maximum thermal efficiency and critical temperature of the working fluid in the LT-ORC.

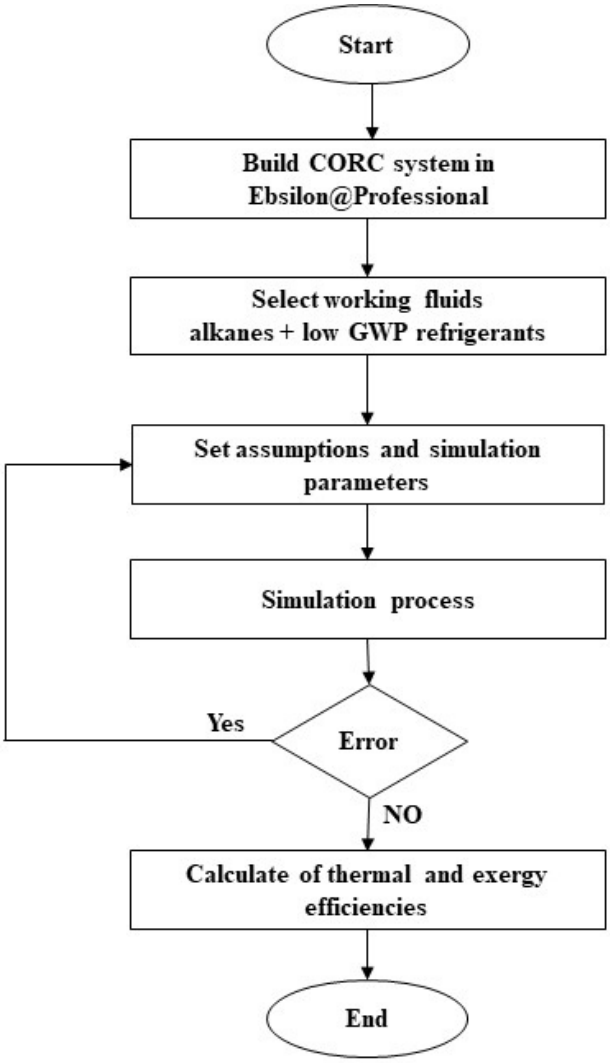

Fig. B3. Methodological approach of the present simulation procedure.

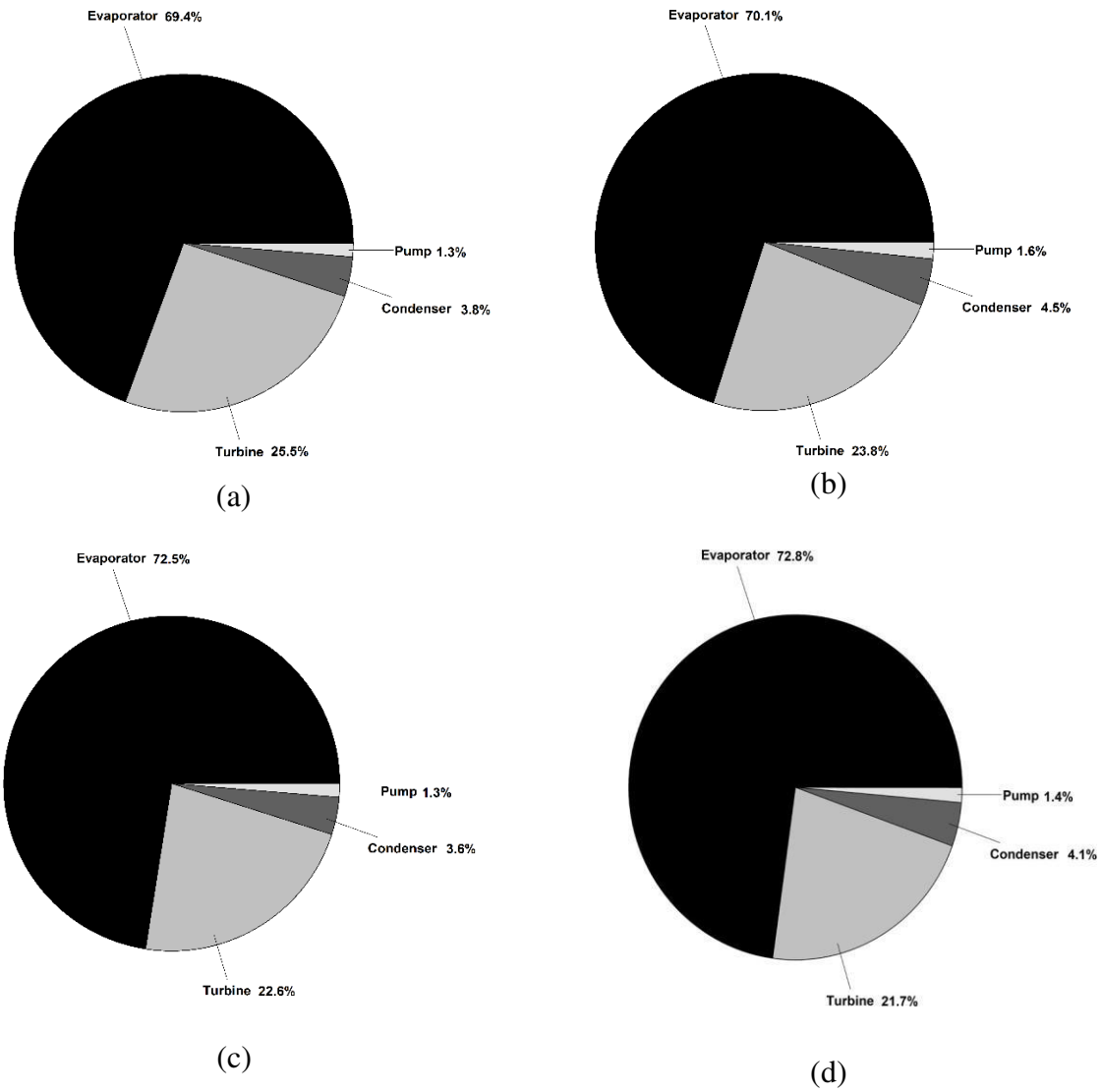

Fig. B4. Percentage of exergy loss in the components of the CORC using the working fluid combinations (a) cyclohexane-R1233zd(E), (b) cyclohexane-butane, (c) cyclohexane-R1234ze(Z), (d) cyclohexane-isobutane.

Table B1. Properties of Therminol 66 [8].

Properties	
Autoignition temperature (DIN 51794)	399°C
Maximum film temperature	375°C
Normal boiling point	359°C
Recommended bulk temperature	345°C
Flash point	184°C
Average molecular weight	252 g/mol
Chlorine content (DIN 51577)	<10 ppm

References

[1] E.W. Lemmon, M.L. Huber, M.O. McLinden, Reference fluid thermodynamic and transport properties (REFPROP), version 10.0, in NIST Standard Reference Database 23. National Institute of Standard and Technology, Gaithersburg, MD, 2007.

[2] K. Braimakis, S. Karellas, Exergetic optimization of double stage Organic Rankine Cycle (ORC), Energy 149 (2018) 296–313. doi:10.1016/j.energy.2018.02.044.

[3] A. Uusitalo, J. Honkatukia, T. Turunen-Saaresti, A. Grönman, Thermodynamic evaluation on the effect of working fluid type and fluids critical properties on design and performance of Organic Rankine Cycles, J. Clean. Prod. 188 (2018) 253–263. doi:10.1016/j.jclepro.2018.03.228.

[4] J. Wang, M. Diao, K. Yue, Optimization on pinch point temperature difference of ORC system based on AHP-Entropy method, Energy 141 (2017) 97-107. doi:10.1016/j.energy.2017.09.052.

[5] M. Jankowski, A. Borsukiewicz, K. Szopik-Depczyńska, G. Ioppolo, Determination of an optimal pinch point temperature difference interval in ORC power plant using multi-objective approach, Cleaner Production 217 (2019) 798-807, doi:10.1016/j.jclepro.2019.01.250.

[6] S. Safarian, F. Aramoun, Energy and exergy assessments of modified Organic Rankine Cycles (ORCs), Energy Reports 1 (2015) 1–7. Doi:10.1016/j.egyr.2014.10.003.

[7] W. Li, X. Feng, L.J. Yu, J. Xu, Effects of evaporating temperature and internal heat exchanger on organic Rankine cycle, Applied Thermal Engineering 31 (2011) 4014-4023.

[8] Eastman chemical company. Product data sheet Therminol 66. Website address: http://www.eastman.com/pages/products/therminol66.asp; accessed on 09th May 2021.

C. Supplementary material for:

Experimental investigation of organic Rankine cycle performance using alkanes or hexamethyldisiloxane as a working fluid

This supplementary provides information about the operating conditions that have been adopted to study the system performance. Moreover, it provides an uncertainty analysis of the experimental work.

Table C1: Parameters and operational conditions.

Parameter	Range
Effects of heat source analysis	
Heat source temperature	80 – 280 °C
Mass flow rate (ORC)	0.08 – 0.12 kg/s
Ambient pressure	1.013 bar
Ambient temperature	5 – 25 °C
Mass flow rate (HC)	0.42 – 0.55 kg/s
Effects of turbine inlet pressure	
Heat source temperature	180-280 °C
Turbine inlet pressure	10 – 44 bar
Mass flow rate (ORC)	0.09 – 0.14 kg/s
Mass flow rate (HC)	0.37 – 0.56 kg/s
Ambient pressure	1.013 bar
Ambient temperature	10 – 25 °C
Effects of superheating degree	
Superheating degree	1 – 18 °C
Mass flow rate (ORC)	0.08 – 0.12 kg/s
Mass flow rate (HC)	0.45 – 0.55 kg/s
Ambient pressure	1.013 bar
Ambient temperature	10 – 20 °C
Effects of critical properties	
Ambient pressure	1.013 bar
Ambient temperature	5 – 20 °C
Heat source temperature	180-280 °C
Mass flow rate (HC)	0.37 – 0.56 kg/s
Mass flow rate (ORC)	0.08 – 0.15 kg/s
Turbine inlet pressure	10 – 45 bar

Table C2: Uncertainties of measuring devices implemented in the test rig.

Variable	Sensor type	Uncertainty
p (HC)	Jumo	± 0.5%
T_1, T_2 (HC)	Pt 1000	± 0.1%
$\dot{m}_{HC}$ (HC)	Pressure difference	± 0.1%
T_3, T_4	Pt 1000	± 0.1%
T_5, T_6	Pt 1000	± 0.1%
p_3, p_4	APT	± 0.5%
p_5, p_6	APT	± 0.5%
$\dot{m}$	Pressure difference	≤ 0.065 %

Table C3: Uncertainties of the equation of state implemented in REFPROP.

Parameter	Uncertainty (%)	Reference
Density	0.02-1	[1-4]
Speed of sound	0.1-1	[1-4]
Isobaric heat capacity	0.2-1	[1-4]
Vapor pressure	0.1-2	[1-4]

References

[1] E.W. Lemmon, M.L. Huber, M.O. McLinden, Reference fluid thermodynamic and transport properties (REFPROP), version 10.0, in NIST Standard Reference Database 23. National Institute of Standard and Technology, Gaithersburg, MD, 2007.

[2] H. Gedanitz, M.J. Davila, E.W. Lemmon, Speed of sound measurements and a fundamental equation of state for cyclopentane, J. Chem. Eng. Data 60 (2015) 1331–1337. doi:10.1021/je5010164.

[3] Bücker D, Wagner W. Reference equations of state for the thermodynamic properties of fluid phase n-butane and isobutane, J. Phys. Chem. Ref. Data 2006;35:929–1019. doi:10.1063/1.1901687.

[3] Thol M, Dubberke F, Rutkai G, Windmann T, Köster A, Span R, Vrabec J. Fundamental equation of state correlation for hexamethyldisiloxane based on experimental and molecular simulation data. Fluid Phase Equilibria 2016;418:133–151. doi:10.1016/J.FLUID.2015.09.047.